FOCAL ACTIVATION AND INTERCELLULAR SIGNALING IN OSTEOCYTE NETWORKS INITIATED BY A NOVEL STOKESIAN FLUID STIMULUS PROBE (SFSP)

by

DANIELLE NICOLE WU

A dissertation submitted to the Graduate Faculty in Biomedical Engineering in partial fulfillment of the requirements for the degree of Doctor of Philosophy,
The City University of New York

2012

This manuscript has been read and accepted for the Graduate Faculty in Engineering in satisfaction of the dissertation requirement for the degree of Doctor of Philosophy.

_____
Date

_____
Professor Sheldon Weinbaum
Chair of Examining Committee

_____
Date

_____
Professor Mumtaz K. Kassir
Executive Officer

_____
Professor Luis Cardoso

_____
Professor Susannah P. Fritton

_____
Professor Mitchell B. Schaffler

_____
Professor Sylvia O. Suadicani
Supervisory Committee

_____
Professor David C. Spray
Supervisory Committee

THE CITY UNIVERSITY OF NEW YORK

Abstract

FOCAL ACTIVATION AND INTERCELLULAR SIGNALING IN OSTEOCYTE NETWORKS INITIATED BY A NOVEL STOKESIAN FLUID STIMULUS PROBE (SFSP)

by

Danielle Nicole Wu

Adviser: Professor Sheldon Weinbaum

Co-Adviser: Professor David C. Spray

Osteocytes are largely distinguished in bone tissue by their dendritic morphology and located in a dynamic cellular labyrinth called the lacunar-canalicular system (LCS). The LCS is surrounded by mineralized matrix that gives bone its unique properties of strength and rigidity and is the major porosity associated with osteocytic stimulation. Osteocytes are a major mechanosensory cell population in bone, but how they communicate within their cellular network and with other cell types under physiological loading conditions require further exploration. Theoretical models have predicted whole bone tissue strains of 0.04-0.3% to be amplified by 1-2 orders of magnitude near regions of loose and rigid attachment of the osteocyte cell process to the canalicular wall. Osteocyte stimulation is widely believed to be linked with load induced bone fluid flow in the pericellular space surrounding osteocytes in the LCS. Mechanisms of osteocyte activation have been explored using fluid flow culture systems, but it is realized that osteocytes have focal regions of mechanotransduction in its 3D microenvironment *in vivo*, which uniform flow patterns do not mimic. To achieve focal stimulation we developed a new force probe, the Stokesian fluid stimulus probe (SFSP), for preferential delivery of quantifiable pN-level hydrodynamic forces to mimic forces predicted to occur *in vivo.* The hydrodynamic disturbance produced a short lived constant strength pressure pulse that propagates nearly instantaneously through the medium creating a nearly spherical expanding fluid bolus that is closely modeled by quasi-steady Stokes flow through a circular orifice in a zero thickness planar wall. Electrophysiological techniques of high temporal and spatial resolution were used to investigate changes in membrane conductance during SFSP stimulation. Forces applied to cell process attachment sites between 1.0 and 2.3 pN initiated cell signaling, and led to responses that were 300 times the average electrical charge and 7 times the average peak conductance of responses produced by cell body stimulation thereby demonstrating osteocyte polarity in signaling initiation.

MLO-Y4 cells also demonstrated intercellular signaling directly through gap junctions and indirectly via purinergic nucleotide receptors. These results indicate that direct as well as indirect intercellular signaling are not mutually exclusive events and do occur in parallel.

Dedication

I dedicate this work to my family. To my husband Nathan James Baldauff, my parents Rini Wu Ziegler, Edward Ray Ziegler, Anthony Bing Wu, Lisa Lyle Wu, my siblings Claudia Jeanne Ziegler and Andrew Anthony Wu, and for my Lee, Wu, Ziegler, and Baldauff family.

Acknowledgements

I am deeply grateful to my advisers Sheldon Weinbaum, Ph.D. and David C. Spray, Ph.D. who invested their time and energy in my work and my career. I express my gratitude to John Tarbell, Ph.D. and the Department of Biomedical Engineering at The City College of New York, New York, NY and to the Department of Neuroscience at the Albert Einstein College of Medicine, Bronx, NY. The caliber of faculty and quality of resources ensured a competitive and nurturing environment for interdisciplinary research in the New York metro area. I thank my committee members Luis Cardoso, Ph.D., Susannah P. Fritton, Ph.D., Mitchell B. Schaffler, Ph.D., and Sylvia O. Suadicani, Ph.D., for their guidance and dedication in overseeing my dissertation work and reviewing my dissertation and manuscript drafts. I thank Peter Ganatos, Ph.D., for his guidance in low Reynolds number hydrodynamics, Robert Majeska, Ph.D. for his expertise and participation in numerous exploratory conversations, and Mia M. Thi, Ph.D. for sharing with me her laboratory knowledge and for being an invaluable resource. I thank Frank Macaluso, M.Sc. and his team, particularly Leslie Gunther-Cummins, M.Sc. and Geoffrey Perumal, for their technical input and assistance with my electron micrographs taken at the Analytical Imaging Facility (AIF) at Albert Einstein College of Medicine. I thank Eliana Scemes, Ph.D. for sharing her perspectives and expertise regarding membrane biology and experimental design, Marcia Maldonado and Adriana Mello for their dedication to the daily management and operations of the laboratory and animal colonies at Einstein, and Eno E. Ebong, Ph.D., Regina Hanstein, Ph.D., Neil Thomas, Ph.D., and Veronica Lopez, Ph.D. for their scientific feedback and comradery over the years. I thank Parisa Mirbod, Ph.D., Laura Causey and Adreanne Kelly Arnold for sharing this journey with me, and for the collegial and supportive inter-office environment that we have established. I thank Francis Andrade at Einstein and Pat Cupid at City College for their tireless administrative dedication and assistance as well as their continued friendship. It was an honor to serve as the Lead Mentor and Teaching Fellow for the NIH Scholars Program for Minorities at The City College of New York, and I thank Phillip Payton, Ph.D. and Marom Bikson, Ph.D. and Sheldon Weinbaum, Ph.D. for their service on the executive committee and vision for the program. I also thank the NIH Scholars, the Ph.D. student mentors, and the Ph.D. student teaching fellows. Their hard work and dedication to the success of the NIH Scholars' created major successes for the program and the Department of Biomedical Engineering at The City College of New York.

Table of Contents

List of Tables

List of Figures

List of Equations

List of Abbreviations

AFM – atomic force microscope

ADP – adenosine diphosphate

ATP – adenosine-5'- triphosphate

BMP – biomembrane force probe

BMU – basic multicellular unit

COX – cyclooxygenase

Cx43 – Connexin43

Cx45 – Connexin45

ECM – extracellular matrix

ERK1/2 – extracellular signal-related kinase 1/2

FSS – fluid shear stress

GAG – glycosaminoglycan

IGF-1 – insulin growth factor 1

IP_3 – inositol trisphosphate

KO – knock-out

LCS – lacunar canalicular system

M-CSF – macrophage colony stimulating growth factor

MLO-Y4 – osteocyte-like cell-line derived from murine long bone

MP - microperoxidase

MPT – magnetic pullers and twisters

NO – nitric oxide

OPG - osteoprotegerin

OPN – osteopontin

OT – optical tweezers

$P2X_7R$ – $P2X_7$ receptor

Panx1 – Pannexin1

PG – prostaglandin

PLC – phospholipase C

PKA – protein kinase A

PKC – protein kinase C

PTA – potassium or sodium phosphotungstate

PTH – parathyroid hormone

Re – Reynolds number

RANKL – receptor activator for nuclear factor κ–B ligand

SACC – stretch-activated cation channel

SEM – scanning electron microscopy

SFSP – Stokesian fluid stimulus probe

SGP – stress-generated potentials

TEM – transmission electron microscope

TGF-β – transforming growth factor β

UDP – uridine diphosphate

UMR–160.01 - osteoblast-like osteosarcoma cells

UTP – uridine triphosphate

VEGF – vascular endothelial growth factor

VOCC – voltage-operated calcium channel

List of Variables

ρ - density

μ - dynamic viscosity

ν - kinematic viscosity

U – velocity

R – radius

Q – volumetric flow rate

p_∞ – pressure far away from micropipette tip

p_o – pressure at t=0

c – tip radius

I_a – area moment of inertia of a single actin filament

I_b – area moment of inertia of the actin filament bundle

$\mu\varepsilon$ - microstrain

δ - deflection

δ_m – maximum deflection

F – force

L – distance between the two attachment sites

E – Young's Modulus

Chapter 1: Mechanotransduction in Bone

General Insight: Loading patterns imposed upon the skeleton during locomotion are observed to regulate bone architecture. Extreme alterations to physiological loading patterns exaggerated the observed effect that mechanical loads had on bone architecture. For example, elite athletes exhibited hypertrophy of the bone tissue in limbs that were hyper-physiologically loaded during rigorous training, and alternatively, astronauts exhibited bone loss after months of living in sub-gravity conditions. Age was also observed to influence skeletal architecture where metabolic activity of bone decreased as physiological activity of individuals with increasing age decreased. These load-induced and age-related changes of bone tissue architecture would cause alterations in its material properties, for example, its ability to absorb impact energy (toughness) and to bear loads (strength). Early observations of skeletal geometry and dynamic strength date back to the times of Galileo Galilei who identified varying geometries with different load bearing thresholds and noted a variance in fracture risk of young versus old bone (Galilei, 1638). Also, architectural observations made by von Meyer in 1867 were captured in his drawings that illustrated similarities between stress trajectories of the man-made Culmann crane and naturally-designed trabecular bone (von Meyer, 1867). This concept was used to relate trabecular geometry and principle stresses in what is often referred to as 'Wolff's Law' (Wolff, 1892), and has been critically examined by modern day biomechanicians (Roesler, 1987; Martin et al 1998; Cowin 2001a,b). Tissue level alterations observed in athletes and astronauts affirmed that mechanical loading or unloading of the skeleton mediated the architecture of whole bone. Cellular level understanding of this mediation would provide great insight into how bone cells contribute to changes that are observed at the tissue level, and provide potential to capitalize on or regulate their contributions.

Overview: Mechanical loading of whole bone tissue causes deformation induced interstitial fluid-flow. Interstitial fluid-flow translates imposed mechanical loads on whole bone tissue into cellular-level forces that act on and activate bone cells within the bone tissue. Mechanotransduction is a term used to refer to mechanisms that are involved in the cellular conversion of mechanical stimuli into chemical signals. Mechanotransduction in the bone depends on the ultrastructure of bone tissue and resident cells, load-induced interstitial fluid-flow, mechanosensitive cellular machinery, and the metabolic microenvironment of bone tissue. Mechanotransduction in bone is sub-divided here into three separate

events: (A) mechanotransmission, (B) mechanosensing, and (C) mechanoresponse, to describe the interaction of mechanotransduction mechanisms during the conversion of whole tissue forces into cellular-level forces and the initiation of intercellular signaling among bone cell networks.

Mechanotransmission of whole tissue mechanical loads to cellular-level forces is achieved by deformation of the viscoelastic bone tissue that produces fluid movement through the hierarchical porosities within the bone. Mechanosensing occurs at the cellular-level and is described as the conformational change or activation of mechanosensitive machinery in response to transmitted cellular forces imposed on the cell. The force-mediated initiation of a cell signal is the mechanoresponse that would mobilize nucleotides and signaling molecules to amplify the cell signal through the cellular network via direct and indirect intercellular signaling pathways. The force-mediated initiation of autocrine and paracrine signaling pathways in addition to transcriptional pathways is essential for cell survival. The initiation of these signaling pathways appears to modulate metabolic activity of bone cells to locally influence bone tissue microarchitecture. These sub-events of mechanotransduction in bone are described in more detail below with a focus on osteocyte activation and its mechanoresponses.

1.1. Mechanotransmission in bone

When whole bone tissue is loaded it undergoes compression, tension, bending, and torsion, and is ultimately distorted in reaction to forces exerted on the skeleton. Viscoelastic properties of bone tissue provide the skeleton its ability to bear weight and flex in response to complex physiological loading patterns. Bone tissue is highly organized and made of mineralized and non-mineralized matrix comprised of 90% collagen type-1 and 10% other proteins such as glycoprotein, osteocalcin, osteonectin, bone sialoprotein, osteopontin, fibronectin, in addition to various proteoglycans (Bartl and Frisch, 2009). The mineralized matrix is comprised of both an amorphous and a crystalline apatitic calcium phosphate phase where experimentally induced nutritional and hormonal deficiencies can alter the amorphous/crystalline ratio in the bone mineral (Termine and Posner, 1967). Tissue-level forces generated by whole bone tissue mechanical loading are translated into forces of tension, compression, fluid shear, and drag that act on bone cells at the cellular-level. Cellular-level forces acting on osteocytes are generated by compression-induced passage of interstitial fluid-flow through hierarchical porosities in

bone tissue. Bone tissue is best described as a hierarchical structure with different levels of porosity, **Figure 1**.

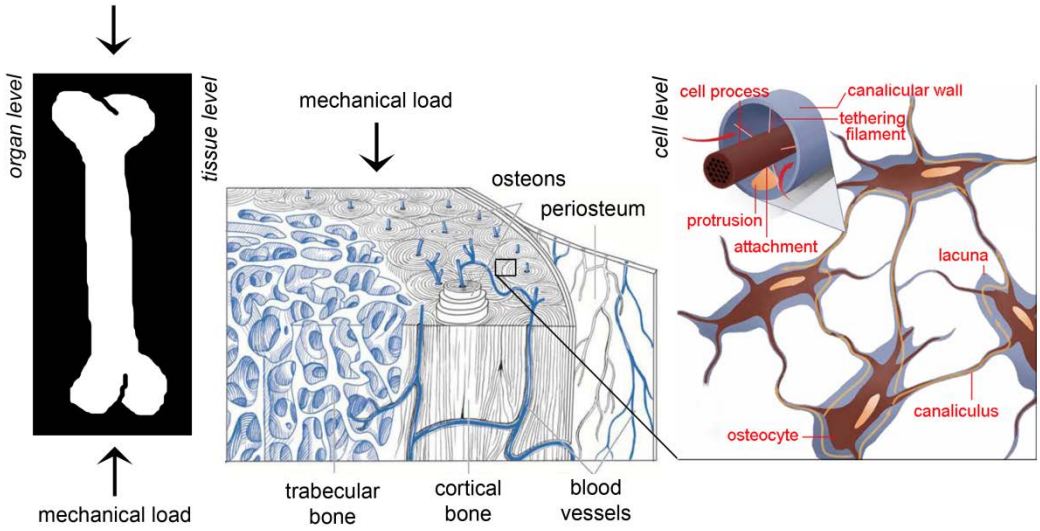

Figure 1 Bone is best described as a hierarchical structure

Mechanical loads from the organ level are transmitted to the tissue level, and further translated to the cellular level by interstitial fluid flow through the bone porosities. Load-induced fluid flow at the tissue level flows through the Haversian canal porosities containing bone vasculature and through the osteocyte containing lacunar-canalicular porosity. Interstitial fluid flow through the lacunar-canalicular system is illustrated with the arrows traversing through the pericellular space surrounding the osteocytes. Cellular level image adapted with permission from Bartl and Frisch (2009) and tissue level image adapted from Akst (2009).

Two levels of porosity provide passageways for interstitial fluid movement through the bone tissue. Fluid flow through the porosity surrounding blood vessels contained in Haversian and Volkmann's canals is driven into the porosity of the osteocyte-containing lacunar-canalicular system by whole tissue compression. Fluid movement throughout bone porosities in response to cyclic loading was first proposed by Piekarski and Munro (1977), and previously associated with increased transport between the

blood supply and osteocytes (Knothe Tate et al., 1998a; Tami et al., 2002). Bone fluid flow was also associated with stress-generated potentials (SGP) produced by load induced fluid-flow through micropores around hydroxyapatite encrusted collagen fibrils (Salzstein and Pollack, 1987; Salzstein et al., 1987; Starkebaum et al., 1979); however, it became apparent that solutes as small as 2 nm (1800 MW) did not penetrate the porosity of the mineralized matrix when intravenously injected (Tanaka and Sakano, 1985). The main transport pathway for interstitial fluid was through the porosity surrounding the bone vasculature and the pericellular space surrounding osteocytes, also referred to as the lacunar-canalicular system (LCS). Load-induced fluid-flow through the LCS is the medium that translates endogenous whole tissue mechanical loads to cellular level forces to stimulate osteocytes.

Early fluid flow studies on bone cells in culture were performed on osteoblasts (Reich and Frangos, 1991; Reich et al., 1990) using a wide range of steady fluid shear stresses (FSS) of 0.5-35 dyne/cm^2, some of which were similar to those that occur in the vasculature on endothelial cells. It was thought unlikely for fluid in bone to create FSS comparable to those seen in blood vessels until Weinbaum et al. (1994) developed a hierarchical model to predict interstitial fluid flow dynamics in the LCS. The model predicted FSS of 8-30 dyne/cm^2 to occur within the canaliculi of the LCS (Weinbaum et al., 1994). These predicted shear stresses were large enough to stimulate osteocytes *in vitro* with pulsatile fluid flow as low as 5 dyne/cm^2 (Klein-Nulend et al., 1995). It was later discovered that physiological whole tissue strains in the range of 0.03-0.4% (Fritton et al., 2000; Rubin and Lanyon, 1982) were not large enough to elicit a cellular response *in vitro* and that strains of > 1% were required (You et al., 2000). A series of theoretical models (Han et al., 2004; Wang et al., 2007; You et al., 2001) were developed to predict cellular-level strains produced by whole tissue compression and predictions were 10-100 times larger than the whole tissue strains measured with strain gauges *in vivo*. The major paradox in bone mechanobiology was addressed by a series of cellular level strain amplification models, described in Section 1.1.2., and these models have highlighted the importance of ultrastructural attachments between the cell membrane and the pericellular space in transducing forces that stimulate the osteocyte.

1.1.1. Whole bone tissue mechanotransmission

Bone tissue is a hierarchical structure with (1) an organ level, (2) a tissue level, and (3) a cellular level.

Mechanical continuity in bone is maintained throughout its structural hierarchy and is mechanically coupled by its matrix and interstitial fluid. Mineralized and compliant regions within the bone are continuous and forces are propagated through different mediums to act on cells within the tissue. Bones do not exhibit perfect symmetry, and therefore, whole tissue strain distributions throughout bone would vary in response to a single loading event. Major alterations in strain distributions would change how bone cells are stimulated and subsequently cause chronic or acute changes in bone metabolism as well as bone microarchitecture to influence its material properties (Fox et al., 2007; Lane et al., 2006). The influence of mechanical loading on bone metabolism at the cellular-level has proven to be critical in the assessment and intervention of fracture risk (Rizzoli et al., 2011) and healing rates (Norrdin and Shih, 1988; Sloan et al., 2010) in pathological conditions of disease or injury.

Different loading patterns that vary in frequency and magnitude are imposed on the skeleton as a result of diverse daily activities. Variations in frequency and magnitude of loading that are translated to the tissue-level are sensed at the cellular-level. These cellular-level responses were explored in animal and culture models, and verified that transcriptional responses were induced in particular bone cells at specific frequencies and magnitudes of load (Lau et al., 2010; Lester et al., 2009; Lohmann et al., 2003; Mack et al., 2004). To characterize these loading patterns in whole tissue, strain gauges were affixed to bone surfaces and the deformation produced in response to whole tissue loading was measured. The recordings of whole bone tissue strain histories of horses, dogs, sheep, turkeys, roosters, opossums, and mice using rosette strain gauges bonded to their long bones during physiological activity (Butcher et al., 2011; Fritton et al., 2000; Lee et al., 2002; Lieberman et al., 2004; Rubin and Lanyon, 1982; Rubin and Lanyon, 1984) has helped characterize whole tissue strains in bone for a variety of loading patterns. When considering a broad spectrum of bone strain, strain histories in different bones across quadrupeds and avian animal species were found to be similar, where physiologically produced strains fell in the range of 0.04-0.3% (Fritton et al., 2000).

Studies on macaques (Demes et al., 2001; Demes et al., 1998) and humans (Burr et al., 1996; Lanyon et al., 1975; Milgrom et al., 2000), have also found skeletons to be surprisingly scaled to maintain uniformity of peak strains; however, bone geometry did not correlate well with regions of maximum strain (Burr et al., 1996). Apparent curvature of long bones seemed to increase rather than decrease strains

(Lieberman 2004), suggesting that the generation of discrete high stress regions within bone was favored. Tissue level alterations of geometric curvature (Rubin and Lanyon, 1982), cortical-cancellous bone ratio, and cancellous tissue orientation (Pidaparti and Turner, 1997) were influenced by mechanical loading. Remodeling of whole bone tissue under various loading environments and in transgenic and disease-induced animal models have revealed relationships between mechanical loading and osteogenesis as well as particular mechanisms that are required for the translation of whole-tissue loads to cellular-level forces.

1.1.2. Cellular mechanotransmission

Mechanotransmission at the cellular-level is the transfer of whole tissue loads to cellular level strains. Poroelastic-bone tissue compression during physiological locomotion transmits mechanical loads to the cells by deformation-induced interstitial fluid-flow. The extension of the concept of fluid-flow through bone (Piekarski and Munro, 1977) to the creation of loading induced cellular-level forces link bone tissue strains to bone cell excitation in Weinbaum et al. (1994), and is now a fundamental concept in bone mechanotransduction. The history of this transition in conceptual understanding and more recent developments is described in Fritton and Weinbaum (2009).

Bone fluid-flow was initially associated with nutrient transport, waste removal, and osteocytic resorption, but osteocytes were initially thought not to have a direct role in local resorption (Parfitt, 1977; Sissons et al., 1984) and the regulation of serum calcium (Baylink and Wergedal, 1971) because of the very small flows induced by mechanical deformation *in vivo*. The role of the osteocyte was not meant to be diminished, but rather to suggest a different function for the osteocyte in regulating bone metabolism. However, the concept of osteocytes influencing their local environment by osteocytic osteolysis has been recently revisited (Bonucci, 2009; Tazawa et al., 2004; Teti and Zallone, 2009), and supports the idea that osteocytes actively influence their local microenvironment.

One early tracer study by Tanaka and Sakano (1985) highlighted the LCS porosity and accurately traced the movement of microperoxidase (MP), MW 1800, between the blood vessels and the LCS in the bone matrix. Fluorescent probes more recently are used to delineate passageways for interstitial fluid flow in the vascular and lacunar-canalicular porosities in bone either by systemic tracer injection (Knothe

Tate et al., 1998b; Price et al., 2010; Sugawara et al., 2011; Tami et al., 2003; Wang, L et al., 2004) or tissue-tracer incubation (Ciani et al., 2009). Computational renderings and image analysis of porosities (Sharma et al., 2012) have been powerful techniques to assess subtle changes in the microarchitecture of whole tissue that would influence forces exerted on bone cells at the cellular-level.

As mentioned previously, the basis of the major paradox in bone mechanobiology was the observation that *in vitro* strains of 0.05-0.5% produced experimentally to mimic physiologic whole tissue strains of 0.04-0.3%, neither evoked a cellular response of prostaglandin (PGE_2) or nitric oxide (NO) release in osteoblastic bone cells (Smalt et al., 1997) nor increased cytosolic calcium levels in osteocytic bone cells (You et al., 2000). However, strains > 1% did evoke an elevation of intracellular calcium in osteoblastic and osteocytic bone cells (You et al., 2000). Strains measured at the whole tissue level were smaller than the strains necessary to activate bone cells in culture, and these observations together gave rise to the major paradox in bone mechanobiology. Whole tissue strains > 0.3% would require rigorous and continuous high impact loading (Milgrom et al., 2000), and whole tissue strains > 0.5% would likely lead to load-induced fracture. The discrepancy between *in vivo* strains produced at the tissue level and *in vitro* strains produced at the cellular level was addressed in a series of theoretical models.

Improvements in tissue sample preparation have allowed for the preservation of ultrastructure surrounding the osteocyte to better visualize potential mechanotransduction complexes in electron micrographs of bone tissue. Theoretical models elegantly incorporated ultrastructural mechanisms identified in electron micrographs of osteocytic canaliculi, and predicted cellular-level strains through the action the identified structures in the pericellular space. When these amplification mechanisms were considered, theoretical model predictions of cellular-level strains matched measured whole-tissue strains *in vivo,* and provided reconciliation between whole-tissue strains measured *in vivo* and strains required to activate bone cells *in vitro*. The series of theoretical models will now be described in detail.

In 1994, it was first proposed that the osteocytes were surrounded by a fiber filled pericellular matrix within the LCS that could be stimulated by relatively small FSS acting on the membranes of their osteocytic processes (Weinbaum et al., 1994). This model was the first to consider the long slender glycosaminoglycan (GAG) fibers of the pericellular matrix located in the annular space between the canalicular wall and the cell process membrane to have a role in mechanotransduction. Brinkman's

equation was used to characterize the flow in this fibrous matrix and predicted FSS in the range of 8-30 dyne/cm^2 to occur at the cell process membrane. The fluid drag associated with the proteoglycan matrix in the pericellular space provided a mechanism for fluid pressure relaxation in the LCS, and this relaxation time was previously predicted to be 100 fold too short for the lacunar-canalicular porosity. Experimentally, FSS in the predicted range were large enough to stimulate calcium signaling (Hung et al., 1995) and prostaglandin E_2 (PGE_2) release (Reich and Frangos, 1991; Reich et al., 1990) when imposed on cultured bone cells. Also, degradation of the hyaluronic acid in the osteocyte glycocalyx with hyaluronidase *in vitro* suppressed FSS induced-PGE_2 release, but FSS-induced intercellular calcium signaling was unaffected (Burra et al., 2010; Reilly et al., 2003). Structures in the pericellular space, i.e. the osteocyte glycocalyx, appeared to be critical mechanisms that facilitated mechanotransmission of forces and mediated intercellular signaling in the LCS.

Another theoretical model based on the ultrastructure of the osteocyte cell process and structures in the pericellular matrix examined the mechanisms of strain amplification in the LCS for the first time. This theoretical model considered the fluid drag force associated with the proteoglycan matrix on the surface membrane of the osteocyte in the LCS and the resulting hoop strain acting on the cell process membrane (You et al., 2001). The ultrastructure was modeled after extracellular matrix (ECM) structures observed in transmission electron microscopy (TEM) micrographs of rat compact bone (Sauren et al., 1992; Tanaka-Kamioka et al., 1998) and tagged ECM proteins identified by immunocytochemistry in isolated osteocytes (Aarden et al., 1996). Tethering elements were observed to span the pericellular space between the cell process membrane and the canalicular wall, and it was noted that the cell process was consistently located at the center of the canalicular cross-section (You et al., 2004). The theoretical model predicted forces produced by bone tissue loads to be amplified by a factor of 20 to 100 at the cell process membrane for whole tissue loading between 1-20 MPa at 20 Hz. This amplification was found to be greatly dependent on the magnitude of loading, and was achieved by the drag imposed on the glycosaminoglycans (GAG) attached to the tethering elements by the fluid flowing in the pericellular space, see **Figure 2**. These amplified forces are predicted to produce cell process strains from 0.3-2%, for physiological whole bone tissue loading between 1-20 MPa, and are large enough to activate primary isolated bone cells and cell lines in culture (You et al., 2000). It was interesting to note the strain

amplification ratio increased non-linearly with linearly decreasing whole bone tissue strains. It has been shown that strains above the loading threshold of 1050 με or about 0.1% at a low loading frequency of 2 Hz increased lamellar bone formation (Turner et al., 1994). Bone mass has also been shown to increase at low magnitude loads of 5 με at 30 Hz (Rubin et al., 2002), and provided supporting evidence for the hypothesis of strain amplification in the LCS, particularly during low-magnitude high-frequency loading.

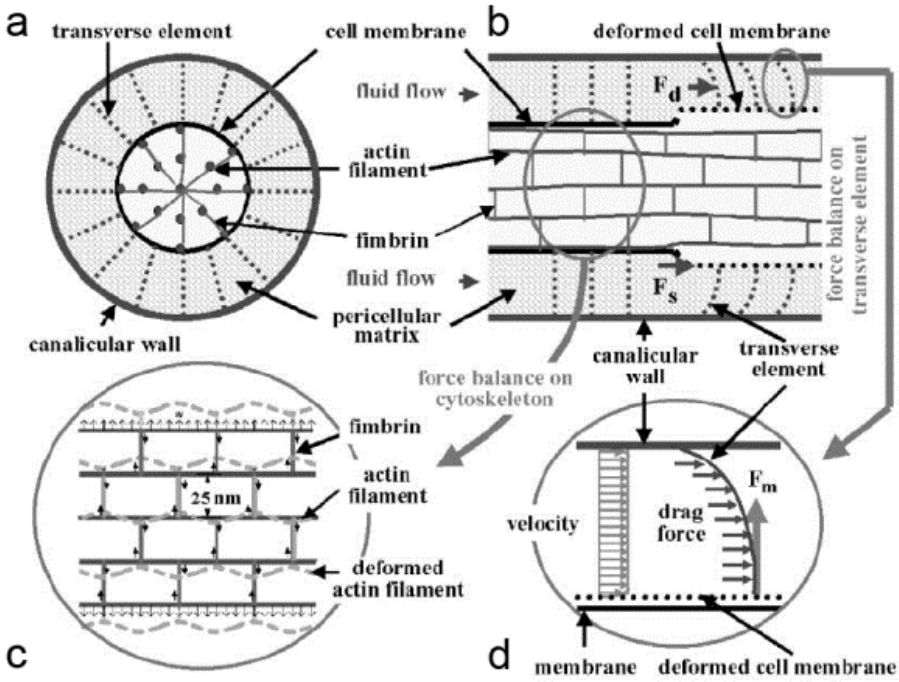

Figure 2 Idealized model of cellular level strain amplification

(a) Transverse cross-section of the osteocyte cell process showing the transverse tethering fibers spanning the pericelluar space between the canalicular wall and the cell process membrane. (b) Longitudinal cross-section showing deformation of the ultrastructures that surround the cell process in response to bone fluid flow through the pericellular space. (c) Illustration of the cytoskeletal organization in the longitudinal cross-section of the cell process used to determine the Young's modulus in the radial direction. (d) Force balance on a transverse element. Adapted with permission from You et al. (2001)

This amplification of force at the osteocyte cell process provided a relationship between whole tissue strain and cellular level strain, and implicated a possible mechanism by which whole tissue loading could achieve cellular strains > 1% found to be pertinent for cellular activation *in vitro*. Ultrastructural verification of geometries used in this theoretical model was performed using transmission electron microscopy (TEM) to determine structures implicated in mechanotransmission at the molecular level; however, the underlying molecular mechanisms sensing these forces are still not completely understood. The tethering elements were shown to traverse the pericellular space to provide a direct linkage to the cell process via CD44, laminin, and now more recently, $\alpha_v\beta_3$ integrin (McNamara et al., 2009; Miyauchi et al., 2006; Wang et al., 2007).

A heightened appreciation for the relationship between the tethering filaments and the cytoskeleton of the cell process as well as the structural make-up of the cell process inspired the next ultrastructural model. In this model, the osteocyte cell processes contain an actin filament bundle with fimbrin cross-links shown in a scanning electron micrograph (SEM) of a primary osteocyte cell process in culture (Tanaka-Kamioka et al., 1998). The periodicity of fimbrin cross-linkages and the double-helical spiral of cross-filaments that are found in the stereocilium (Tilney et al., 1983), was not previously realized in osteocyte cell processes and idealized in **Figure 3.** The actin filament bundle provided a structural rigidity of the cell process that was predicted to be 600 times larger than that of the cell body (Han et al., 2004). Peripheral regions of osteocytes in culture had a significantly higher elastic modulus than nuclear regions demonstrated by experimental nanoindentation (Sugawara et al., 2008). A rigid structure would exhibit superior force transmission than a compliant body, suggesting the cell process to be the likely candidate involved in mechanotransmission. Inclusion of these ultrastructural details led to hoop strain predictions that were smaller by a factor of 3 compared to previous predictions in (You et al., 2001). However, cell process strains produced were still large enough in magnitude to elicit cellular responses from whole tissue loads > 5 MPa at a 10 Hz loading frequency (whole tissue strains > 250 με), see **Figure 4**. Also, the fluid drag force per unit length of the osteocyte cell process is predicted to be around 20 times larger than the fluid shear forces per unit length of the osteocyte cell process (You et al 2001). This indicated that fluid-induced drag forces on the GAG side chains that are transmitted to the tethering fibers were dominant excitation forces *in vivo*. Punctate staining of mechanosensitive molecules such as β_3 integrin along the

cell process *in vivo* (McNamara et al., 2009) supports the notion that osteocyte cell processes have integrin attachment sites along its length and are mechanosensitive regions of the cell. T-type voltage sensitive calcium channels have been shown to be more prominent on the osteocyte cell process than on the cell body (Shao et al., 2005), and could be a cell signaling mechanism located at cell processes that mediates calcium wave potentiation in the cell network.

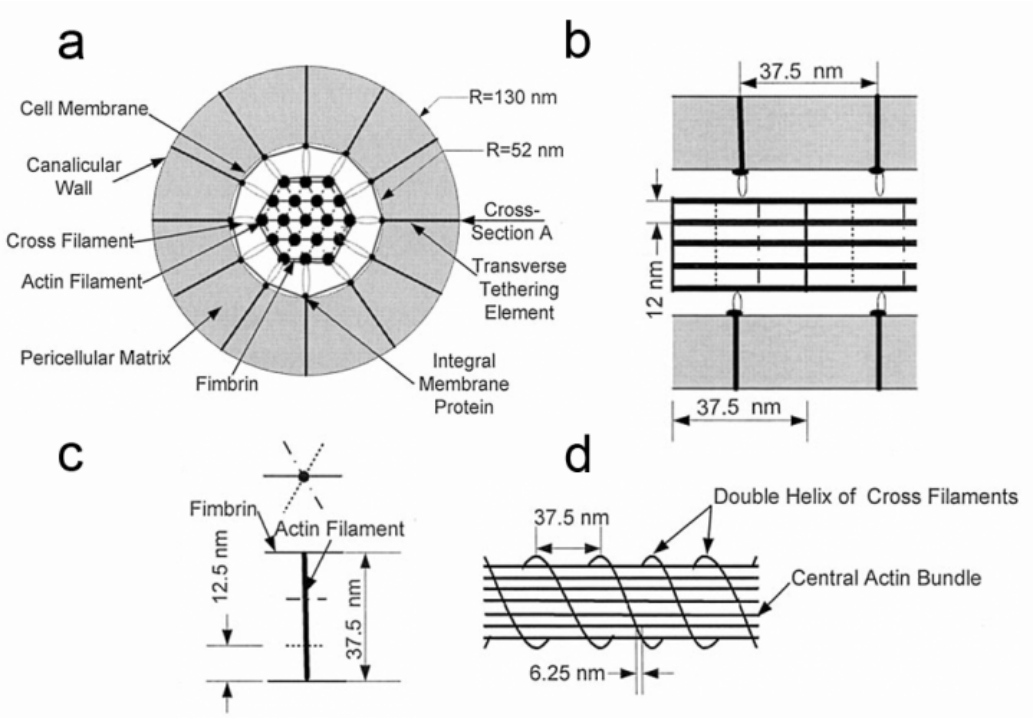

Figure 3 Idealized ultrastructure of the osteocyte cell process and its attachment to the canalicular wall

(a) Transverse and (b) longitudinal cross-section of the cell process where the actin filament bundle is comprised of a hexagonal array of actin filaments bundled by (c) periodic fimbrin cross-linkages and bound by a (d) spiraling double-helical coil of cross-filaments around the actin filament bundle. Adapted with permission from Han et al. (2004)

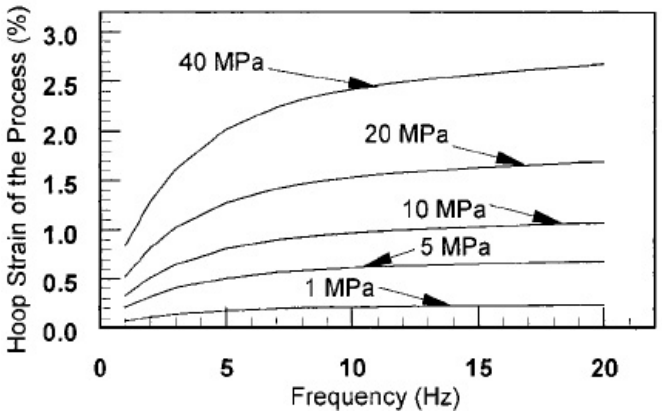

Figure 4 Hoop strains of the osteocyte cell process plotted as a function of whole bone tissue loading frequency and amplitude.

Adapted with permission from Han et al. (2004)

A new geometry found in TEM micrographs of longitudinal cross-sections of the osteocyte cell process from whole tissue (McNamara et al., 2009) (**Fig. 5**), inspired the adapted cellular strain amplification model that predicted load-induced forces at these canalicular projections (Wang et al., 2007) (**Fig. 6**).

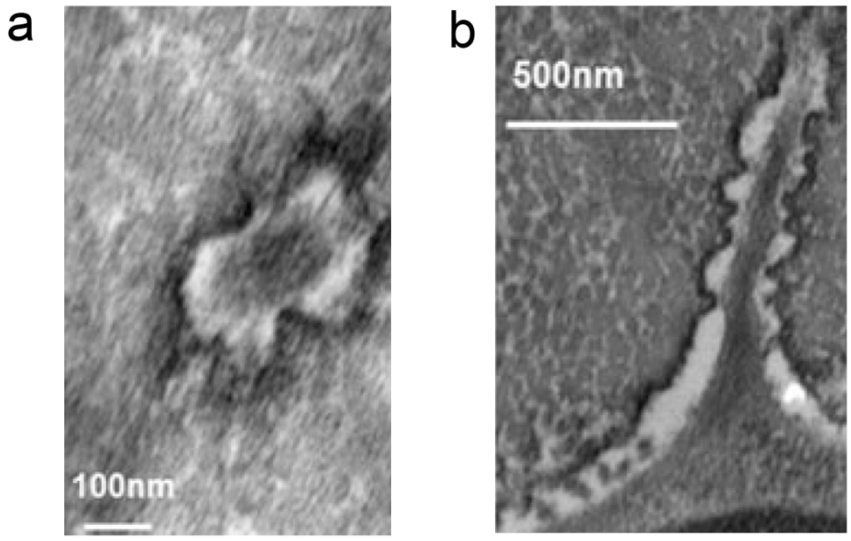

Figure 5 Transmission Electron Micrographs of osteocyte cell processes

(a) Cross-section of cell process within its canaliculi to show canalicular protuberances (b) Discrete collagen protuberances emanating from the canalicular wall traverse the pericellular space toward the cell process membrane

and occur in a periodic manner. Adapted with permission from McNamara et al. (2009)

Discrete collagen protuberances emanating from the canalicular wall to traverse the pericellular space toward the cell process membrane were observed to occur in a periodic manner (**Fig. 5b**). New predictions of the cellular strain amplification model with the new geometry calculated tensile forces < 15 pN to occur at interfaces between discrete conical protuberances and the canalicular wall. This model demonstrated that the axial strains produced in the vicinity of rigid attachment sites were 10 times larger than radial strains previously predicted in the cellular-level strain amplification model in Han et al. (2004). High stress concentrations are produced at these discrete regions of attachment and are implicated as additional and effective mechanisms to further amplify strains created by load induced fluid-flow in the LCS. Whole tissue strains necessary to produce adhesion-mediated axial strains up to 6% at the apex of the protrusion were 1-2 orders larger in magnitude, and in agreement with experimentally measured whole tissue strains *in vivo*. Physiological tensile forces produced at those focal attachment sites were in the range of 1-10 pN, and were largely below the force range shown to rupture $\alpha_v\beta_3$ integrin attachments (Litvinov et al., 2003). These predictions suggested that osteocytes in bone would be stimulated at whole tissue strains between 0.04-0.3% and also at lower-magnitude high-frequency loading, to explain how persistent high frequency (10 - 50 Hz)-low amplitude postural strains < 5 με due to muscular contractions would suffice in maintaining bone mass and influencing the microarchitecture of bone (Rubin et al., 2002).

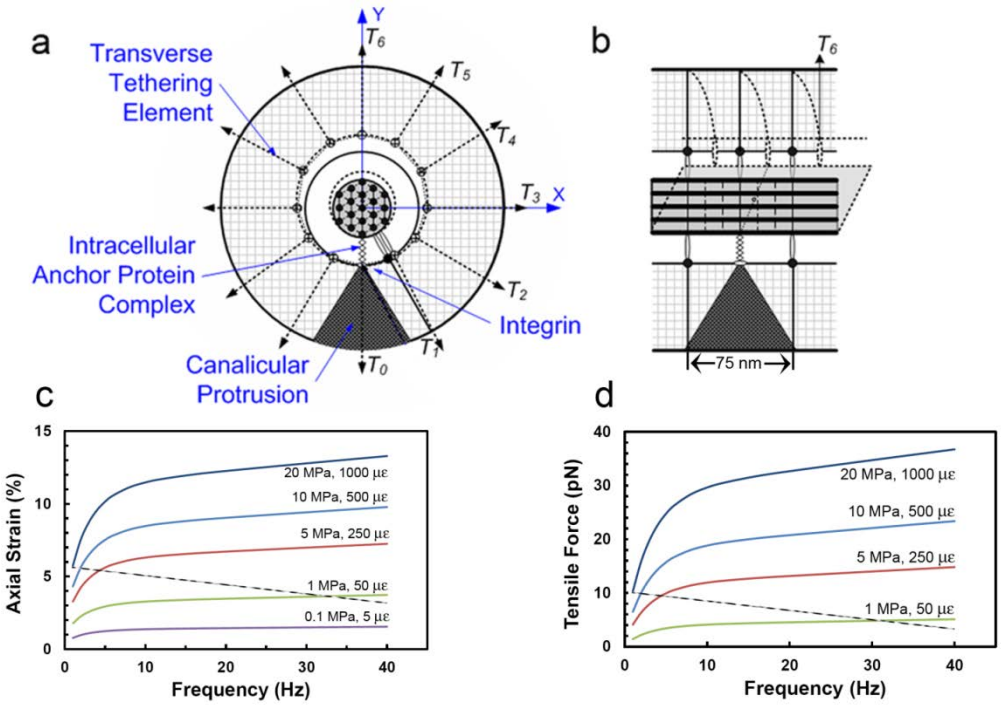

Figure 6 Deformation diagrams near a canalicular projection and its strain and force predictions from the idealized mathematical model.

As bone fluid flow travels through the pericellular matrix in the LCS and around the canalicular projections, cell process deformations are produced at focal attachment sites at the apex of canalicular projections that intermittently appear throughout the length of osteocyte canaliculi. Deformation diagrams of the cell process are shown in the (a) transverse cross-section to illustrate location of transverse tethering elements and focal attachment site and in the (b) longitudinal cross-section to illustrate deformation of tethering elements and sliding of the actin filament bundle centered in the cell process. (c) Axial strain and (d) tensile force predictions in the vicinity of the attachment site are shown as a function of loading frequency and amplitude where the area under the dashed line represents physiological loading measured by Fritton et al. (2000). Axial strains up to 6% are achieved under physiological loading conditions and are on the same order as strains required to elicit a cellular response in culture. Tensile forces in the range of 1-10 pN are predicted to occur from local axial strains around the attachment

site and are now believed to be the dominant source of cellular excitation *in vivo*. Axial strains predicted in this model were an order of magnitude larger than axial strains previously predicted in the absence of canalicular protrusions. Adapted with permission from Wang et al. (2007)

It has become increasingly evident that mechanical loading events in bone are an integral part of bone mechanotransduction that influences whole tissue architecture, and mediates the orchestration of other cellular mechanisms within the skeletal system. Cellular level computational and theoretical models are used to analyze what cannot be experimentally measured, and have been instrumental in relating whole tissue loads to cellular level strains. They have predicted forces within the bone microenvironment that have proven to be vastly different than what may be measured at the tissue level, and have elegantly addressed the major paradox in bone mechanobiology. It is widely believed that the orchestration of communicating bone cells has localized influence on the microarchitecture of bone and subsequently whole bone tissue. The elucidation of cellular level communication between bone cells to influence bone formation and resorption focused mainly on osteoblast and osteoclast activity because of their established role in bone matrix deposition and degradation. Osteocytes more recently were recognized to greatly contribute to the metabolic interplay between bone cells because they are mechanosensitive and release osteogenic metabolites and numerous intercellular signals when mechanically stretched or strained. Theoretical models that have focused on identifying the strains and forces imposed on the osteocyte cell processes *in vivo* and have illustrated the microenvironment of the osteocyte to be highly stimulatory. Stimulation of osteocytes even at low-magnitude high-frequency whole tissue loading would likely mediate intercellular signaling pathways among all cells networks distributed throughout the bone tissue during daily physiological activity. Although osteocytes have experimentally demonstrated high sensitivity to strains theoretically predicted in the LCS, the amplification of these strains to stimulate osteocytes *in vivo* are dependent upon the microarchitecture of the LCS in native bone tissue the subsequent load-induced interstitial fluid-flow in the pericellular space.

In summary, the series of theoretical models in this section have elegantly described the relationship between whole tissue strains and cellular level strains *in vivo.* Predicted amplified strains in the LCS that

incorporated mechanotransduction mechanisms discovered through ultrastructural analysis were on the same order of strains that were necessary to initiate intracellular signaling responses in bone cells *in vitro* (Owan et al., 1997; Smalt et al., 1997; You et al., 2000). These cellular level strain amplification models have addressed the long standing paradox in bone with predictions that are 10-100 times larger than measured whole tissue level strains of 0.04-0.3% produced by physiological ambulation and activity (Fritton et al., 2000; Rubin and Lanyon, 1984). Mechanotransduction mechanisms implicated in mediating the strain amplification in the LCS and potentiation of signals by the osteocyte include adhesion-mediated mechanosensitive complexes, non-junctional hemi-channels, mechanosensitive ion channels, and ligand-gated purinergic P2 receptors. These mechanisms and the intercellular signaling which they mediate will be described in more detail in Chapter 3 and 4.

1.2. Mechanosensation

Molecular components of a cell that resist external forces and undergo conformational changes resulting in signal transduction in response to a mechanical force are considered mechanosensitive. Conformational changes of a mechanosensor would initiate a cellular response and give the cell its capacity to respond to its extracellular environment. Investigated mechanosensers expressed in osteocytes that resist forces within the pericellular space of the LCS include integrins (Litzenberger et al., 2010; Miyauchi et al., 2006), mechanosensitive ion-channels (Rawlinson et al., 1996; Zaman et al., 1999), hemichannel complexes (Cherian et al., 2005; Genetos et al., 2007), adhesion complexes (Pavalko et al., 2003b), and primary cilia (Malone et al., 2007; Whitfield, 2003). Other ligand-activated mechanisms found in osteocytes, for example purinergic receptors (Ke et al., 2003; Li et al., 2005; Orriss et al., 2010) and hormone receptors (Gu et al., 2001b; Kimmel et al., 2011; Miyauchi et al., 2000), are often associated with mechanosensor-activation that induces “transmembrane mobilization” of signaling molecules. The activation of receptors by these signaling molecules would also mediate numerous signaling cascades of other molecular interactions to regulate cell function. Calcium signaling (Miyauchi et al., 2006), cellular (adenosine-5’- triphosphate) ATP release, and PGE_2 release (Reilly et al., 2003) in bone cells are examples of mechanoresponses and discussed in more detail in Section 1.3. Altered mechanotransmission of force to the cell, i.e. lack of force transmission via compromised cellular

attachments or unloaded bone tissue, may also have influence on bone tissue metabolism which can be observed at the tissue level (Jee et al., 1992; Phillips et al., 2008). Removal of expression of mechanosensitive mechanisms with the use of transgenic integrin knock-out (KO) animal models (Litzenberger et al., 2009) or removal of mechanical loading (Aguirre et al., 2006), yielded tissue-level consequences that obviated the role of mechanosensation mediated by cellular attachment as well as the transmission of forces at the cellular-level. Also, alteration of mechanosensitive mechanisms by using antibodies/peptides in culture under variable FSS/strain conditions yielded morphological and transcriptional changes in osteocytes (Kawata and Mikuni-Takagaki, 1998). The ability for cells to sense changes in their mechanically and metabolically dynamic environment is critical for the maintenance of the bone cell network and their local microenvironment. Key mechanosensitive mechanisms found in osteocytes and MLO-Y4 cells are now briefly reviewed.

1.2.1. Integrins

Cells are decorated with cell membrane spanning surface receptors called integrins that specifically link the cell cytoskeleton located inside the cell to extracellular matrix proteins located outside the cell. Integrins are associated with cytoskeletal structures and signaling proteins and serve as important sites of attachment between the cell and its extracellular matrix (ECM) (Burridge and Chrzanowska-Wodnicka, 1996) to mediate mechanotransduction (Hynes, 2002). Furthermore, integrins are composed of transmembrane heterodimers that have a non-covalently bonded α- and β- subunit pair that link the integrins to the cytoskeleton directly by focal adhesion kinase (FAK), talin, vinculin, and paxillin (Alenghat and Ingber, 2002) as well as adaptor proteins p130Cas and Crk that also act as molecular signaling scaffolds to bring kinases and substrates together (Wozniak et al., 2004). Changes in the macromolecular scaffold of the cell coupled to its extracellular environment through integrins facilitated alterations and phosphorylation of numerous proteins within the cell (Ingber, 1997) to mediate proliferation (Folkman and Moscona, 1978; Gershey and Alisa, 1980; Ingber and Folkman, 1987; Stoker, 1970), migration (Keely et al., 1997), differentiation (Menko and Boettiger, 1987), gene expression (Bissell et al., 2002; Emerman and Pitelka, 1977; Haskill et al., 1988; Li et al., 1987; Werb et al., 1989), protein synthesis, and apoptosis (Plotkin et al., 2005).

At least 24 known integrin subunits have been identified and sequenced, providing numerous combinations for attachment to various ECM proteins (Globus, 2007). Many of these ECM proteins have the RGD sequence recognized by the α_v integrin subunit that can bind to five different β chains (De Arcangelis and Georges-Labouesse, 2000). Two particular β integrin subunits, β_1 and β_3, are expressed in osteocytes *in vivo* (Bennett et al., 2001; Hughes et al., 1993; McNamara et al., 2009), and have been shown to play an important role in mechanotransduction for bone remodeling. The $\alpha_v\beta_3$ heterodimer is linked to substrate molecules particularly fibronectin (FN), osteopontin (OPN), bone sialoprotein, and vitronectin (VTN). ECM proteins found in bone: FN, OPN, bone sialoprotein, VTN, and laminin (Ross et al., 1993; Saito et al., 1994), serve as substrates for integrin binding.

The ECM surrounding osteocytes in the lacunar-canalicular space is comprised of ECM proteins that bind to β_1 integrin (Gohel et al., 1995; Hughes et al., 1993) and β_3 integrin (Bennett et al., 2001; McNamara et al., 2009). The distribution of these integrin subunits was distinct, i.e. α_v integrin subunits were homogeneously expressed on osteoblasts but heterogeneously expressed on osteocytes (Hughes et al., 1993), and ECM composition surrounding the osteocytes could be inferred by particular receptor-ligand interactions or vice versa. Gohel et al. (1995) used immunogold-labeling to locate β_1 integrin at the plasma membrane of bone cells and found β_1 integrin expression on osteocyte cell bodies. Again notable was the abundant β_1 integrin expression found on osteoblast cell bodies, but less frequent expression along its specialized cytoplasmic processes near the mineralizing front containing collagen fibrils. McNamara et al. (2009) reported that osteocytes express β_3 integrin only along osteocyte cell processes and the periodicity of the β_3 integrin expression was in good agreement with the frequency at which protrusions of the canalicular wall spanned the cellular space toward the cell process. Furthermore, it has been suggested that $\alpha_v\beta_3$ forms in the absence of β_1 integrin (Wennerberg et al., 1996). In light of these findings, it is strongly suggested that integrin mediated mechanotransduction is, at least in part, initiated by β_3 integrins at osteocyte cell processes.

Integrin signaling is dependent on the conformational state of integrin heterodimers. Integrins in the active-state or extended form have exposed epitopes for activation, visualized in high-magnification EM images (Takagi et al., 2002), and integrins in the inactive- or bent-state have hidden epitopes and residues that do not bind to ligands (Beglova et al., 2002). The integrin must be in functional form to mediate

signaling, and mechanical loading of bone is largely implicated to induce these conformational changes in integrins and in numerous membrane bound signaling proteins in bone cells (Pavalko et al., 2003b).

Physiological consequences of integrin function have been evaluated using transgenic knock-out (KO) animal models where an integrin gene of interested is ablated and expression of that integrin chain in all tissues is removed. Ablation of the α_v integrin subunit gene caused embryonic lethality from impaired organogenesis, a consequence of the removal of 10 heterodimers which α_v may form, and validated the importance of α_v integrins particularly during development (Bader et al., 1998). Observed normalcy in skeletal development in α_v-null mice born, 20% of embryos, mitigated the importance of the α_v integrin subunit during bone tissue development; however, the exact regulatory role(s) of α_v integrin in bone maintenance and homeostasis after development is not fully realized, particularly for the $\alpha_v\beta_3$ integrin localized to the osteocyte cell processes (McNamara et al., 2009). A study using EGFP-tagged $\alpha_v\beta_3$ integrins within living cells discovered that de-novo integrin complexes could be formed independent of the actin cytoskeleton over the time course of only minutes (Cluzel et al., 2005). Mn^{2+} was used for effector activation that recruited talin and formed an adhesion complex in these cells, and mechanical activation of these heterodimers could induce a similar recruitment of talin to encourage integrin clustering independent of F-actin in osteocytes. Clustering was also demonstrated after F-actin disassembly with cytochalasin D prior to stimulation, but neither the affinity nor the strength of these particular adhesion complexes was explored. It is known that activated $\alpha_v\beta_3$ integrin rupture forces may rise to 100 pN where their peak rupture forces range between 40-50 pN. Non-stimulated $\alpha_v\beta_3$ integrins had a lower force threshold for rupture that never exceeded 35 pN. $\alpha_v\beta_3$ integrin adhesion complexes are found in osteocyte cell processes and are implicated to mediate the loose and firm cell process adhesion to the pericellular matrix where de-novo integrin clusters independent of the hexagonal actin flament bundle could form and adapt under the influence of bone fluid flow.

β_3 knock-out mice were not embryonic lethal, but contained 3.5-fold more osteoclasts than their heterozygote littermates and developed osteosclerosis (McHugh et al., 2000). The development of osteosclerosis was attributed to deficient matrix-derived resorption by β_3-deficient osteoclasts. The lack of β_3 integrin would suppress integrin-mediated signaling from osteocytes and also contribute to osteoclastogenesis, since osteocytes are widely implicated in the force-mediated suppression of

osteoclastogenesis (You et al., 2008). However, the requirement for osteoclast substrate-attachment to ensure cell survival (Sakai et al., 2000) further complicates osteoclastogenesis in β_3 knock-out mice and points to other mechanisms that would regulate this process. With respect to bone formation, $\alpha_v\beta_3$ integrins were found necessary for the enhancement of IGF-1 mRNA levels in osteocytes exposed to 2% strain using a deformable substrate where high levels of IGF-1 mRNA are associated with bone growth (Miyauchi et al., 2006). This enhancement of IGF-1 mRNA levels was abolished when osteocytes were treated with the $\alpha_v\beta_3$ integrin blocker, echistatin, and exposed to strain.

Another integrin subunit found in osteocytes is the β_1 integrin subunit that can associate with over 10 α integrin subunits. Ablation of the gene for the β_1 integrin subunit was embryonic lethal. To circumvent embryonic lethality in β_1 KO-mice and to investigate consequences of mechanical loading in β_1-null animals, conditional KO mice were developed using a Cre-lox system that targeted deletion in cells of the osteoblastic lineage. In these β_1-null mice, β_1 integrins mediated load-induced cortical bone formation at the tissue-level (Litzenberger et al., 2009; Phillips et al., 2008), and mediated the upregulation of COX-2 and subsequent release of PGE_2 as well as the downregulation of RANKL and OPG at the cellular–level in cultured osteocytes in response to oscillatory flow (Litzenberger et al., 2010). These cellular-level responses were associated with whole-tissue responses where there was an increase in number and activity of osteoblasts and osteoclasts. β_1 integrins had a clear role in bone formation and metabolic regulation of osteocytes in the presence of whole tissue mechanical loads.

Different classes of cellular adhesion have been described and distinguished by their associated proteins and function. Focal complexes are distinct from focal adhesions in that they also contain vinculin, paxillin, and focal adhesion kinase (FAK), but are formed independently from rho family of GTP-binding proteins that regulate actin filament organization (Nobes and Hall, 1995; Small et al., 1998). Focal complexes can further recruit integrins and linker proteins to grow into micron sized focal adhesions and the recruitment is facilitated by members of the rho family of GTPases. This recruitment is force-mediated for adhesions greater than 1 μm^2; however, a correlation between force and focal adhesion was not apparent for adhesion complexes < 1μm^2 (Tan et al., 2003). Smaller adhesion complexes generated greater traction forces than larger focal adhesions that contain numerous associated integrins and signaling molecules (Beningo et al., 2001). These focal complexes are likely the attachments that

are found in the canaliculi that attach the osteocyte cell process membrane to the canalicular wall.

The osteocyte cell processes in whole tissue measure ~ 80 nm in diameter (You et al., 2004) and are intermittently approached by collagen protrusions emanating from the canalicular wall (McNamara et al., 2009). Adhesion complexes associated with the apex of the canalicular protrusions and the cell process membrane likely contain $\alpha_v\beta_3$ integrins (McNamara et al., 2009). $\alpha_v\beta_3$ integrins have contributed to the stability in adhesion complexes, particularly when associated with talin, but not to the adhesion strength (Roca-Cusachs et al., 2009). Distinct mechanical contributions of different integrin heterodimers expressed on the surface of cells would be advantageous in that certain linkages would provide weaker bonds to focally facilitate mechanotransduction and others could provide strength to focally transmit extracellular forces to the cytoskeleton of the cell, see **Figure 7**.

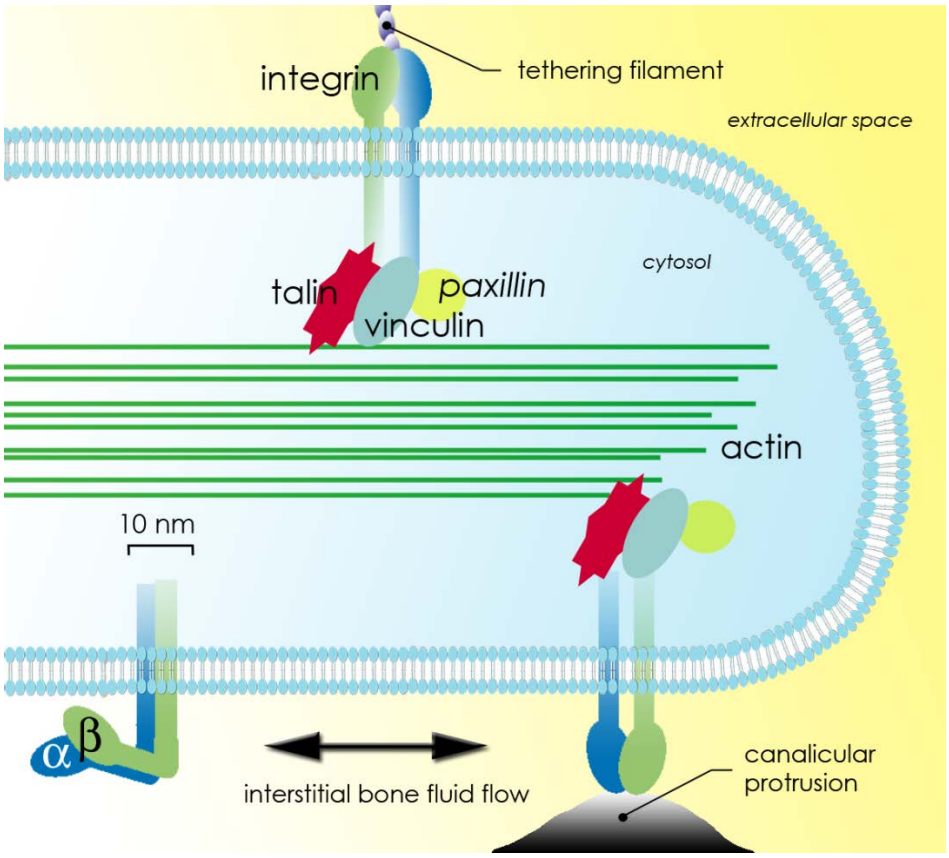

Figure 7 Adhesion complexes in osteocyte cell processes

Adhesion complexes are mediated by active transmembrane spanning integrin heterodimers that connect the extracellular matrix to cytoskeletal structures inside the cell. The ECM in bone is comprised of fibronectin, collagen, bone

sialoprotein, vitronectin, osteopontin and laminin that serve as ligands for several integrin heterodimers. Integrins transfer mechanical forces in the extracellular space to cytoskeletal structures and associated signaling proteins. Force-mediated integrin activation initiates cellular signaling pathways for cell function and intercellular signaling.

It is established that integrins are essential in mechanical coupling of the cell cytoskeleton with the extracellular environment to mediate cell function and intercellular signaling in a cell network. Integrins initiated mechanoresponses such as the mobilization of cations, nucleotides, and other chemical messengers into the extracellular space through mechanisms that will be discussed in detail in Section 1.3. A lack of integrin mediated survival signals can induce apoptosis, a process called anoikis (Stupack et al., 2001), and occurs in osteocytes induced by glucocorticoids (Plotkin et al., 2007). Characterization of various adhesion mechanisms in osteocytes is important for understanding the initiation and mediation of cell signaling in bone that is responsible for cell survival (Pavalko et al., 2003a; Plotkin et al., 2005; Sakai et al., 2000), formation (Chyun and Raisz, 1984; Keller et al., 1993), resorption (Cardoso et al., 2009; Dietrich et al., 1975) and maintenance (Baylink et al., 1996; Genetos et al., 2007; Lau et al., 2010).

1.2.2. Mechanosensitive channels and stretch-activated channels

All plasmalemmal channels are not gated by the same stimulus. Channels can be activated by chemical, mechanical, and electrical stimuli. Stretch-activated ion-channels are mechanically linked to the cell membrane and opened by membrane stretch (Guharay and Sachs, 1984). The gating of these cation-selective channels depends on the amount of stretch applied to the membrane.

Three species of mechanosensitive channels have been discovered based on their activation properties, kinetic characteristics, and ion selectivity: MscL, MscS, and MscM (Morris, 1990), and have pharmacologically been explored in osteocytes in the presence of membrane stretch. In these studies, membrane stretch was provided by either a mechanical loading device for whole-tissue, a deformable substrate on which a population cells are seeded, or suction from a micropipette on the cell membrane. Gadolinium chloride was used to block mechanosensitive-cation channels in rat bone explants, and

abolished load-induced PGE_2, PGI_2 and NO release from osteocytes (Rawlinson et al., 1996). It also abolished the increase of cytosolic calcium concentrations induced by osmotic swelling of osteocytes over a time course of 3 min, where Ca^{2+} increases were predominantly seen in regions along the cell process (Miyauchi et al., 2000). Cellular buffering of calcium would also activate non-mechanosensitive Ca^{2+}-activated K^+ channels, as well as other Ca^{2+}-activatable channels to assist in calcium wave propagation in the bone cell network.

Mechanosensitive channels have been studied in osteoblasts by membrane aspiration using a glass micropipette. Gating of non-selective cation channels with conductances between 15-50 pS was initiated by membrane stretch in osteoblastic cells (Charras et al., 2004; Davidson et al., 1990; Duncan, RL and Misler, S, 1989). Charras et al. (2004) found that an average negative pressure of 8.9 kPa or 9800 $pN/\mu m^2$ was needed to obtain the first mechanosensitive channel opening. This pressure yielded a membrane extension that was 23 μm in height and imposed a membrane strain of 800% at the apex of the bleb. These membrane strains far exceeded any strains in bone that are osteogenic at the physiological level, and pointed to other membrane associated mechanisms that would provide osteogenic signals which did not require membrane tensions of 500 pN/μm for activation. However, Duncan, R and Misler, S (1989) observed mechanosensitive non-selective cation channels using up to 2 kPa of suction on osteoblatoma UMR-106 cells. These strains far exceed strains used in culture experiments to mimic physiological conditions for mechanosensistive osteoblasts and especially osteocytes.

Integrin-mediated responses and stretch-activated channel responses from osteocytes do overlap at times, and to distinguish which activated mechanosensitive mechanism produced a specific response is difficult. It is clear that mechanotransduction is mediated by integrins and plasmalemmal channels, and evidence of integrins and ion channels working together in a complex is compelling in the case of the osteocyte. The mature osteocyte embedded in the mineralized bone matrix is not highly motile nor found readily navigating the LCS, and would not require large focal adhesions needed for migratory processes as do osteoblasts or osteoclasts. Osteocytes likely form less permanent adhesions that do not require a large amount of signaling and scaffolding proteins to be trafficked throughout the cell processes during the mediation of adhesion formation and disassembly. Therefore, suggested mechanisms that mediate intercellular signaling initiated at cell process attachments are integrin and ligand mediated mechanisms

that are activated by pN level forces induced at these attachment sites by the bone fluid flow.

1.3. Mechanoresponse

Mechanoresponses within bone are not limited to those highlighted in this chapter, and chosen because of their contributions to direct and indirect intercellular signaling between bone cells that are mediated by force. It is difficult to categorize mechanoresponses of cells because they can use similar cellular machinery for different signals. Although this would provide the cells with a level of efficiency for intercellular communication, revealing signaling specificity in osteocytes has been a major goal in the field.

Cellular mechanisms involved in the transmission of mechanoresponses to neighboring MLO-Y4 cells are also discussed throughout this section. These mechanisms facilitate the release of calcium, prostaglandin (PGE_2), nitric oxide (NO), and nucleotides, and are evidenced in the mediation of mechanically-induced autocrine/paracrine signaling in osteocytes. Mechanical loading also facilitated receptor signaling and induced transcriptional regulation in bone cells (Robling et al., 2008; Sawakami et al., 2006), but is beyond the scope of the faster force-mediated intercellular mechanoresponses and will not be discussed in detail.

Direct and indirect intercellular signaling in osteocytes is mediated by numerous mechanisms including membrane bound non-selective ion-channels, purinergic P2 receptors, and gap junction proteins. These mechanisms are not all mechanosensitive, but are involved in the fast-acting autocrine and paracrine responses that last for a few seconds to a few minutes. Fast-acting responses to mechanical strain, i.e. ATP-release and calcium mobilization into the cell from extracellular space, initiate regulatory cascades and potentiate intercellular signals throughout the bone network. The mobilization of calcium, ATP, and PGE_2 during indirect intercellular signaling in bone and osteocytes as well as the direct intercellular signaling in bone mediated by gap junctions will now be detailed below.

.

1.3.1. Calcium signaling

Calcium exists in blood in three different forms: protein bound, complexed, and ionized. In humans, the plasma and interstitial fluids have a cumulative calcium ion concentration of 1.2 mM, and the other 50% of the calcium in blood is ionized and diffusible through the capillary membrane (Guyton and Hall, 2006).

Calcium in the ionized form is important for cellular functions in the circulatory, nervous and particularly the skeletal system. Calcium concentrations in the medullary cavity of sheep were measured using implanted ultrafiltrate membrane probes, and the measured calcium concentration in plasma was 4.4 mg/dL or 1.1 mM of which 3.2 mg/dL or 0.8 mM was ionized and available and diffusible to mediate bone metabolism (Janle and Sojka, 2001). Direct measurement of ionized calcium concentrations in bone collected from the medullary cavity measured 1.7 mg/dL or 0.4 mM in sheep. Calcium concentrations in the local microenvironment of bone have been calculated using computer simulations and microelectrodes. Calcium concentrations predicted in the bone fluid in humans is 0.6 mM where the normal concentration of ionized calcium in plasma is 1.2 mM (Járos et al., 1980). Extracellular calcium concentrations in the microenvironment of osteoporotic bone measured up to 40 mM in the erosion sites with a pH of 4.7 where the average pH recorded was 6.01 (Silver et al., 1988). Extracellular calcium concentrations up to 76 mM have also been reported. Changes in the concentration of extracellular calcium are caused by exogenous stimulation by hormones (Gu et al., 2001b), autocrine substances (Zeng et al., 2008), neurotransmitters, or mechanical deformations (Adachi et al., 2009a). Mechanical stimuli, such as fluid flow or cell-substrate stretch, can induce intercellular calcium responses in bone cells (Huo et al., 2008; Rubin et al., 2006) which can be further enhanced by parathyroid hormone (PTH) (Miyauchi et al., 2000; Ryder and Duncan, 2001). It has been shown that calcium responses can propagate between neighboring bone cells via an intercellular calcium wave (Guo et al., 2006; Yellowley et al., 1998) mediated by inositol trisphosphate (IP_3)-triggered cytosolic calcium release. IP_3 production via phospholipase C (PLC) is diffused through the cytoplasm and through gap junctions between neighboring cells (Brophy et al., 1993; Kuroda et al., 2008) to bind to IP_3 receptors on the endoplasmic reticulum (ER) to induce a Ca^{2+} release that can also trigger calcium-induced-calcium-release signaling cascades. Calcium wave propagation in certain cells and under certain conditions can also occur in the presence of gap junctional blockers (Huo et al., 2008), being mediated by the P2Yreceptor/IP_3 signaling pathway (Jørgensen et al., 2002; Suadicani et al., 2003; Zeng et al., 2008).

Calcium signaling is essential for bone metabolism and for numerous bone cell functions including proliferation and differentiation. Ca^{2+} influx regulates transforming growth factor-β (TGF-β) (Sakai et al., 1998), activating protein kinase A (PKA) signaling pathways for the downstream anabolic responses such

as production of IGF-1 and osteocalcin (Miyauchi et al., 2000) for cytoskeletal reorganization. Calcium is also involved in regulating PGE_2 (Ajubi et al., 1996; Cheng et al., 2001a; Huo et al., 2008) with an intact glycocalyx (Reilly et al., 2003), as well as PTH-stimulated production of the inducible prostaglandin synthesis enzyme, cyclooxygenase-2 (COX-2) (Bakker et al., 2003; Huang et al., 2010). Calcium activation and release differs in each bone cell type, and to identify those mechanisms involved and associated responses should aid in deciphering bone cell metabolism and how they communicate with one another to influence their local microenvironment.

A mechanosensitive channel activated by physical strain with prospects for initiating bone remodeling was discovered using the patch-clamp technique (Duncan and Hruska, 1994). In this study, effects of chronic, intermittent strain on mechanosensitive-cation channels in osteoblast-like osteosarcoma cells (UMR-106.01) suggested that cyclic strain reduced the activation threshold of stretch-activated cation channel activity in strained cells. Also, whole-cell conductance was markedly increased in response to further mechanical strain. How these mechanisms are utilized in bone cells *in vivo* remain debatable particularly when complexed with other mechanosensitive machinery.

It has been hypothesized that load-induced deformation of the bone cell membrane opens the stretch-activated cation channel (SACC) (Pavalko et al., 2003b). Membrane stretch induced conformational changes in the SACC followed by an immediate influx of Ca^{2+} through the channel that increased cytosolic calcium via release of internal stores. This mobilization of Ca^{2+} initiated numerous kinase cascades converting the membrane force into a biochemical signal. In an immunocytochemical study localizing the expression of Ca^{2+} channels on bone cells, distribution in channel expression differed along the cell process from that of the cell body (Shao et al., 2005). Expression of T-type and L-type voltage sensitive Ca^{2+} channels were observed in osteoblasts and osteocytes; however, lower levels of L-type subunits were present on the osteocyte with primarily T-type subunit expression along osteocyte cell processes. Osteocyte cell processes are also shown to be sensitive to PTH-potentiated Ca^{2+} influxes (Miyauchi et al., 2000). In addition to the VSCC, that significantly mediated Ca^{2+} influx in mechanically activated cells (Miyauchi et al., 2000; Ryder and Duncan, 2001), other mechanosensitive channel complexes including mechanosensitive Pannexin1 (Panx1) channels permeant to ATP in oocytes and likely most cell types (Bao et al., 2004a; Bao et al., 2004b; Barbe et al., 2006) and mechanosensitive

connexin ‘hemi-channels’ are also thought to be involved in ATP release and PGE_2 release in osteocytes (Bao et al., 2004b; Cherian et al., 2005). Although numerous studies indicate the presence of a mechanically sensitive ion channel in both osteocytes and osteoblasts (Kizer et al., 1997; Miyauchi et al., 2000; Ryder and Duncan, 2001), there is much left to be discovered in the bone cell channelome especially in the osteocyte.

1.3.2. Purinergic signaling & the Pannexin channel

Purinergic receptors known to mediate extracellular signaling arse classified into two groups: (1) P1 receptor are activated by adenosine and (2) P2 receptors are activated by nucleotides such as adenosine triphosphate (ATP), adenosine diphosphate (ADP), uridine triphosphate (UTP) and uridine diphosphate (UDP) (Burnstock and Kennedy, 1985). P2 receptors are further subdivided into P2X and P2Y which are ligand-gated ion channels and G-protein-coupled receptors, respectively. Currently seven P2X receptors and eight P2Y receptors have been identified, see the review by Orriss et al. (2010) for a larger spectrum of purinergic signaling in bone.

Homeostasis of cytoplasmic ATP levels of 2-5 μM has been shown to be mediated by local purinergic signaling in excitatory and nonexcitatory cells, especially following damage or necrosis, and osteoblasts have demonstrated this homeostasis when exposed to fluid shear stress (Genetos et al., 2005), hypoxia (Orriss et al., 2009), and vitamin D (Biswas and Zanello, 2009). In bone, expression of $P2X_7R$ has been reported in osteoblasts and osteoclasts, and are proposed to be involved in ERK1/2 activation (Liu et al., 2008), apoptosis regulation (Jørgensen et al., 2002; Li et al., 2005), intercellular communication (Jørgensen et al., 2002; Modderman et al., 1994), regulation of osteoclast formation and activity (Gartland et al., 2003; Korcok et al., 2004), PKCα translocation to basolateral membrane (Armstrong et al., 2009), cytoskeletal reorganization (Gardinier et al., 2009), and bone formation (Panupinthu et al., 2008; Panupinthu et al., 2007). P2 receptor expression in osteoblasts has also been shown to be strongly differentiation-dependent (Orriss et al., 2006). Expression of P2 receptors in osteocytes is not widely reported (Li et al., 2005), however, the $P2X_7R$ has been associated with fluid shear stress induced anabolic responses in osteoblasts (Reich and Frangos, 1991; Reich and Frangos, 1993; Reich et al., 1997; Reilly et al., 2003; Saunders et al., 2003; Thi et al., 2003; Thi et al., 2010a) and is likely that $P2X_7R$

also serves as a mechano-regulated signaling mechanism in osteocytes. ATP release from osteocyte-like cells in response to oscillating fluid flow was demonstrated (Alford et al., 2003; Genetos et al., 2007) and likely mediated by P2 receptor complexes. P2 receptors in osteoclasts are closely related to ATP-induced osteoclast apoptosis *in vitro* and hypothesized to contribute to increased fracture risk (Ohlendorff et al., 2007). However, $P2X_7$ deficient mice possess functional osteoclasts *in vivo* (Ke et al., 2003). The metabolic environment in bone is indeed regulated by P2 receptors; however, how osteocytes utilize P2 signaling is still loosely defined and has encouraged further exploration.

More recently, another group of proteins have been shown to form non-selective high-conductance channels permeable to ATP, called pannexins (Barbe et al., 2006; Scemes and Spray, 2012). The functional form of Panx1 is likely an unpaired hexamer in a single plasma membrane (Boassa et al., 2008), and performs similar tasks that 'hemi-channels' are suggested to mediate, i.e. ATP release through non-junctional channels caused by mechanical stimulation. Panx1 channels have followed a similar description and shown to be a mechanosensitive channel of large unitary conductance permeant to ATP and molecules up to 629 Da (Iglesias et al., 2009; Locovei et al., 2007) Panx1 is responsible for large voltage-dependent non-junctional membrane conductance. It is increasingly apparent that pannexins do not form direct intercellular channels, and that particularly Panx1 forms functional plasmalemmal channels that display properties similar to those that have been attributed to connexin hemichannels (Dahl and Locovei, 2006; Scemes et al., 2009; Spray et al., 2006). Pannexins were previously classified as gap junction proteins because of their significant but low (~20%) homology to gap junction proteins of invertebrates, innexins (Scemes et al., 2007).

These non-junctional plasmalemmal channel proteins have potential in mediating anabolic activity between bone cells and may also offer an alternative for the 'hemichannel' proposed to be involved in the release of PGE_2 in osteoblast-like and osteocyte-like cells (Burra et al., 2010; Cherian et al., 2008; Genetos et al., 2007). For example, integrin activation would mobilize ATP, a fast acting ligand that activates purinergic receptors (Bretschneider et al., 1995; Liu et al., 2008; Orriss et al., 2010) to further increase intracellular calcium (Jorgensen and Kroese, 1995), and repeated or prolonged activation of the $P2X_7R$ would recruit a non-selective pore permeable to molecules of 900 Da (Locovei et al., 2007) or possibly larger for osteocytes during bone maintenance which can drastically alter local pH and cationic

concentrations in the bone microenvironment.

.

1.3.4. Prostaglandins

The release of paracrine factors, such as prostaglandin E_2 (PGE_2) and prostacyclin (PGI_2) in response to bone tissue loading has been shown (Chyun and Raisz, 1984; Rodan et al., 1975) and has become a well-characterized signaling pathway required for mechanically induced bone formation. Many studies demonstrate a marked anabolic effect of PGE_2 treatment in bone of humans and animals showing increased bone formation in limbs and ribs (High, 1987; Keller et al., 1993; Li et al., 1990; Norrdin and Shih, 1988; Ringel et al., 1982), in metaphyseal and cortical mass (Jee et al., 1987; Ueno et al., 1985), and in trabecular bone (Jee et al., 1992; Mori et al., 1990), and also evaluated in cultured bone cells (Baylink et al., 1996). PGE_2 stimulation at nM concentrations induced cellular proliferation in human bone cells, but PGE_2 concentrations higher than 0.1 μM inhibited proliferation. The importance of prostaglandins in the mechanoregulation of bone is further emphasized by *in vivo* findings showing that mechanical loading-induced bone formation could be inhibited by the administration of cyclooxygenase inhibitors that block PG G/H synthase or cyclo-oxygenase (COX) (Forwood, 1996). COX-2 transcription is associated with PGE_2 production that is released from bone cells under mechanical stress (Ponik and Pavalko, 2004), and blockade of COX-2 eliminated mechanically induced bone formation (Forwood, 1996). However, more recent evidence suggested that COX-2 does not contribute to the mechanosensitivity of bone since no difference in bone formation between the two genotypes: COX-2 KO mice and control wild-type mice was found (Alam et al., 2005). Possible compensatory production of COX-1 derived PGs in the presence of COX-2 deficiency (Wang, H et al., 2004) might explain the lack of phenotypic change in the COX-2 KO mice.

More specifically, PGE_2 release is followed by increases in cyclic adenosine monophosphate (cAMP) production, DNA synthesis, and activation of cAMP/PKA and β-catenin signaling pathways to prevent osteocyte apoptosis (Kitase et al., 2010). Mechanisms for PGE_2 release are thought to include integrins (Ingber, 1991; Ponik et al., 2007), mechanosensitive cation channels (Klein-Nulend et al., 1995), and G protein-dependent pathways (Berthiaume and Frangos, 1992; Reich et al., 1997) to activate signaling pathways such as phospholipase C (PLC) (Brophy et al., 1993), and protein kinase C (PKC) (Reich and

Frangos, 1993). Disruption of the osteocyte actin cytoskeleton with cytochalasin B (Ajubi et al., 1996), degradation of the glycocalyx with hyaluronidase (Reilly et al., 2003), and blockage of cellular adhesion with RGDS peptides (Ponik and Pavalko, 2004) significantly diminished the fluid flow induced PGE_2 release to indicate PGE_2 release be mediated by a channel mechanism dependent on the cytoskeleton.

1.3.1. Gap Junctions

Gap junctions provide a direct pathway for intercellular communication between neighboring cells. Earliest observations of gap junctions occurred in the 1960s with the use of an electron microscope. Structural observations have shown that gap junctions are comprised of connexon units that span the plasma membrane of a cell. Each gap junction contains two docked connexons, one from each cell in the pair containing the gap junction. Each connexon contains six radially-arranged intramembrane connexin proteins that span the plasma membrane four times (M1-M4) forming two extracellular loops (E1, E2). Both amino and carboxyl termini (NT, CT) and a cytoplasmic loop (CL) of the connexin protein are found at the cytoplasmic side of the membrane. When two connexons dock, their connexin proteins form a hydrophilic channel that spans the two apposed plasma membranes including the 2-3 nm gap between the cells. Gap junction channel nomenclature was based on its species of origin and molecular mass in kDa deduced by the cloned DNA sequence (Beyer et al., 1987; Beyer et al., 1990; Bruzzone et al., 1996). Transmembrane and extracellular domains exhibited high homology across connexins determined by sequence analysis; however, the CL and CT domains are unique to each connexin (Bruzzone et al., 1996).

Hexagonal arrays of connexin proteins were discovered in synaptic membrane complexes (SMC) of the Mauthner cell in the goldfish brain fixed with potassium permaganate (Robertson, 1963), in plasma membranes in rat liver stained with potassium or sodium phosphotungstate (PTA) (Benedetti and Emmelot, 1965), and in tissue sections of mouse heart and liver after lanthanum salt treatment (Revel and Karnovsky, 1967). When adjacent cells merge, docking of pairs of adjacent connexons will form gap junction channels with the potential for passage of ions and small molecules from one cell to the next (Caspar et al., 1977; Goodenough and Revel, 1970). These hexagonally arranged elements on the plasma membrane were different from that of any other portion of the plasma membrane (Benedetti and Emmelot, 1968; Goodenough and Stoeckenius, 1972).

Apposing connexon proteins consistently exhibit a 2-3 nm gap space between their associated adjacent plasma membranes of 5-6 nm thickness (Revel and Karnovsky, 1967), and the average center-to-center spacing of the connexins within a plaque is generally in the range of 8-10 nm (Benedetti and Emmelot, 1965; Benedetti and Emmelot, 1968; Goodenough and Stoeckenius, 1972). Permeability of gap junctions were explored with injected dyes where molecules < 1 kDa would freely diffuse between cells coupled by gap junctions (Benedetti and Emmelot, 1968; Finbow and Pitts, 1981; Pitts and Simms, 1977). Non-selective permeability of the gap junction channel allowed passage of molecules < 1 kDa; however, for molecules > 1 kDa, permeability was more complex and in the presence of chemical gradients, these channels exhibited voltage sensitivity and ionic selectivity (Goodenough et al., 1996; Spray et al., 1979).

Cells that were electrically coupled were found to be joined by close membrane appositions (Bennett and Trinkaus, 1970) by gap junctions and were distinct from tight junctions (Revel and Karnovsky, 1967). Gap junctions provided a low resistance pathway for ionic movement between the cytoplasm of adjacent cells in invertebrates (Bennett, 1966; Gilula et al., 1970; Sheridan, 1968), and similarly allowed for the exchange of electrically charged ions and small metabolites in the form of second messengers, hormones, amino acid, and high energy compounds through channels that penetrate the plasma membranes of adjacent cells for bi-directional transport in vertebrates (Loewenstein, 1966). Ions and metabolites are used as building blocks to compose messages delivered as far as signals may propagate between adjacent cells and distant cells via cellular networks. Electrical coupling is of considerable importance in development in which the electrical pathways transmit substances between cells that act in the coordination of growth and differentiation. Connexin proteins exhibited dynamic behavior and their activity is determined by their phosphorylation state (Saez et al 1998). Trafficking, turnover, and degradation of connexin within the cell have been shown to be critical determinants of channel gating and intercellular communication, and alterations of these regulatory mechanisms of intercellular communication naturally occur during physiological and pathological circumstances (Mazet et al., 1985; Meyer et al., 1981; Traub et al., 1983).

Gap junctions have been found in numerous tissues such as heart (Duffy et al., 2006), liver (Spray et al., 1994), brain (Rozental et al., 2000), and bone (Doty, 1981). Electron micrographs of gap junctions

between bone cells (Doty, 1981; Marotti, 1996) has made electrical coupling a likely pathway for intercellular communication between adjacent osteoblasts and osteocytes throughout the hard mineralized matrix in bone. Increased interest developed surrounding junctional communication and propagation of signals in bone (Donahue, 2000; Steinberg et al., 1994; Yellowley et al., 2000) to explore how bone cells respond to mechanical strain and fluid shear (Rawlinson et al., 1996; Thi et al., 2003).

Cx43, Connexin45 (Cx45), and Connexin46 (Cx46) proteins are expressed in bone tissue and in cultured osteolasts (Bhattacharjee et al., 2009; Donahue et al., 1995; Geneau et al., 2010; Schirrmacher et al., 1998; Steinberg et al., 1994) and in osteocytes (Ishihara et al., 2008; Kato et al., 1997; Thi et al., 2003; Yellowley et al., 2000). Cx43 is abundantly expressed in osteocytes and provides a principal pathway for intercellular communication between junctionally connected osteocyte networks. Fluid flow studies on osteocytes are designed to mimic the microfluidic environment in bone to study Cx43 activity in intercellular communication between bone cells. Fluid flow between 30 minutes to 4 hours upregulated Cx43 protein, increased migration of Cx43 to the plasma membrane in MLO-Y4 cells, and increased coupling post-stress but without an increase in phosphorylated Cx43 levels (Cheng et al., 2001b). Another study showed both low and high fluid shear for 1 to 3 hours caused a translocation or an internalization of membrane bound Cx43 and Cx45 accompanied by a decrease in cellular communication through appositional membranes in both osteocyte-like MLO-Y4 (MLO-Y4) cells and osteoblast-like MCT3T-E1 (MCT3T-E1) cells (Thi et al., 2003). Both studies demonstrated translocation of Cx43 proteins and changes in mRNA levels in response to fluid flow, and more importantly both exhibited alterations in intercellular coupling in response to mechanical stimulation.

Connexons have also been hypothesized to perform as a mechanosensitive ‘hemi-channels’ that form non-junctional membrane pores thought to be involved in the release of paracrine acting messengers, such as ATP, in response to a mechanical stimulus (Bao et al., 2004b; Leybaert et al., 2003), and (Spray et al., 2006) has reviewed the connexin “hemichannel” in greater detail. Mechanical stimulation has been shown to induce PGE_2 and ATP release in response to fluid flow through Cx43 ‘hemichannels’ in osteoblasts and osteocytes (Cherian et al., 2008; Genetos et al., 2007). Burra et al. (2010) found that the opening of ‘hemi-channels’ is likely to be modulated by the association of Cx43 and α5 integrin. Other channels such as the $P2X_7$ receptor, the voltage dependent anion channel (VDAC), pannexin1 and

mechanosensitive channels are also reported to mediate chemical and electrical metabolites ascribed to 'hemi-channels' (Spray et al., 2006).

The role of connexins in bone development was largely evident in the Cx43-null mouse model that illustrated delayed ossification, craniofacial abnormalities, and osteoblast dysfunction in the absence of Cx43 (Lecanda et al., 2000). Cx43 was found important in skeletal development, and also in bone maintenance and remodeling. Gap junctions have been shown to be important for proper calcification *in vitro* (Thi et al., 2010b), and this gap junctional communication could be largely responsible for the essential coordinated participation of osteoblasts, osteocytes, and osteoclasts in bone homeostasis.

1.4. Summary

Whole bone tissue is influenced by the metabolic activity of bone cells within and on surfaces of cortical and trabecular bone matrix where osteoblasts, osteocytes, and osteoclasts greatly differ in cellular machinery and in response to the same stimulus. Cell proliferation, differentiation, cytoskeletal remodeling, protein synthesis, and signal propagation is mediated by various metabolic pathways initiated at the cellular level. Mechanoresponses, such as metabolic fluxes through the cell membrane, can be quantified and aided in elucidating mechanisms of mechanotransduction in bone cells. Further investigation of signaling machinery and the ultrastructure of the osteocyte, that is widely believed to be the mechanosensory cell in bone, will reveal possible signaling pathways used by the osteocyte during mechanotrasduction and its overall contribution to bone homeostasis at the molecular level.

Chapter 2: The Stokesian Fluid Stimulus Probe (SFSP)

2.1. Introduction

Osteocytes are implicated to be a major mechanotransducer in bone. How they sense forces in their microenvironment has been challenging to explore for a few reasons. Osteocytes are located within mineralized matrix and are difficult to access without compromising its native environment. Therefore cell culture techniques have been used on isolated osteocytes to mimic its dynamic microenvironment to better study osteocyte responses to flow, hydrostatic pressure, and stretch. However, *in vivo* forces exerted on osteocyte cell process predicted by theoretical models are different than that of the osteocyte cell body. A biophysical technique capable of preferential stimulation to mimic *in vivo* hydrodynamic forces in a culture system had not previously been developed.

It was necessary to develop a technique to preferentially stimulate specific regions of the osteocyte to address how an osteocyte may detect forces exerted on the cell in its native environment. The study of cellular polarity in the osteocyte-like MLO-Y4 cell was performed using a newly developed force probe called the Stokesian Fluid Stimulus Probe (SFSP). The SFSP, capable of focally and preferentially stimulating sub-cellular regions, stimulated the cell while cellular responses were recorded in real-time with the electrophysiology technique in the whole-cell voltage-clamp mode.

The novel SFSP was used to investigate mechanosensitive complexes in single cells using physiological forces. The SFSP was based on pressurized fluid delivery through fine pipettes, a methodology in routine use by pharmacologists for focal application of chemical messengers when studying single cell responses. The pressurized fluid used in the SFSP is not filled with pharmacological agonists or blockers, but with extracellular fluid to establish only a hydrodynamic simulation.

A drawback of other currently used force probe techniques, further detailed in Section 2.4.1., is that all require physical contact to deform membranes, and thus, may alter the system through this contact with a rigid body in a live single-cell experiment. Also, biophysical techniques previously used on bone cells, i.e. micropipettes for membrane depression, exert forces 1000 times larger than what is physiologically predicted to occur *in vivo* which do not produce physiologically relevant responses. They also do not target osteocyte adhesions sites which are widely implicated to be the site of mechanotransduction initiation.

Generally, micropipette ejection systems operate in a tip Reynolds number (Re_t) regime where a vortex-shedding axial jet is produced that breaks up into turbulence (Hanani, 1997). To produce not a jet, but a nearly spherical reproducible bolus, whose growth and pressure field can be theoretically predicted and experimentally measured, required operating in a much lower Re_t regime than, heretofore, examined. An initial series of experiments was performed with tracers ejected at low pressure from a micropipette with a 0.8 μm tip diameter to visualize the fluid bolus. However, diffusional blurring prevented clear demarcation of the edge of the growing bolus, and vastly improved results were obtained using a 1000 fold larger laboratory scale model employing hydrodynamic similarity. This laboratory scale model clearly demonstrated that a nearly spherical bolus, closely corresponding to Sampson flow through a circular orifice, could be achieved provided $Re_t < 0.03$, and that Sampson's solution could be used to describe the velocity and pressure field in the vicinity of the micropipette tip.

The SFSP has now enabled preferential stimulation of particular regions on a single cell. This new technique would assist in the detection of molecular mechanisms responsible for the initiation of osteocyte signaling. Immediate cellular responses are detected after stimulation with the SFSP, and the SFSP is used to identify the mechanosensitive regions of the osteocyte *in vitro*. Characterization of the SFSP is required to ensure that stimulation of the cell is physiological.

2.2. Materials and Methods

2.2.1. Solutions and Fluorophores

Lucifer yellow CH dilithium salt (Sigma-L0259, MW 457) or Dextran Conjugated Fluorescein (Molecular Probes-D1822, MW 70k) was used in the tracer experiments. Extracellular solution used to dilute fluorophores into the working solution was comprised of the following chemicals and concentrations [mM]: 140 NaCl., 2 CsCl, 2 $CaCl_2$, 1 $MgCl_2$, 5 HEPES, 4 KCL, 5 glucose, 2 Sodium Pyruvate, 1 $BaCl_2$; pH 7.4 using NaOH. The extracellular solution was filtered using a 0.22 μm pore size bottle top filter (Corning).

3.2.2. Tracer studies

An initial series of experiments was performed whereby Lucifer yellow CH dilithium salt (Sigma-L0259, MW 457) or Dextran Conjugated Fluorescein (Molecular Probes-D1822) labeled intracellular solution was ejected into unlabeled extracellular solution contained in a glass bottom culture dish (MatTek) from a micropipette (Single barrel filament borosilicate capillary glass, A-M Systems, Inc.) with a tip diameter of 0.8 μm and a back pressure controlled by a Picospritzer (Parker). Micropipettes are pulled with a P-97 Pipette Puller to achieve an initial tip resistance of 2-3 MΩ when filled with extracellular solution. Epi-fluorescent image sequences of spreading dye, Lucifer Yellow or Dextran Conjugated Fluorescein diluted in extracellular solution, were obtained using an epifluorescence microscope (Nikon) at an acquisition interval of 20 or 50 ms during SFSP application at 20 psi for 100 ms.

2.2.3. Tip Reynolds number relationship

It was apparent from these initial tests that here were two key Reynolds numbers (Re) in the problem:

$$\mathrm{Re}_t = \frac{2\rho U_t R_t}{\mu}, \qquad 1$$

where R_t and U_t are the inner radius of the micropipette and the average velocity at the tip exit, and

$$\mathrm{Re}_s \frac{2\rho U_s R_s}{\mu}, \qquad 2$$

where R_s and $U_s = \frac{dR_S}{dt}$ are the instantaneous radius and expansion velocity of the bolus corresponding to a constant ejection rate Q, at the micropipette tip. From continuity,

$$Q = \pi R_t^2 U_t = 4\pi R_{s_s}^2 U_s \text{ or } U_t = 4\left(\frac{R_s}{R_t}\right)^2 U_s, \qquad 3$$

substituting this relationship between U_t and U_s into the foregoing definition of Re_t and Re_s one finds that

$$\mathrm{Re}_t = 4\left(\frac{R_s}{R_t}\right)\mathrm{Re}_s. \qquad 4$$

3.2.4. Laboratory Model

A screw actuated syringe pump was constructed to eject fluid at constant flow rate from a large-scale pipette using a 20 mL syringe (BD Biosciences) in-line with a motor (RF-310TA, Mabuchi) (**Fig. 8**). Four drive shaft revolutions advanced the syringe to expel 1 mL of fluid over 31.2 s. A vertically secured 5 mL serological pipette (BD Falcon) was hermetically connected in series to 6 cm of glass tubing, 1.2 m of Teflon FEP tubing (Upchurch Scientific), and the syringe, where the pipette tip was submerged and positioned in the 500 mL reservoir in view of the camera (Sony DSC-W55) to video ejected fluid. Newtonian fluid (Pantene Pro-V shampoo) was used in the reservoir and pipette, but the latter differed in color to clearly demarcate the advancing border of the ejected fluid bolus. To determine the time dependent variation of fluid bolus shape as a function of Re_t from 0.03-20.4, four different viscosities were investigated where the fluid viscosity was changed by dilution with water over a 600 fold range. Image frames were extracted from the video of the expanding bolus at four time points (HandyAvi) where, 0 s < t < 31.2 s, for each viscosity.

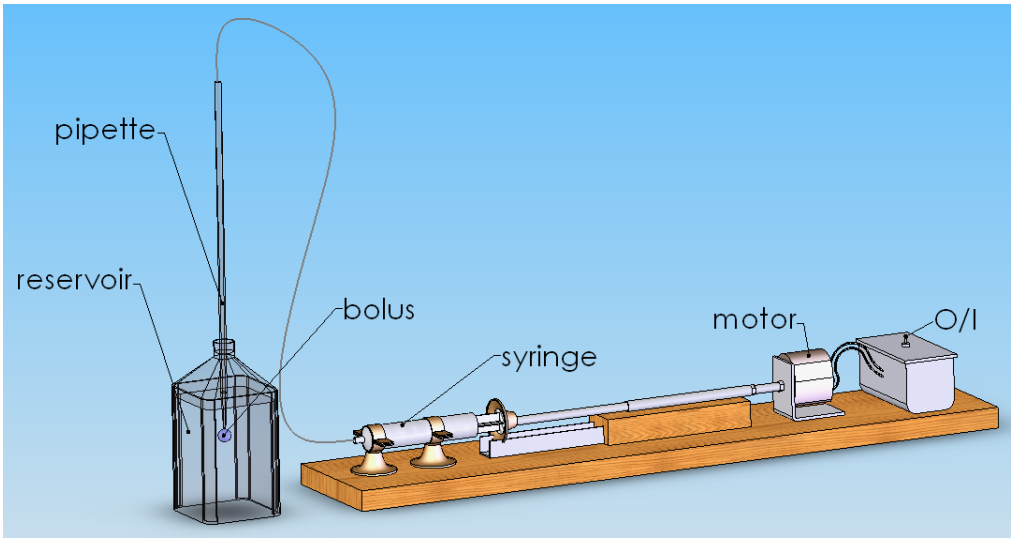

Figure 8 Laboratory model

A schematic of the scaled-up laboratory model built to visualize expansion of the ejected fluid bolus. The screw-actuated syringe pump ejects Newtonian fluid at a constant flow rate of Q = 32 mm^3/s. The same Newtonian fluid is used to fill the pipette tip and the reservoir, but differed in color to clearly distinguish the leading edge of the expanding bolus. One mL of fluid is expelled from the pipette

tip into a 500 mL reservoir and imaged for 31 s.

3.2.5. Samson solutions for velocity and pressure field

Laboratory model experiments showed that the growth of the bolus is closely approximated by Sampson flow through a circular orifice in a zero thickness plane wall. The pressure p_o experienced at the plane of the orifice (micropipette tip) is given by

$$p_o = p_\infty + \frac{3\mu Q}{2c^2}. \qquad 5$$

Here p_∞ is the fluid pressure far from the tip, μ is the absolute viscosity and Q is the volumetric flow rate. The pressure field is given by

$$p = p_0 - (p_0 - p_\infty)\frac{2}{\pi}\left(\frac{\lambda}{\lambda^2+\zeta^2} + \tan^{-1}\lambda\right), \qquad 6$$

where the oblate spheroidal coordinates (λ,ζ) are related to cylindrical coordinates (r,z) via the relations

$$\lambda^2 = \frac{\beta-\alpha}{2},\ \zeta^2 = \frac{\beta+\alpha}{2},\quad \text{where}\quad \alpha = 1-\left(\frac{r}{c}\right)^2-\left(\frac{z}{c}\right)^2,\ \beta = \sqrt{\alpha^2+\left(\frac{2z}{c}\right)^2}. \qquad 7$$

The radial and axial velocity components of the fluid are given by

$$u_r = U_o\frac{\lambda\zeta^2}{\lambda^2+\zeta^2}\sqrt{\frac{1-\zeta^2}{1+\zeta^2}},\quad u_z = U_o\frac{\zeta^2}{\lambda^2+\zeta^2}, \qquad 8$$

where U_o is the centerline velocity in the plane of the orifice given by

$$U_o = \frac{3Q}{2\pi c^2}. \qquad 9$$

The bolus shape at any time t > 0 is obtained by numerically solving the differential equations for a fluid particle trajectory

$$\frac{dr}{dt} = u_r,\ \frac{dz}{dt} = u_z \qquad 10$$

subject to the initial condition that at t = 0, r = r_0, where $0 \le r_0 \le c$ and $z = 0$.

2.3. Results

2.3.1. Tracer studies

The Lucifer yellow tracer results (**Fig. 9**) clearly demonstrated the feasibility of ejecting a reproducible nearly spherical fluid bolus. However, the Lucifer yellow images did not clearly demarcate the edge of the growing bolus because of rapid diffusional spreading of this low MW tracer. The blurring of the image is roughly estimated from the characteristic diffusion length, $\delta=\sqrt{4Dt}$, where D, the diffusion coefficient for Lucifer yellow, is $3x10^{-6}\frac{cm^2}{s}$ (Imanaga et al., 1987). For t=100ms, δ~11 μm. Experiments were also conducted with a high molecular weight fluorescein conjugated dextran, which provided a much clearer series of images (**Fig. 10**), but it still remained difficult to track the leading edge of the expanding bolus as a function of time with the current experimental set-up. The shortest acquisition interval, 20 ms, was too long to accurately capture the evolving bolus shape.

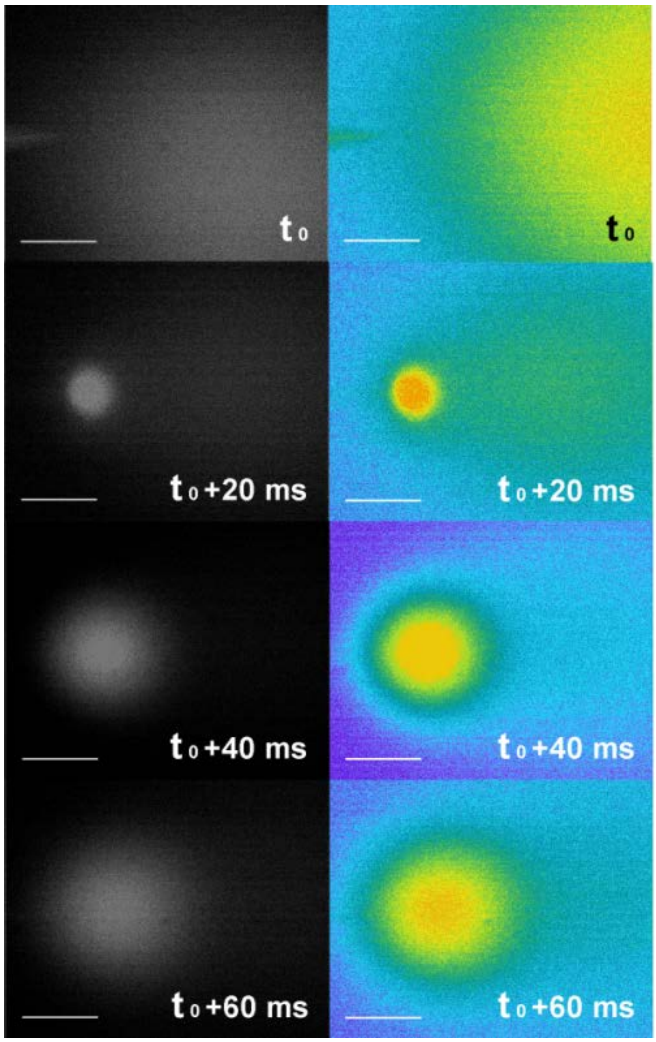

Figure 9 Tracer study with Lucifer yellow (MW 457)

SFSP experiment using Lucifer yellow dye (MW 457) showing growth of bolus with diffusion in extracellular solution. The picospritzer applied a back pressure of 20 psi for 100 ms to a micropipette with a tip diameter 0.8 μm. A 20 ms image acquisition interval was used to capture a series of bolus expansion images. Both greyscale fluorescent and pseudo color images are shown. Scale bar is 50 μm.

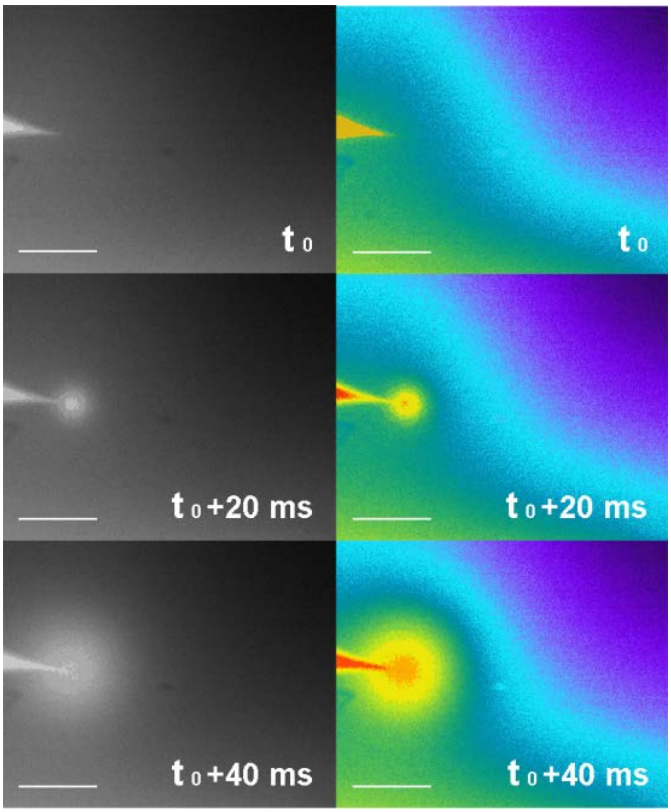

Figure 10 Tracer study using dextran conjugated fluorescein (MW 70,000)

Image series of the expanding bolus when backfilled with high MW dextran conjugated fluorescein (MW 70,000) to mitigate diffusional spreading. Yellow boundary was more clearly defined than with Lucifer yellow dye, but blurring still existed and time intervals were still too long to accurately measure expansion of bolus or clearly define its edge. Back pressure of 20 psi was applied for 100ms. Both greyscale fluorescent and pseudo color images are shown. Scale bar is 50 μm.

2.3.2. Tip Reynolds number

In **Table 1**, the diameter of the bolus after 100 ms is estimated from images in **Figure 9**, and this growth rate of the bolus is used to estimate Re_s. Re_t is then calculated from the relation in Equation 4 that is derived from Equation 3. For an applied pressure of 10-20 psi, the expelled bolus was nearly spherical. However, for pressures > 25 psi with the same micropipette tip size the bolus started to distort.

Pressure (psi)	Q (μm^3/ms)	D_t (μm)	Re_s	Re_t
10	23	0.8	0.0003	0.04
20	51	0.8	0.0006	0.10

Table 1 Tip Reynolds numbers calculated from Lucifer yellow tracer studies

Measurement of Q at back pressures of 10 and 20 psi and determination of sphere and tip Reynolds numbers Re_s and Re_t, Equation (1). Lucifer yellow (MW 457) was used to image the expanding SFSP bolus, but diffusional blurring prevented accurate observation of the bolus shape and its growth. Thus, a laboratory model in **Figure 1** was developed to more clearly observe the leading edge of the expanding bolus and its changing shape.

2.3.3. Laboratory model

A laboratory model, 1000 fold larger than the SFSP experiment, was developed to observe the expansion of the ejected bolus over a much longer timescale of 31.2 s (**Fig. 11**). Bolus growth for the flow from a circular orifice in a plane wall (**Fig. 11a**) closely approximated the pipette flow at a Re_t=0.03, where there is a closed form solution to model this case using Sampson solution. It may also be noted that a nearly spherical bolus is achieved at Re_t=0.03 (**Fig. 11b**), very similar to the previous case with a Re_t very close to the first row in **Table 1**. A pear like distortion is observed at Re_t=0.1 (**Fig. 11c**), an exaggerated distortion of the bolus at Re_t=0.5 (**Fig. 11d**), and a fully developed laminar jet has started to break up into turbulence about its rolled up vortex at Re_t=20.4 (**Fig. 11e**).

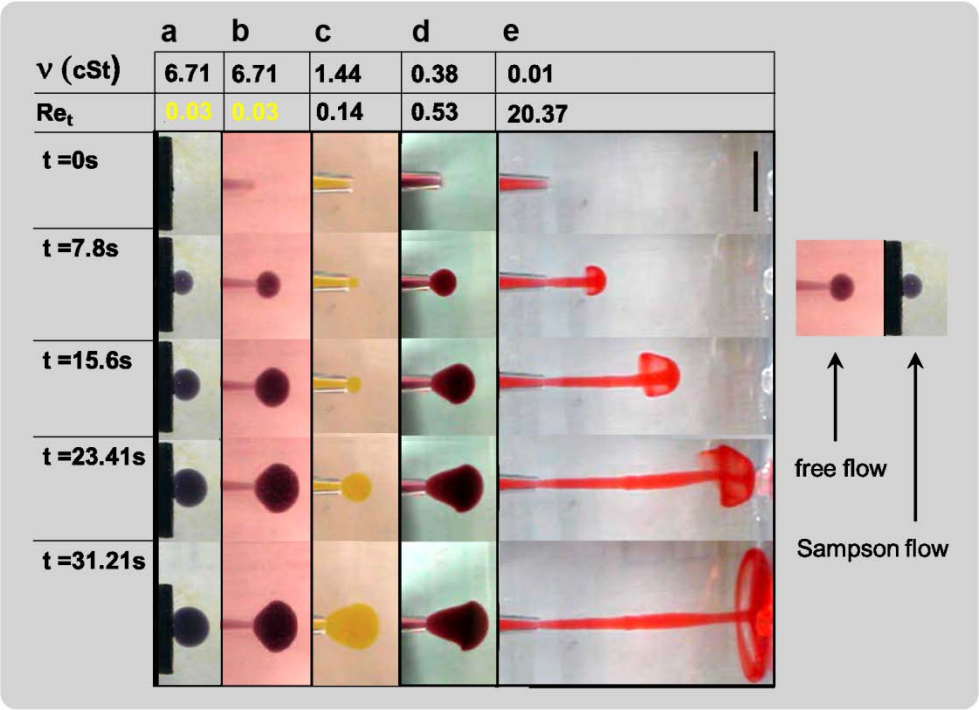

Figure 11 Laboratory model bolus expansion with varying Reynolds number and viscosity

Laboratory model results were presented to illustrate the time dependent change in bolus shape obtained by varying solution viscosity from 0.01 to 6.71 cm^2/s. For all experiments, the reservoir solution and the bolus solution were identical in viscosity but differed in color. The laboratory pipette tip diameter was 0.2 cm. The reservoir size and pipette tip position were chosen to minimize the influence of the boundaries and the bolus was considered to expand into free space. (a,b) The nearly spherical bolus shape was preserved at a Re_t of 0.03, and (c) pear-like bolus distortions are observed at a Re_t as small as 0.1. (d) Large distortions are observed at Re_t = 0.5 and (e) for Re_t > 1 an axial jet develops. When the pipette exit was replaced by an orifice in a plane wall, the bolus shape closely resembled a Sampson flow. Scale bar is 1.5 cm.

2.3.4. Sampson solutions for velocity and pressure profiles

Laboratory model experiments showed that the growth of the bolus could be closely approximated by Sampson flow. While there are no analytical solutions for Stokes flow at the exit of a hollow bore circular cylinder, there is a closed form solution for creeping flow through a circular orifice in a wall of zero thickness, Sampson flow (Happel and Brenner, 1973). Since the length of the bore has little effect on the exit velocity profile (Dagan et al., 1982), one would expect that the exit flow at the pipette tip is very similar to Sampson flow (**Fig. 11**). This similarity is clearly observed when $Re_t = 0.03$ (**Fig. 12a** from **Fig. 12a**) where the growth of the bolus, at equivalent time points with only minor differences in overall bolus shape, is nearly identical to Sampson flow predictions (**Fig. 12b**). Thus, Sampson's solution for the bolus growth for the laboratory model, $Q = 32$ mm^3/s, and the micropipette, $Q_t = 255$ μm^3/ms (**Fig. 12c**), and its associated pressure field in the vicinity of the micropipette exit (**Fig. 12d**) provide a remarkably good description of the bolus expansion and pressure field. Equations (6) and (7) provide the isobars shown in **Figure 12d**. Although the flow starts from rest and there is an initial transient, this is short lived. If the characteristic vorticity diffusion distance, $\sqrt{4vt}$, is 10 µm and $v=0.01$ $\frac{cm^2}{s}$ (water 20 ºC), the duration of this initial transient $t=6x10^{-4}$ s. Thus, the steady state pressure field is set up almost instantaneously, and the velocity field is a quasi-steady Stokes flow and does not change during the entire pressure pulse. A key observation is, although the bolus has an approximate diameter of 35 mm at the end of the pressure pulse (**Fig. 12c**), the region of interest in the pressure diagram (shaded region in **Fig. 12d**) is confined to 1–5 µm from the orifice exit. Here the pressure rapidly decays from approximately 100–1 pN/µm^2 along the axis of the bolus.

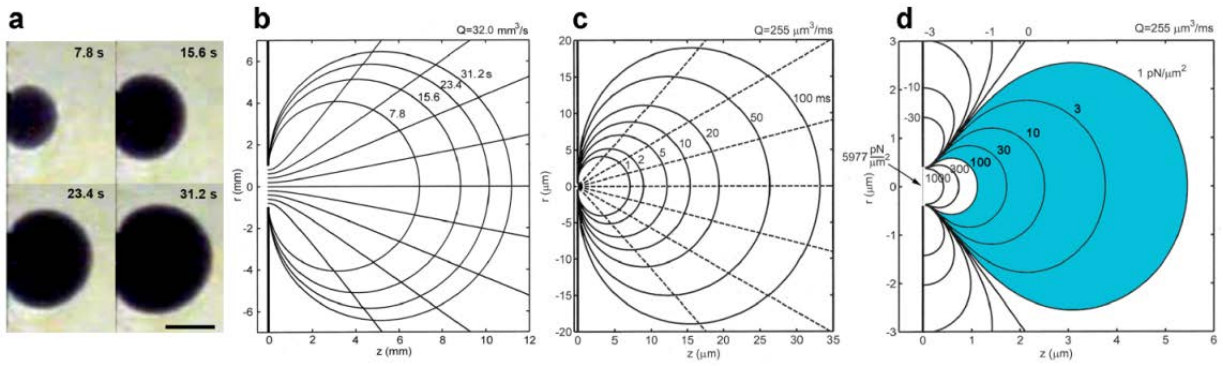

Figure 12 Theoretical predictions of bolus shape and pressure field

(a) Laboratory model of growing bolus for Sampson flow through a circular orifice, from **Figure 11a** where Re_t = 0.03. Scale bar is 0.5 cm. (b) Theoretical prediction for the laboratory model bolus growth for $Q = 32.0\ mm^3/s$ in which the pipette tip diameter was 0.2 cm and Re_t = 0.03. The Sampson solution closely predicts the leading edge of the bolus expansion over time, and closely approximates the bolus growth in the laboratory model pipette experiment (**Fig. 11a**). (c) Theoretical prediction of bolus shape for Sampson flow for a micropipette with a tip diameter of 1 μm where $Q = 255\ \mu m^3/ms$. (d) Theoretical predictions of the pressure field (isobars) in the vicinity of the micropipette tip exit corresponding to the bolus expansion. This pressure field describes the decay in the velocity field from the plane of the orifice.

2.4. Discussion

2.4.1. Motivation for development

The goal of achieving focal hydrodynamic stimulation in a single cell to identify differences in responses along the length of the cell was the primary motivation for SFSP development. It was also critical to stimulate the cell at a physiologically relevant force and mimic fluid flow that would put cell membrane attachment sites in tension similar to what fluid flow drag would produce at discrete sites of attachment in its native LCS. Current force probes that have uniquely contributed to biophysical and biochemical discovery: the biomembrane force probe (BMP), atomic force microscope (AFM), optical

tweezers (OT), and magnetic twisters and pullers (MPT) all required probe decoration with antibodies or ligand specific molecules, had probe-cell surface interaction, and operated in the pN - nN force range. Most of these techniques operated at a higher force range than desired for these particular live-cell experiments and the force probes could only target one focal region per experiment. The SFSP has the capability to target multiple sites within the same cell during one experiment, and has captured unique mechanosensitive characteristics in a single cell. In the field of calcium imaging, many groups have adopted mechanical indentation with a micropipette as the gold standard for dimpling and poking cells (Duszyk et al., 1989) to initiate calcium signaling, but the forces have proven difficult to measure and are believed to be in the nanoNewton range or larger.

2.4.2. New mode of operation

An entirely new approach has been developed utilizing a pressure pulse generated from a Picospritzer traditionally used for ejections of RNA into oocytes (Kalinowski et al., 2004) and application of pharmacological agents to particular regions of cells (Smith and Uteshev, 2008). The ejection technique is hardly new; however, we have now been able to convert a somewhat crude volumetric ejection device into a precise and quantifiable force application device. This advance requires sophisticated theoretical modeling both for device design and calculation of forces produced.

Investigators previously using the ejection system were not readily concerned with forces or the profile of the fluid applied as much as the volume ejected, so they would apply axial jets similar to ejections with a tip Reynolds $Re_t > 100$, five times larger than the case illustrated in **Figure 11e**. A laboratory model has been designed to visualize the behavior of the ejected fluid from the pipette at varying viscosities to understand the relationship between the micropipette tip Reynolds number and the profile of the ejected fluid, and how it may be controlled by pipette tip size and back pressure used to eject the volume.

2.4.3. New force probe for pN level loading

A novel hydrodynamic force probe has been developed to use concurrently during electrophysiology experiments in whole-cell voltage-clamp mode to yield functional information about the electrical and signaling characteristics of osteocytes under pN loading in culture. The novel force probe does not

require decoration with anti-bodies or ligand specific molecules and does not physically interact with the cell membrane of interest, as many force probe techniques have required (Bausch et al., 1998; Binnig et al., 1986; Evans et al., 1995; Litvinov et al., 2003), so the probe can be applied multiple times at different locations on the same cell.

Chapter 3: Mechanotranduction mechanisms on the osteocyte cell process

3.1. Introduction

There has been a longstanding debate regarding bone mechanotransduction summarized in a recent review (Fritton and Weinbaum, 2009). The two fundamental questions are: (1) whether the osteocyte cell body or its dendritic processes serve as the mechanosensor of fluid flow in the lacunar–canalicular porosity, and (2) if the cell process is the sensing component, whether intracellular signaling is initiated at discrete attachment sites along the cell process, as hypothesized by Wang et al. (2007) and McNamara et al. (2009) or at the much more numerous flexible tethering attachments described in You et al. (2001) and You et al. (2004). We hydrodynamically exposed the cell body and its dendritic processes in a repeatable and physiological manner using the newly developed Stokesian Fluid Stimulus Probe (SFSP). The SFSP tip does not touch the cell or its substrate, yet creates tensile forces on focal attachments at magnitudes that are predicted to occur *in vivo* (Wang et al., 2007). These tensile forces *in vivo*, which are reproduced experimentally *in vitro*, are concentrated at small focal contacts observed at the apex of the canalicular protuberances described in McNamara et al. (2009). These forces in the range of 1–10 pN likely perturbate just a few integrins, since only a few integrins would fit on the apex of protuberances observed *in vivo*, and are roughly three orders of magnitude smaller than the mechanical forces typically exerted during indentation of a cell with a micropipette tip or AFM cantilever tip to elicit a Ca^{2+} response (Huo et al., 2010).

In order to test whether an osteocyte is mechanically activated at its dendritic processes or at its cell body, we have performed the first electrophysiological experiments to measure the focal activation of ion channels in the dendritic processes of osteocytes using our newly developed SFSP. A unique aspect of the experiment is that the SFSP can apply pN level forces locally along the length of the dendritic process at various locations or at the cell body, where cellular responses initiated at different regions of the cell may be compared.

3.2. Materials and Methods

3.2.1. MLO-Y4 culture

MLO-Y4 osteocyte-like bone cells were maintained in α-MEM (Invitrogen) supplemented with 5% fetal

bovine serum (Invitrogen), 5% bovine serum (Invitrogen), and 1% penicillin-streptomycin solution (Meditech). MLO-Y4 cells were plated on 12 mm glass microscope coverslips (Fisher Scientific) at low density and cultured for two days before performing whole-cell voltage-clamp experiments.

Expression of integrin subunits known to associate with mechanosensitive channel complexes or the cytoskeleton could vary with different substrates. To test whether or not MLO-Y4 cells plated on varying substrates expressed mechanisms implicated in mechanotransduction, MLO-Y4 cells had been plated on the following substrates: rat tail collagen Type-1, osteopontin, and glass, and probed for the implicated mechanotransduction proteins using immunocytochemistry, staining details are described below. Expression of $\alpha_v\beta_3$ integrin and paxillin implicated in mechanotransduction, were observed in MLO-Y4 cells plated on rat tail collagen Type-1, osteopontin, and glass (**Fig. 13**). Expression of the purinergic P2 receptor implicated in indirect pathways of intercellular signaling was also observed. Electrophysiology experiments were performed on glass substrates to mitigate micropipette tip clogging between SFSP stimulation caused by ECM proteins that are not bound to the substrate. MLO-Y4 cells with rounded cell bodies and multiple cell processes were selected for electrophysiological recordings (**Fig. 14c**).

$\alpha_v\beta_3$ integrin, paxillin, and P2X$_7$R Fixation of cells was performed with 4% formaldehyde, permeabilized with 0.4% Triton X-100 (Sigma), and blocked with 1% BSA in 1XPBS. For $\alpha_v\beta_3$ integrin, paxillin, and P2X$_7$R staining, the cells were incubated with primary polyclonal antibodies against $\alpha_v\beta_3$ (Sigma, LM-609), paxillin, and P2X$_7$R followed by incubation with secondary antibody conjugated to Alexa 488 or 594 (Molecular Probes). The coverslips were mounted on microscope slides with mounting media containing DAPI for nucleus staining, and imaged using a 40X oil objective on the Nikon Eclipse TE300 microscope with SPOT-RT software (Diagnostic Instruments, Sterling Heights, MI).

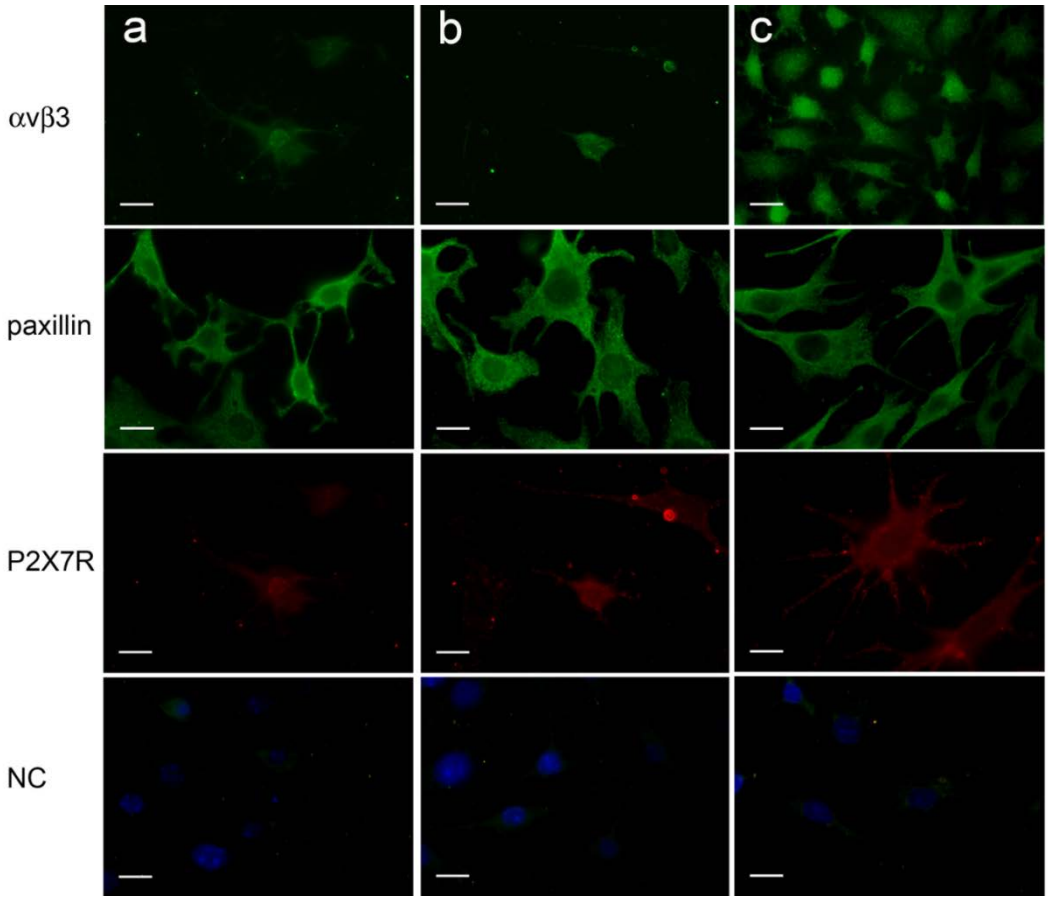

Figure 13 Epifluorescence images of MLO-Y4 cells plated on three different substrates

MLO-Y4 cells (a) plated on collagen Type-1, (b) osteopontin, and (c) glass then stained for $\alpha_v\beta_3$, paxillin, and $P2X_7R$ expression. Non-specific staining was not observed on the negative control (NC) incubated with only the secondary antibody.

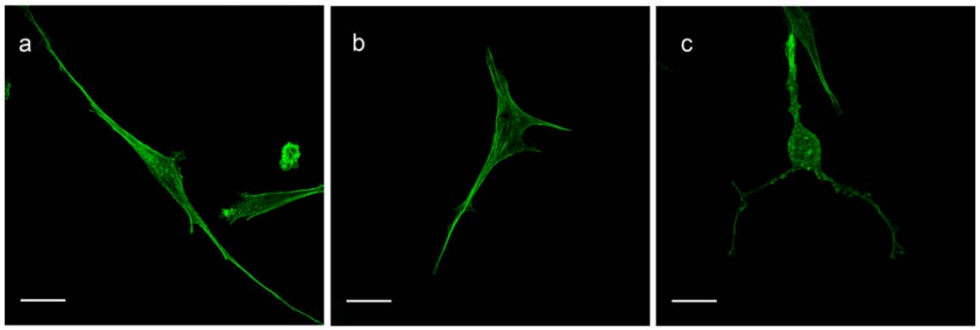

Figure 14 Confocal images of MLO-Y4 cells stained for phalloidin

Confocal images of F-actin structures within the cell clearly illustrated three morphologically distinct cells within the MLO-Y4 cell culture. (a) An elongated cell with two cell processes, (b) a multi-dendritic cell with a flat cell body, and (c) stellate cell with secondary cell processes and a rounded cell body. (c) The cell with a more rounded cell body and stellate cell processes is used for all electrophysiology experiments. Scale bar is 20 μm.

3.2.2. Extracellular and intercellular solutions

Extracellular solution in the SFSP pipette contained [mM] - 140 NaCl., 2 CsCl, 2 $CaCl_2$, 1 $MgCl_2$, 5 HEPES, 4 KCL, 5 glucose, 2 Sodium Pyruvate, 1 $BaCl_2$; pH 7.4 using NaOH, filtered using a 0.22 μm pore size bottle top filter (Corning). Intracellular solution in the patch pipettes contained [mM] - 130 CsCl, 10 EGTA, 10 HEPES, and 0.5 CaCl2; pH 7.3 with KOH, filtered using a 0.22 μm pore size bottle top filter (Corning).

3.2.3. The Stokesian Fluid Stimulus Probe (SFSP)

The SFSP is a novel force probe technique capable of focally administering hydrodynamic forces on cells in culture (Wu et al., 2011). The SFSP is used to apply 1-10 pN level forces on a single osteocyte-like cell to identify mechanosensitive regions of the cell. The SFSP pipette tip must be placed 2-5 μm away from the cell membrane to achieve the desired pressures of 1-10 pN/μm^2, **Fig. 15**.

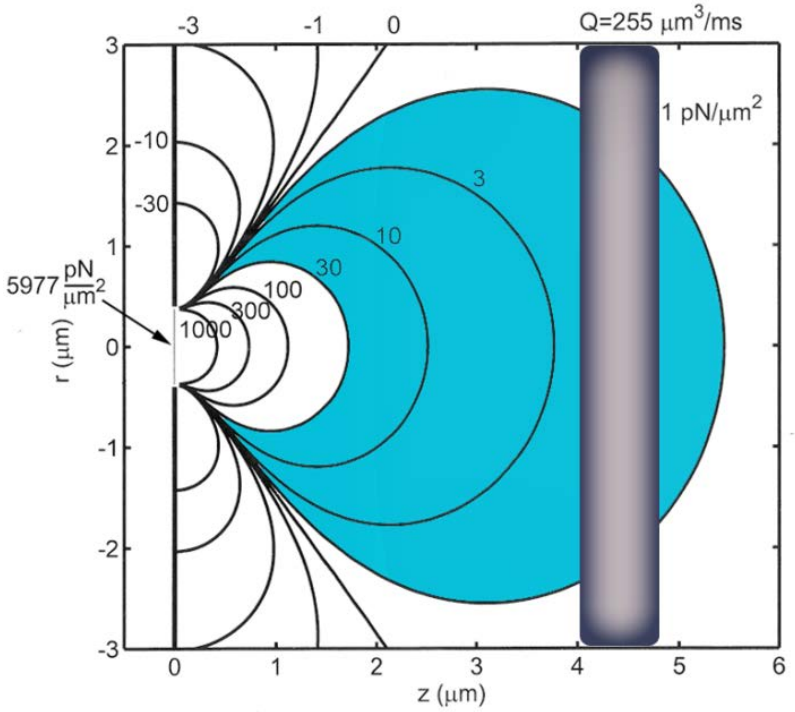

Figure 15 The Stokesian fluid stimulus probe

Theoretical predictions of the pressure field (isobars) in the vicinity of the micropipette tip exit corresponding to the bolus expansion. This pressure field describes the decay in the velocity field from the plane of the micropipette tip. The osteocyte cell process, shaded grey, is overlaid on the isobars to illustrate the critical parameter of micropipette tip distance from the center of the cell process, d_t, in relation to the pressures achieved on the target object. For forces of 1-10 pN, d_t must be 2-5 μm.

3.2.4. Micropipette preparation and placement

SFSP micropipettes were pulled with a P-97 Pipette Puller to achieve an initial tip resistance of $2-3$ MΩ when backfilled with extracellular solution, and placed at $2-5$ μm distance from the cell body or its processes, **Fig. 16**, at a 35-40 degree angle from the substrate, **Fig. 17**. The acute angle of the micropipette from its substrate was necessary to ensure a torsional force that rotates the cell process by the dominant force in the x-direction that puts molecules of adhesion at the substrate in tension. A single SFSP pressure pulse is applied at 20 psi and held constant for a duration of 100 ms. The quasi-steady

state velocity and pressure field are established nearly instantaneously and motion ends abruptly with the termination of the pressure pulse.

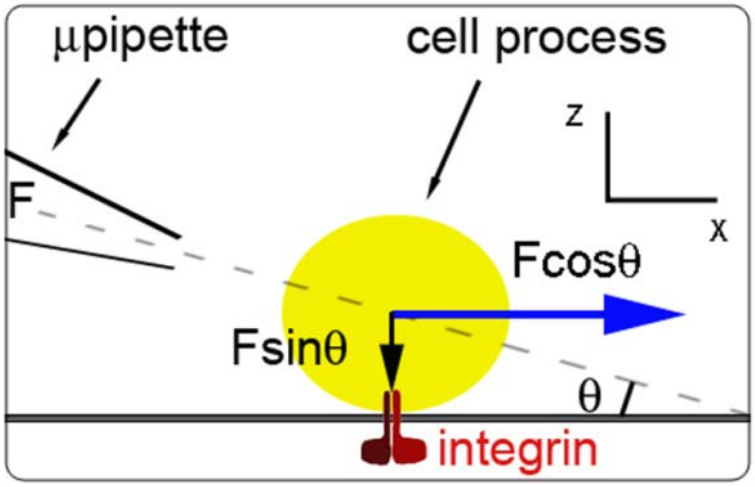

Figure 16 Force diagram

Force diagram showing vectors of SFSP force: traction force, F_x (Fcosθ), and compression force, F_z (Fsinθ). Only F_x creates tensile force on integrin attaching cell process to substrate. Line of action is through the center of the cell process cross-section.

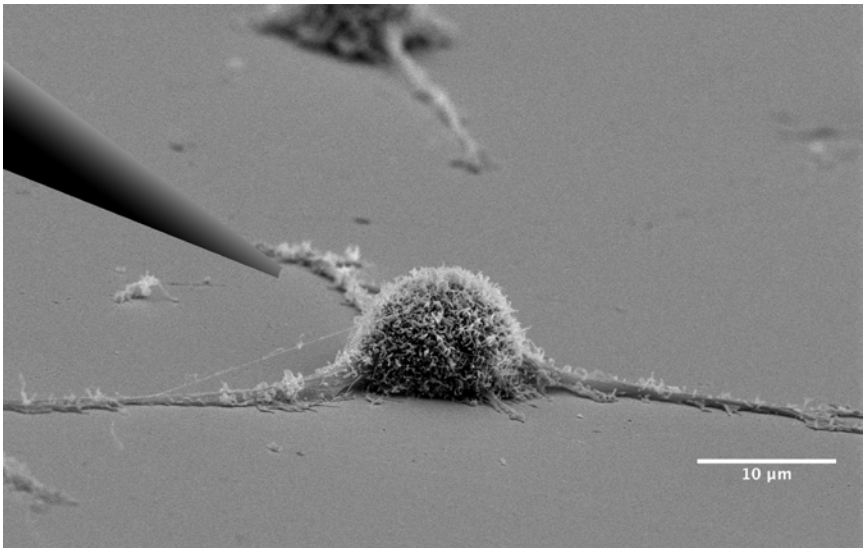

Figure 17 Micropipette placement

A SEM micrograph of a MLO-Y4 cell plated on a glass coverslip with a

superimposed micropipette to illustrate its placement during SFSP excitation. SFSP micropipette is positioned at a 35-40 degree angle from the substrate and 2-5 μm away from the cell process or the cell body prior to stimulation. A 3-axis hydraulic manipulator is used to position the micropipette, and may be repositioned multiple times during a single experiment. The patch-pipette is not shown.

3.2.5. Whole-cell voltage-clamp experiments

Patch microelectrodes were pulled as described in Section 3.2.3, but to an initial electrode resistance of 4-5 MΩ and backfilled with intracellular solution. All experiments were performed at room temperature (20-26 °C) with an epi-fluorescent microscope (Nikon), patch clamp amplifier (Axon Instruments), PClamp 8.5 software (Axon Instruments), 3-axis hydraulic micromanipulators (SD Instruments), and a pneumatic vibration isolation table. Conventional whole-cell voltage-clamp recordings were performed on individual MLO-Y4 cells held at -60 mV with high resistance seals ≥ 1GΩ. Recordings from cells were extracted from PClamp 8.5 and analyzed in Origin 5.0 (Microcal), ImageJ (NIH), and Prism 5.0 (GraphPad). When more than one cell process response was recorded in a single-cell, the cell process responses were paired with their respective cell body response and analyzed. A second or sequential SFSP stimulation was only applied after the membrane potential of the cell had returned to its initial state prior to the primary stimulation. The electric charge and peak conductance in response to SFSP stimulation directed to the cell process at attached sites or the cell body were calculated and analyzed using a two-tailed paired Student's t-test. All values were expressed as means ± s.e.m.

The whole-cell patch-clamp technique was chosen to evaluate biophysical responses of single osteocytes because of its spatial and temporal resolution capable of quantifying fast and transient cellular responses on the order of milliseconds to seconds after stimulation by forces predicted to occur *in vivo*. In cultured MLO-Y4 cells, calcium wave propagation on the order of seconds to minutes can be detected using Ca^{2+} indicators, and the release of prostaglandins (PGE_2) and nitric oxide (NO) over minutes to hours may be measured using quantitative assays, see **Figure 18**. The techniques used to detect cellular responses in osteocytes is arranged from higher to lower temporal resolution, but the initial release

of the signal detected, i.e. Ca^{2+}, PGE_2, or NO, may occur earlier than the time-frame detected. Particularly in the case of the osteocyte with thin dendritic cell processes, detection of molecular messengers at low concentrations in regions of small cytoplasmic volume presents difficulty. Whole-cell patch-clamp overcomes these challenges and can detect small current fluxes passing through the cell membrane. Whole-cell patch-clamp could also detect signals that occur upstream of what calcium imaging and molecular messenger assays may detect.

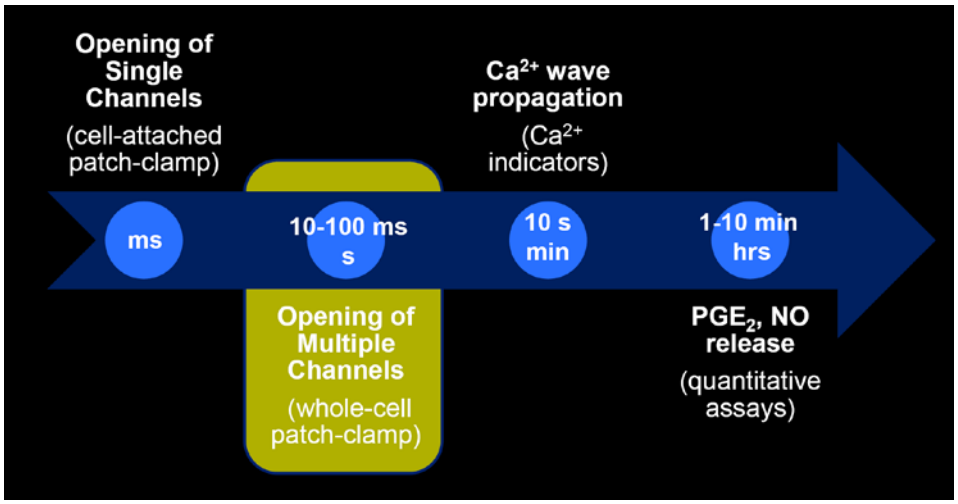

Figure 18 Detection of cellular responses in MLO-Y4 cells

Temporal resolution of techniques used to detect biophysical responses in MLO-Y4 cells are arranged from higher to lower temporal resolution. Electrophysiology techniques in the cell-attached and whole-cell mode can detect current or voltage changes in cells on the order of a few to 100 ms. Calcium wave propagation in osteocytes may be detected on the order of 10 s to a few minutes when stimulated at their dendritic cell processes. Prostaglandin (PGE_2) and nitric oxide (NO) release may be detected using quantitative assays after a few minutes to hours of stimulation.

3.2.6. Determination of the area moment of inertia of the central actin filament bundle

The flexural rigidity EI of the central actin filament bundle in the cell process is the product of the Young's modulus E of a single actin filament and the area moment of inertia of the actin filament bundle I_b. Calculation of I_b is performed using the parallel axis theorem for multiple bodies where I_a,

$$I_a = \frac{1}{4}\pi r^4 \qquad 11$$

is the area moment of inertia for a single actin filament, with an effective cross-sectional area of $25\,\text{nm}^2$, parallel to the line of action through the 5 central actin filaments along the x-axis. The contribution of each actin filament to I_b,

$$I_b = \sum (I_a + A_a \cdot y_1^2) + \sum (I_a + A_a \cdot y_2^2) \qquad 12$$

is its area moment of inertia plus the product of the actin's cross sectional area A_a and its squared distance from the line of action. Thus I_b,

$$I_b = 8 \cdot \left(I_a + \pi r_a^2 \cdot \left(\frac{\sqrt{3}a}{4} \right)^2 \right) + 6 \cdot \left(I_a + \pi r_a^2 \cdot \left(\frac{\sqrt{3}a}{2} \right)^2 \right), \text{ where } I = I_b \qquad 13$$

is defined as the summation of the contribution of each actin filament in the 19 actin filament hexagonal bundle described in detail in (Han et al., 2004) shown in **Figure 19**, where r = 2.8 nm and the filament spacing is $\frac{a}{2} = 12\,\text{nm}$.

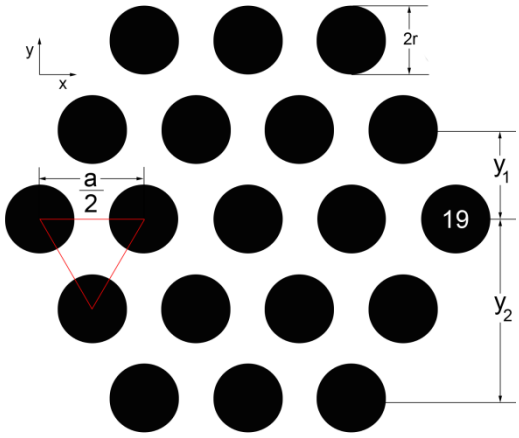

Figure 19 Axial geometry of cell process actin filament bundle

Calculation of the area moment of inertia of the 19 central actin filament bundle the cell process

3.2.7. Measurement of process deflection and predictions of forces

The determination of the force acting on the processes is subtle since the flow geometry is fully three dimensional and unbounded and, thus, not easily amenable to a computational analysis at low Re. It is easy to observe and measure the deflection of the process and the separation distance *L* between discrete attachment sites where there was visible deflection, see **Figure 20**. Thus, if one can estimate the flexural rigidity *EI* of the central actin filament bundle in the process, one can apply elastic beam theory to relate the force on the process to the displacement at its center. The detailed structure of the fimbrin cross-linked actin filament bundle is a highly organized hexagonal structure, five actin filaments across, and described in detail in Han et al. (2004). This structure is based on the electron microscopic observations of dendritic process cross-sections (You et al., 2004) and exposed actin filament bundles in which the process' membrane has been enzymatically removed (Tanaka-Kamioka et al., 1998). The Young's modulus of individual actin filaments, $E = 2.6x10^3$ pN/nm^2, has been accurately measured by *in vitro* nanomanipulation (Kojima et al., 1994), and *I* is the area moment of inertia of the central actin bundle, where the effective cross-sectional area of an individual actin filament is 25 nm^2. Elastic beam theory may be applied to relate the measured deflection δ_m of the cell process midway between rigid attachment points and force applied to the cell process. The distance *L* between integrin attachment sites where there was an observed deflection was measured from light images of the cell process during SFSP application. The area moment of inertia of the 19 filament central actin bundle is calculated to be $I=8.6x10^4$ nm^4.

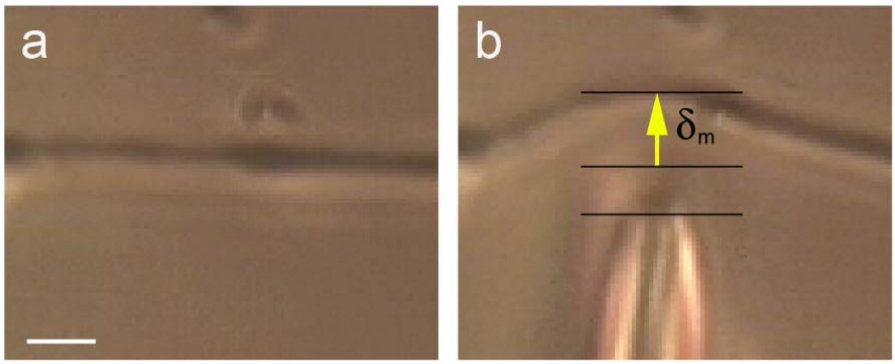

Figure 20 Measurement of maximum cell process deflection

Position of the cell process (a) before SFSP stimulation and (b) after SFSP stimulation with horizontal bars marking the pipette tip, the initial position of the center of the cell process before stimulation, and the final position of the center of the cell process after SFSP stimulation. δ_m indicates the maximum deflection of the cell process. Note: This case of SFSP stimulation did not evoke a cellular response because it lacked a firm or loose adhesion near the centerline of the SFSP. The scale bar is 5 μm

The relationship between the force acting at the midpoint between attachment sites and the local deflection is given by:

$$\delta_{0<x<\frac{L}{2}} = \frac{Fx}{48EI}\left(3L^2 - 4x^2\right). \qquad 14$$

The maximum deflection at x = L/2 is given by:

$$\delta_m = \frac{FL^3}{48EI} \qquad 15$$

where the force is related to δ_m by

$$F = \frac{48EI\delta_m}{L^3}. \qquad 16$$

3.3. Results

3.3.1. Whole-cell voltage-clamp experiments

The whole-cell voltage-clamp technique was used to measure membrane currents in cells subjected to SFSP stimulation at different locations along the cell process and on the cell body. In the case of the cell process, two strikingly different traces were obtained depending on whether the probe tip was directed precisely at an attachment site or midway between attachment sites. A single cell is stimulated at a series of locations **Fig. 21a**, and its whole-cell voltage-clamp recordings in response to stimulation at attachment sites of the cell process and on the cell body, are shown in **Figure 21b**. Collectively, out of 10 cells and 31 cell processes, significantly larger electric charge was observed when local pN level forces were directed at focal attachment sites along the cell process, 1.02 ± 0.32 nC, than when directed at the cell body, 0.0032 ± 0.0011 nC, where p=0.004 (**Fig. 21c**). Much larger peak conductance in response to SFSP stimulation was also observed when the bolus was directed at a cell process attachment, 2.76 ± 1.20 nS, compared to impingement on the cell body, 0.38 ± 0.14 nS, (**Fig. 21d**) where p=0.041. Only data from high resistance seals of $1-3$ GΩ were included in the analysis; however, data from lower resistance seals of ~ 300 MΩ provided evidence of similar osteocytic polarity where $n = 105$, data not shown. Most important is the observation that traces for CP 1, 2, and 3 were all collected at points where there was little to no deflection of the cell process indicating that these were loci of discrete attachments. A vivid comparison between a cellular response at a strong adhesion site (**Fig. 22a,b**) and a weak adhesion site that demonstrated process deflection (**Fig. 22d,e**), is shown in **Figures 22c,f.** Also noteworthy, recordings from the deflected cell process, **Fig. 22f,** were similar to recordings from cell body stimulation, **Fig. 21b**.

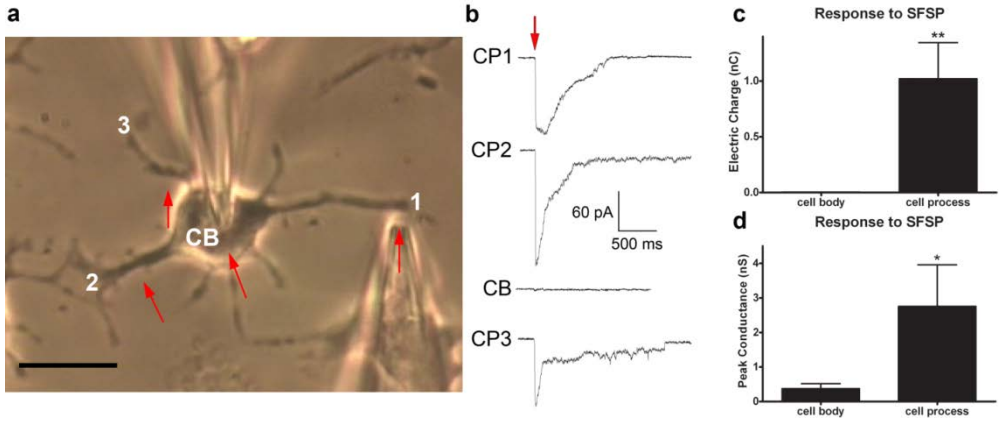

Figure 21 Whole-cell voltage-clamp of MLO-Y4 cells

Prior to SFSP stimulation, seals ≥ 1GΩ are formed at the cell body (CB) with a patch microelectrode and the SFSP tip is positioned perpendicular to and 2-5 μm away from the cell process (CP). (a) A light micrograph of a MLO-Y4 cell with SFSP tip 3 μm from CP1. Red arrows indicate SFSP tip positions during this experiment. (b) Whole-cell voltage patch-clamp recordings during SFSP stimulation of the MLO-Y4 cell at CP1, CP2, CB, and CP3 consecutively. SFSP application is indicated by the red arrow. (c) SFSP stimulation at the CP induced larger electric charge, 1.02 ± 0.32 nC, through the membrane than when the SFSP is directed at the CB, 0.0032 ± 0.0011 nC, and (d) conductance amplitudes were larger in response to SFSP stimulation at the CP, 2.76 ± 1.20 nS compared to those from stimulation at the CB, 0.38 ± 0.14 nS. (n = 31, two-tailed paired Student's t-test, **p < 0.01 and *,p < 0.05, mean ± s.e.m) Scale bar is 20 μm.

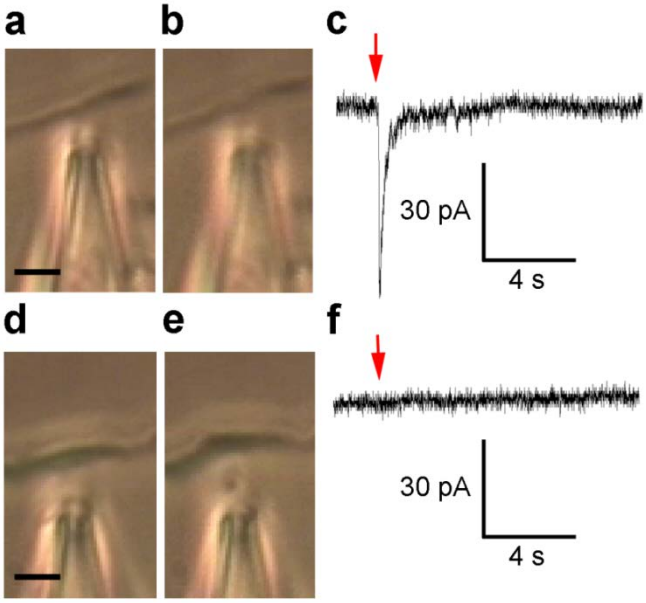

Figure 22 Variation in cellular conductance in response to focal pN loading

Comparison of cellular responses when stimulated by the SFSP at two separate locations along the same cell process. (a) First location along cell process (b) is stimulated by the SFSP without deflecting, and (c) a change in cellular conductance is detected from the recording. (d) Second location along the same cell process (e) is stimulated by the SFSP with visual deflection of the cell process and (f) yielded no change in cellular conductance. Scale bar is 5 μm, red arrow indicates SFSP application, cells were held at -60 mV with a seal > 1GΩ.

3.3.2. Predictions of forces from cell process deflection under SFSP loading

Detailed measurements of five maximum cell process deflections δ_m at the central location between firm attachment sites on the process are summarized in **Table 2**. Radii *a* and distance between attachments *L* are shown for each process. The maximum deflection of the process varies inversely as the third power of the distance *L* and the value of $EI = 2.2 \times 10^8$ pN nm^2. Here I=8.6x10^4 nm^4 is calculated using the detailed theoretical model for the central actin filament bundle.

In general, the distance *L* is significantly larger than the radial spread of the pressure profile in **Figure 23**, which depends on the distance of the probe tip from the centerline of the process d_t where the

maximum deflection d_m is measured (**Fig. 20**). A rough approximation to the lateral force distribution can be obtained from the Sampson pressure field given by Equation 6, at varying distances z from the SFSP tip. These lateral profiles are plotted in **Figure 23**. This distance d_t was typically in the range 4.4–6.3 mm and the radial pressure profiles along the process estimated from the solutions for Sampson flow are shown in **Figure 23,** where the radius of the pipette tip *c* is 0.4 μm. The rapid lateral decay in pressure from the centerline compared to the distance L between focal attachment sites, see Table 2, allows us to treat the force as a concentrated load instead of a distributed load applied midway between firm attachment sites on the cell process. Theoretically predicted forces based on Equation 15 on cell processes are shown in the last column of **Table 2** where the force is related to δ_m by $F = \frac{48EI\delta_m}{L^3}$.

A rapid lateral decay in pressure occurs from 19.4 to 0 pN/μm^2 within a radial distance of 2.6 μm when d_t=2 μm, and from 1.9 to 0 pN/μm^2 when d_t=5 μm. A deflection in the cell process will further decrease these forces acting at the integrin attachment sites at the center line of the SFSP and 0 pN/μm^2 will be exerted on the pivot points of attachment if the distance between focal attachment sites exceed 2 μm when d_t>2 μm. Note that the predicted forces all fall in the range 1–2.3 pN, well within the range of forces predicted by Wang et al. (2007) for the hypothesized integrin attachments at canalicular projections.

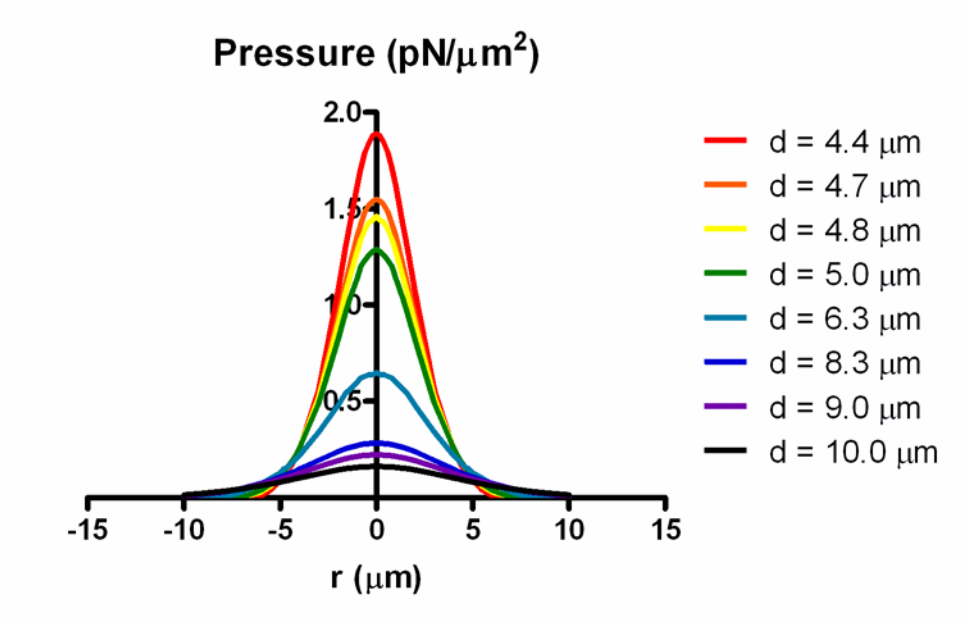

Figure 23 Theoretical pressure distributions at varying distances from the pipette tip

The pressures distributions exerted on an MLO-Y4 cell process at varying SFSP pipette distances *in vitro* produced forces from 1-2.3 pN at the centerline of the probe where maximum cell process deflection occurred. The pressures rapidly dissipated laterally from pipette tip, and dropped to zero before reaching the pivot points or neighboring attachment sites along the cell processes.

	a (μm)	d_t (μm)	L (μm)	δ_m (μm)	F (pN)
cell A	0.7	4.4	28.9	5.2	2.3
cell B	0.7	4.8	35.2	4.1	1.0
cell C	0.9	5.0	26.2	3.3	2.0
cell D	1.6	6.3	26.9	3.8	2.1
cell E	1.3	6.3	28.0	3.3	1.6

Table 2 Force predictions from cell process deflection analysis

Measurements of radius a, distance between SFSP tip and cell process d_t, length between two firm attachment sites on the cell process L, maximum deflection δm,,

and predicted force F for five different cell process deflections are given. Predictions of F acting at the midpoint of L are in the range of 1 to 2.3 pN, and are within the range of forces predicted to occur at focal attachment sites along the cell process in vivo (Wang et al., 2007).

3.4. Discussion

The SFSP was developed to deliver highly focal hydrodynamic forces to single osteocyte-like bone cells in culture of comparable magnitude to the pN level forces that Wang et al. (2007) predicted to occur *in vivo* due to physiological loading to address whether intracellular signaling is initiated at discrete attachment sites along the cell process, as hypothesized in Wang et al. (2007) and McNamara et al. (2009), at the cell body (Vatsa et al., 2008), or at the much more numerous flexible tethering attachments (You et al., 2004). Our present electrophysiological experiments in **Figure 21** indicated that dendritic processes induce a far greater mechanosensitive response than the cell body when stimulated by the SFSP at comparable distances. By contrast, observed membrane deformations of the cell body were larger than those of the cell process when subjected to the SFSP stimulus. This demonstrated that the soft cell body, which easily dimples in response to pN level forces, is a poor force transducer and that membrane deformation alone is not sufficient to initiate a detectable change in cellular conductance. Even more important than the polarization of the cell, is the observation that electrical signaling (**Fig. 22c**) is initiated only when the probe is directed at focal attachment sites along the cell process (**Fig. 22b**). There was no response when the SFSP is directed at locations along the process void of focal attachments and discernible cell process deflection (**Fig. 22e**), or when the SFSP is applied on top of the process putting it in compression (results not shown) to suggest that only tensile forces trigger a response.

We addressed the involvement of an adhesion complex and its possible role in activating a mechanosensitive channel whereby metabolites are released to initiate signaling event(s) in a single osteocyte cell. While the molecular structure of the attachment complex is uncertain, likely candidates for the attachment are β_1 and β_3 integrins. Litzenberger et al. (2010) have stably transfected a dominant negative form of β_1 integrin into MLO-Y4 cells and consequently have observed a reduction in PGE_2 release. McNamara et al. (2009) observed β_1 integrins *in vivo* with immunocytochemistry on both the cell

body and cell process membranes, but only β_3 integrins on the cell process. More specifically, *in vitro* studies on rat osteocytes using echistatin to demonstrate an adhesion-mediated effect on stretch-activated cation channels and Ca^{2+} signaling suggested the functional importance of $\alpha_V\beta_3$ integrin (Miyauchi et al., 2006). Collectively, these results indicate that the electrical response we have observed is most likely mediated by an integrin-associated complex whose identity at present is unknown.

Two-dimensional culture systems using MLO-Y4 cells have been viewed as crude approximations of osteocytes in the lacunar–canalicular system *in vivo*. A key difference has been the absence of numerous tethering fibers attaching the cell process to the canalicular walls *in vivo* captured by You et al. (2004). These tethering fibers when subjected to fluid flow through the lacunar–canalicular system are put in tension and create a hoop strain on the cell process membrane, which mathematical models have predicted to be more than an order of magnitude larger than whole tissue strains. It would be very difficult to distinguish *in vivo* whether the electrophysiological response observed herein originated from axial strains associated with focal integrin attachments or from these hoop strains *in vivo*. In contrast, the hoop strains in culture are absent since there are no tethering fibers, and the response is clearly due to the discrete focal attachments.

The foregoing results strongly support the observations of two recent cell culture studies. Adachi et al. (2009b) observed that slender dendritic processes were more sensitive to mechanical deformation than the cell body when coated microparticles were attached to the cell membrane and subject to measured displacements. Burra et al. (2010) showed that intact integrin attachments on the processes were required for entry of Lucifer yellow tracer into the cell after hydrodynamic stimulation of dendritic processes. Stimulating forces in these studies were in the nN range rather than in the pN range, and exceeded the force range predicted to occur at integrin attachment sites *in vivo*, however, they have also implicated important mechanotransduction mechanisms to be in osteocyte cell processes.

A unique aspect of the SFSP was its ability to focally deform regions of the cell at pN level forces along the length of the dendritic process. One could accurately determine local attachment sites along the length of the dendritic processes by identifying locations where there was no discernible cell process deflection. Cellular responses to these pN level forces could be recorded real-time causing a hyperpolarization of the cell, and this provided insight into how an osteocyte would respond to

physiological loading *in vivo.* This experimental system is used to mimic tensile forces of 1-10 pN produced near focal attachment sites *in vivo* by load induced radial strains in the cell process, and were below the force necessary to rupture $\alpha_v\beta_3$ integrin attachments (Litvinov et al., 2003).

In summary, our results in **Fig. 21c, d** and the results in Table 2 indicate that physiological forces between 1 and 2.3 pN applied at focal attachment sites on cell processes led to responses that were 300 times the average electrical charge and 7 times the average peak conductance of those of the cell body. These observed changes in cellular conductance in MLO-Y4 cells are indicative of molecular and ionic fluxes passing through the cell membrane in response to external stimulation occurring upstream or independent of signaling pathways such as Ca^{2+} release, and only detected by the whole-cell voltage-clamp technique of high sensitivity. Studies are currently underway to determine the components of the complex, possibly containing $\alpha_v\beta_3$ integrin and a mechanically sensitive ion channel permeable to molecules such as ATP, PGE_2, and other signaling molecules pertinent to osteogenesis and bone maintenance.

Chapter 4: Intercellular signaling pathways in MLO-Y4 cells

4.1. Introduction

Increasing evidence indicates that bone homeostasis and osteogenic remodeling require mechanical loading of whole bone tissue (Chow et al., 1998; Moustafa et al., 2011; Rubin et al., 2002; Turner and Robling, 2005). Interstitial fluid in bone passes through hierarchical levels of porosity when bone tissue is deformed by external loads, and is the medium that translates endogenous whole tissue mechanical loads to cellular level forces in bone. The magnitude of endogenous forces acting on osteocytes *in vivo* has been a major challenge to measure experimentally, but a principal parameter when investigating force-induced cell signals *in vitro*. Theoretical models of *in vivo* forces acting within the bone porosity of the lacunar-canalicular system (LCS) that contain osteocytes were developed (Han et al., 2004; You et al., 2004), and have predicted forces on attachment sites along the osteocyte cell process (Wang et al., 2007) that guided the development of a hydrodynamic force probe to focally stimulate osteocytes *in vitro* at *in vivo* level forces (Wu et al., 2011). Intercellular signaling throughout an extensive network of mechanosensitive osteocytes is of particular interest for understanding the degree of influence osteocytes have on their microenvironment.

Osteocytes are positioned throughout the bone tissue and respond to forces distributed at a cellular level. Force-induced cell signals are relayed throughout the network directly through gap junction channels and indirectly via the release of chemical messengers acting on neighboring cells. Intercellular signaling is mediated directly by gap junctions that allow diffusional exchange of nucleotides, ions, and metabolites between coupled cells (Spray et al., 1985). Gap junctions in bone cells (Doty, 1981; Palumbo et al., 1990) are comprised of connexin 43 (Cx43) (Civitelli et al., 1993) and connexin 45 (Cx45) (Steinberg et al., 1994), but the major gap junction protein between osteoblasts and between osteocytes is Cx43, encoded by the *Gja1* gene. A recent illustration of calvarial osteocytes *in vivo* directly communicating through gap junction*s* was shown by fluorescence recovery after photobleaching (FRAP) (Sugawara et al., 2011). Conditional ablation of the *Gja1* gene in mice osteoblasts and osteocytes attenuated the anabolic effect of mechanical stimulation on bone (Grimston et al., 2008) and demonstrated the importance of Cx43 in mechanically induced osteogenic bone remodeling. Dye injection assays in primary cultures of isolated osteocytes demonstrated that they similarly form gap junctions and communicate directly *in vitro*

(Gu et al., 2006; Kamioka et al., 2007). Osteocyte-like MLO-Y4 cells also exhibited a level of dye coupling comparable to that of primary cultured osteocytes (Yellowley et al., 2000), and have been shown to communicate via transmission of calcium waves across large distances within a cultured cell network (Huo et al., 2010).

Major signaling molecules reported to interact with osteocytes in bone to achieve tissue level homeostasis and remodeling include adenosine-5'-triphosphate (ATP) (Li et al., 2005; Orriss et al., 2010), prostaglandins (PG) (Raisz et al., 1993), nitric oxide (NO) (Chow et al., 1998), Wnt (Baron and Rawadi, 2007), vascular endothelial growth factor (VEGF), receptor activator of nuclear factor kappa-B ligand (RANKL), osteoprotegerin (OPG) (Cheung et al., 2011; Kennedy et al., 2012), and macrophage colony stimulating factor (M-CSF) (Al-Dujaili et al., 2011). Demonstration of intercellular signaling via indirect pathways, such as intercellular potentiation of Ca^{2+} waves was recently performed in intact native osteocyte networks (Ishihara et al., 2012). Autocrine/paracrine signaling of osteocytes has been shown to occur in culture through the force-mediated mobilization and action of molecules such as ATP (Li et al., 2005), PGE_2 (Kitase et al., 2010; Klein-Nulend et al., 1997), NO (Vatsa et al., 2007; Zaman et al., 1999), VEGF (Thi et al., 2010a), RANKL, OPG (You et al., 2008), and Ca^{2+} (Adachi et al., 2009b). Signaling molecules are mobilized by activation of integrins (Litzenberger et al., 2010; Miyauchi et al., 2006), mechanosensitive channels (Bett and Sachs, 2000; Ryder and Duncan, 2001), and purinergic P2 receptors (Abbracchio and Burnstock, 1994; Ito and Dulon, 2002; Li et al., 2000). These signaling mechanisms are expressed in osteocytes (Thompson et al.; Young and Pavalko, 2011) and are implicated to initiate and potentiate pertinent intercellular signals within an osteocyte network to influence its microenvironment.

The investigation of distinct intercellular signaling pathways between osteocytes during steady state and dynamic environments mediated by force would provide insight into how osteocytes communicate in a network. Dual whole-cell patch-clamp electophysiology, initially devised to characterize voltage sensitivity in gap junction channels in embryonic cells (Spray et al., 1979) and routinely used to investigate electrical coupling in isolated cells (del Corsso et al., 2006), was integrated with the SFSP technique to provide physiological hydrodynamic stimulation to osteocyte cell processes while monitoring real-time cellular changes. These techniques were used to characterize direct gap junctional signaling and indirect

intercellular signaling between cells with high spatial and temporal resolution.

Experimental objectives were to (1) characterize intercellular signaling dynamics under steady-state conditions and during focal stimulation, and (2) to evaluate mechanisms that mediate rapid direct and indirect signaling in the bone cell network by using a culture model of osteocyte-like MLO-Y4 cell networks. Our finding, that MLO-Y4 cells utilize at least two distinct intercellular communication pathways in response to physiological force perturbation, is the first demonstration of discrete parallel communication pathways of mechanotransduction utilized by the cells to initiate and potentiate signals throughout an osteocytic network. This finding provides important new understanding of how bone cells respond to their dynamic external environment.

4.2. Materials and Methods

4.2.1. Cell culture

The osteocyte-like cell line MLO-Y4 (Bonewald, 1999; Kato et al., 1997) was cultured on 12 mm coverslips coated with 0.3% rat-tail collagen type-1 (BD Biosciences, 354236) in α-minimal essential medium (α-MEM) (Gibco, 12571) supplemented with 2.5% fetal bovine serum (FBS) (EMS, 15710), 2.5% bovine serum (BS) (Sigma, C3881) and 1% penicillin and streptomycin (PS) (Sigma, P7643) and maintained at 37°C in a 5% CO_2 incubator. All experiments were performed within 2-4 days after plating.

4.2.2. Electron Microscopy

Cells were grown as described above, and fixed at room temperature with 2.5% glutaraldehyde (EMS, 16020) in a 0.1M sodium Cacodylate buffer for 20 min. The samples were then sputter-coated with carbon prior to imaging with a JEOL 100 CX II high resolution scanning electron microscope at 80 keV and 500-35k magnification. ImageJ (NIH) was used for dimensional analysis.

4.2.3. Immunohistochemistry

Connexin43 and F-actin Cells were fixed with 4% paraformaldehyde (EMS, 15710), permeabilized with 0.1% Triton X-100 (Gibco, 25052), and blocked with 1% albumin from bovine serum (BSA) (Sigma, A7906) in 1xPBS at pH 7.4. Cells were incubated with Cx43 primary polyclonal antibodies (Sigma,

C6219), followed by secondary antibody conjugated to Alexa Fluor 594 (Molecular Probes, A-11012) to tag Cx43 proteins, and with Alexa 488-labeled Phalloidin Conjugate (Molecular Probes, A-12379) at 1:200 for 1 hr to label F-actin. The 12 mm coverslips were mounted on microscope slides (FisherBrand, 12-550-343) with mounting media containing 4', 6-diamidino-2-phenylindole (DAPI) (Sigma, D9542) for nucleus staining, and imaged using a 60X oil objective (N.A.= 1.4) on a Confocal Microscope (Zeiss) and analyzed using LSM Image software (Zeiss).

Connexin43 and $\alpha_v\beta_3$ integrin Fixation of cells was performed with 4% formaldehyde, permeabilized with 0.4% Triton X-100 (Sigma), and blocked with 1% BSA in 1XPBS. For Cx43 and microtubule staining, the cells were incubated with primary polyclonal antibodies against Cx43, β-tubulin, or $\alpha_v\beta_3$ (Sigma, LM-609) followed by incubation with secondary antibody conjugated to Alexa 488 or 594 (Molecular Probes). For F-actin staining cells were incubated in Alexa 488-labled phalloidin (Sigma) immediately after fixation. The coverslips were mounted on microscope slides with mounting media containing DAPI for nucleus staining, and imaged using a 40X oil objective on the Nikon Eclipse TE300 microscope with SPOT-RT software (Diagnostic Instruments, Sterling Heights, MI) or using a 60X oil objective (N.A. 1.4) on the Confocal microscope (Zeiss) with LSM Image software (Zeiss).

4.2.4. Electrophysiology

Conventional electrophysiological techniques were used in the whole-cell voltage-clamp mode to study membrane conductance during steady state and dynamic conditions. Borosilicate glass pipettes of 4-5 MΩ resistance were pulled with a P-97 Pipette Puller (Sutter Instruments) filled with internal solution ([mM], 130 CsCl, 0.5 $CaCl_2$, 10 EGTA, 10 HEPES; pH 7.3 using KOH) and were used to control the potential of the cell and for measuring current. MLO-Y4 cells were studied in external solution ([mM], 140 NaCl, 2 CsCl, 2 $CaCl_2$, 1 $MgCl_2$, 5 HEPES, 4 KCl, 5 glucose, 2 sodium pyruvate, 1 $BaCl_2$; pH 7.4 using NaOH) during recordings, and currents were acquired with an amplifier (Axopatch 200B, Molecular Devices) and digital oscilloscope (GDS-1022, GW Instek); signals were recorded using a data acquisition system (Axon Digidata 1400A, Molecular Devices), and analyzed with pClamp10 software (Molecular Devices). $BaCl_2$ and CsCl were used in external and internal solutions to block non-junctional K^+ currents

in order to increase input resistance and thereby improve isopotentiality of MLO-Y4 cells. Light images of cell pairs were captured using an epifluorescence microscope (Nikon Diaphot 300) and a SLR camera (Nikon 5000).

Dual whole-cell patch-clamp was utilized to directly measure junctional conductance (g_j) in cell pairs to assess electrical coupling within a network of MLO-Y4 cells. In this configuration, the cellular potential of each cell was clamped at -60 mV and controlled while measured currents were amplified and recorded, see schematic in **Figure 24a**. Voltage of two cells were independently clamped and controlled by two distinct voltage protocols. Cell 1 (C1) was subjected to a hyperpolarizing voltage-step of 10 mV for 30 ms at 10 Hz, and the voltage of Cell 2 (C2) was held constant. Resistances imposed by plasma membranes of C1 and C2 (R_1, R_2), by microelectrodes and micropipettes (series resistances: R_{s1}, R_{s2}), appositional cell process membranes of C1 and C2 (access resistances: R_{a1}, R_{a2}), and by the junction (R_j), see equivalent circuit schematic in **Figure 24b**. Current flowing via the junctions from the pulsed cell C1 into the second cell C2 is matched by the first cell with current of opposite polarity supplied by its voltage clamp to maintain a constant membrane potential (Spray et al., 1979). Therefore, junctional conductance g_j between C1 and C2 is calculated from the measured junctional current I_j that passes through junctional channels between the cell pair divided by the magnitude of the transjunctional voltage V_j ($g_j=-\Delta I_j/\Delta V_j$, where $\Delta V_j=V_{1f} - V_{1i}$ and $\Delta I_j=I_{2f} - I_{2i}$). Magnitude of g_j (nS) in cell pairs under steady-state conditions and changes in g_j as well as non-junctional electric charge (pC) under focal force stimulation via the SFSP were reported.

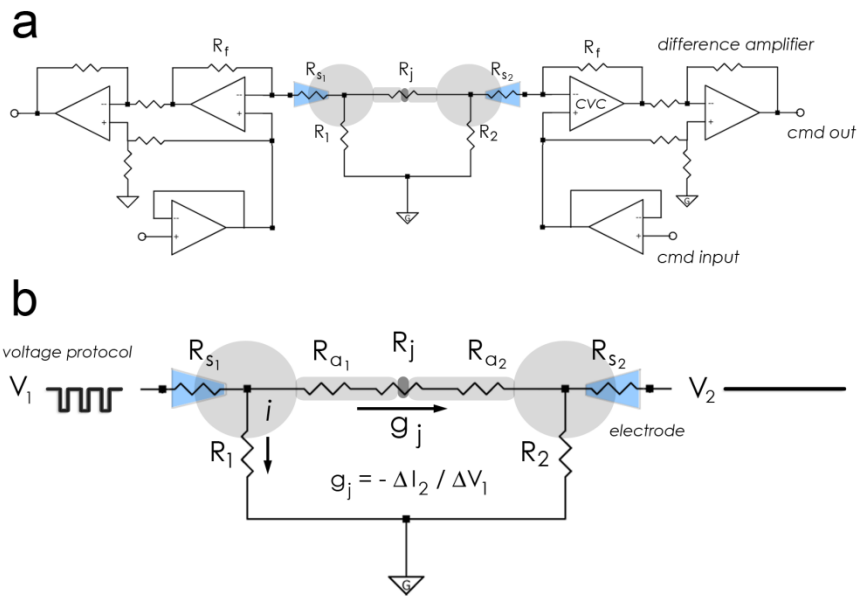

Figure 24 Schematic of the dual whole-cell patch-clamp electrophysiology technique applied to MLO-Y4 cell pairs

(a) A schematic of the dual whole-cell patch-clamp configuration used to measure junctional and non-junctional conductance in MLO-Y4 cell pairs in steady-state conditions and under dynamic SFSP stimulation. (b) An electrical equivalent circuit of a cell pair with resistances introduced from the equipment and the cell pair: series resistance R_s, cell membrane resistance R, access resistance R_a, and junctional resistance R_j. Voltage protocols were used to control the voltage of the cells. The voltage protocol applied to C1 (V_1) was a series of hyperpolarizing steps of 10 mV for 30 ms at 10 Hz and the voltage applied to C2 (V_2) was held constant at -60 mV. Cells were coupled if the junctional conductance was > 0 and was calculated from the current that passes into C2 through the junction(s): $g_j = -\Delta I_2/\Delta V_1$.

4.2.5. Dye Transfer

Lucifer Yellow CH dilithium salt (LY) (457 MW, Sigma, L0259) was used to stain MLO-Y4 cells that communicated through gap junctions. The gap junction permeable bright fluorescent dye filled the

cytoplasm of the injected cell and passed into that of neighboring cells via gap junctions. Images of the LY dye transfer were captured with an epifluorescence microscope (Nikon Diaphot 300) and a SLR camera (Nikon 5100) at an acquisition rate of 1 frame/s for at least 3 min. In some cases, electrical quantification of g_j using dual patch-clamp was performed concurrently with LY dye transfer in the same pair. LY dye was readily retained in cells and did not interfere with electrical measurements.

4.2.6. Connectivity

Connectivity between pairs of MLO-Y4 cells was defined by the number of connections between cells. To objectively characterize connectivity in a pair, we assigned topological orders of each branch segment in a cell process emanating from cell bodies of the pair, and counted the number of junctions between adjacent cell processes at adjacent segments with highest topological order, see **Figure 30**. Cell pairs were categorized by the number of cell process junctions (CPJ) between two cells where the numeric followed by the *CPJ*- is the number of junctional interfaces between the pair: CPJ-1, CPJ-2, CPJ-3, and CPJ-4^+ (CPJ-4^+ denotes connectivity of four or higher).

4.2.7. Stokesian Fluid Stimulus Probe

The Stokesian Fluid Stimulus Probe (SFSP) was used to apply focal pN level loads to distinct regions of a cell process as previously described in Wu et al. (2011) while real-time cellular-level responses were recorded. Cell processes were either stimulated at (1) an appositional cell process region between the pair or (2) a distal region of an un-apposed cell process emanating from a cell in the pair, see **Figure 25** for illustration of microelectrode and micropipette placement. Cellular responses were only seen when little to no cell process deflection (<1 μm) resulted from SFPS stimulation.

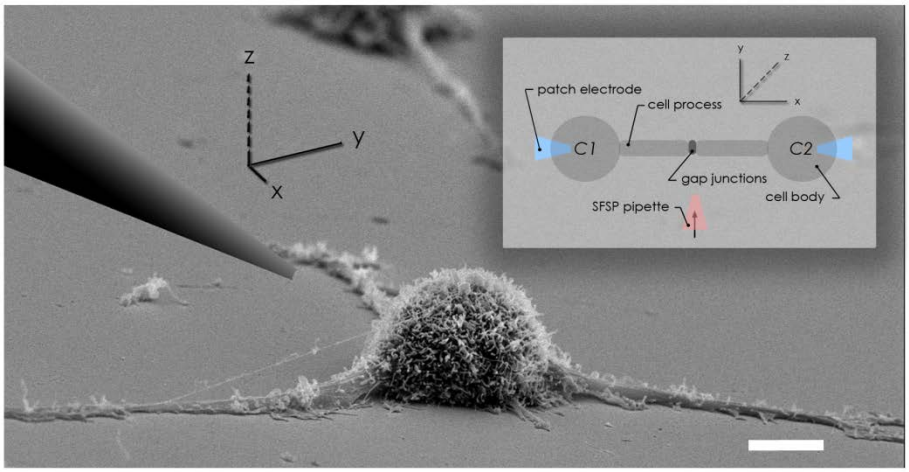

Figure 25 Stokesian Fluid Stimulus Probe (SFSP) integrated with dual whole-cell patch-clamp electrophysiology

A scanning electron micrograph of a single MLO-Y4 cell with superimposed images to illustrate placement of experimental microelectrodes and/or micropipettes. Translation of the SFSP microelectrode in three dimensions enabled fine positioning of the force probe set for focal stimulation. SFSP stimulation was directed at regions along appositional (red micropipette in inset) or un-apposed cell processes (shaded micropipette in SEM image) to introduce physiologic pN level forces to principal mechanosensitive regions.

4.2.8. Pharmacology

A broad-spectrum purinergic receptor blocker, suramin (50 µM, Sigma, P7643) was applied to explore the role of P2Rs in intercellular signaling (Hoyle et al., 1990; Suadicani et al., 2010). Membrane currents were measured in response to stimulation of distal regions of an un-apposed cell process in the presence and absence of suramin (incubation for 2-3 min). In order to compare effects of suramin on C1 and C2 and to keep effector responses of C2 paired with its force-induced response of C1, C2 responses were normalized to its respective C1 responses in the presence and absence of suramin. In all experiments, subsequent SFSP-stimulations were applied after the membrane potential returned to baseline.

4.2.9. Statistical Analysis

All quantified values were shown as mean ± SEM and *n* is the number of cell pairs on which measurements were made. Unpaired and paired student t-tests were used to identify differences between groups, asterisks indicated significant differences compared with reference controls (*p<0.05, **p<0.01). A one-way ANOVA was used in the connectivity analysis to identify differences between groups and a p-value<0.05 indicated significant differences. Transient changes in coupling were calculated using normalized values to compare relative changes of direct intercellular communication among cells differing in junctional conductance. Non-junctional SFSP-induced effector responses of C2 were normalized with respect to the force-induced response of C1, and similarly for responses in pharmacological conditions. Electrophysiological recordings were analyzed using PClamp10 (Molecular Devices), Origin 5.0 (Microcal), and ImageJ (NIH). Prism 5.0 (GraphPad) was used for statistical analysis.

4.3. Results

4.3.1. Electrical coupling in MLO-Y4 cells

MLO-Y4 cells on collagen type**-**1 coated coverslips in culture exhibited a dendritic morphology, with cell processes forming interconnected networks with neighboring cells (**Fig. 26**). MLO-Y4 cell pairs with apposed cell processes (**Fig. 26a**) had cells bodies that were rounded and cell surfaces that appeared somewhat ruffled with microvilli- and ribbon-like protrusions of varying dimension (**Fig. 26b**). These microvilli-like structures had cytoplasmic and cytoskeletal components, such as F-actin (immunocytochemistry data not shown), and varied in length with diameters in the range of 100-140 nm. These structures that surrounded the cell body were more uniformly ~ 1 μm and occasionally up to 3 μm in length, and were less prominent and more sparsely distributed on cell processes. In confocal images (**Fig. 26c,d**), apposed cell processes exhibited puncta of Cx43 (red), possible pathways of direct intercellular communication mediated by Cx43 gap junction channels, and F-actin (green) that highlighted the cytoskeleton of appositional cell processes. The measured diameters at the midpoint of the appositional cell processes in the SEM (**Fig. 26a**) and cell process diameter near the puncta of Cx43 in the confocal image (**Fig. 26c**) were both 0.4 μm in diameter. In the case with a pair having more than one cell

process junction (**Fig. 26d**), Cx43 puncta also appeared midway along appositional cell process likely to contribute to the passage of electrical current observed between MLO-Y4 cell pairs.

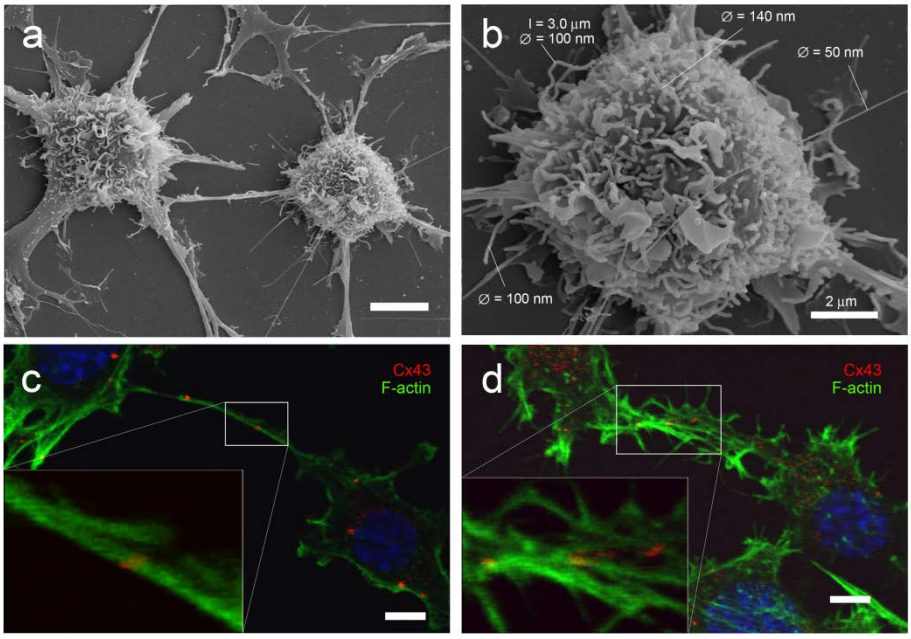

Figure 26 MLO-Y4 cells express Cx43 within appositional cell processes

(a) Scanning electron micrograph shows MLO-Y4 cells in contact with neighboring cells via dendritic cytoplasmic extensions, 5000X magnification (b) SEM of a cell body with microvilli- and ribbon-like structures protruding from the cell membrane, 9000X magnification (c) Immunohistochemistry was used to label Cx43 (red) and filamentous actin (green) in MLO-Y4 cell monolayers to locate Cx43 gap junctions in appositional cell processes that would mediate cell coupling (d) Cx43 puncta was located in more than one appositional cell process in a pair. Scale bars = 5 µm unless indicated otherwise.

Junctional conductance values of MLO-Y4 cell pairs in culture for 2-4 days ranged from 0 to 7.8 nS. A weakly coupled osteocyte cell pair had a junctional conductance of 1.5 nS (**Fig. 27**). Appositional cell processes between the pair of interest as well as other cytoplasmic cell process connections with neighboring cells were evident in light micrographs (**Fig. 27a,b**). To trace network connections between coupled cells, LY was injected into C2 and observed for 3 min. There was little dye spread to C1,

consistent with the weak electrical coupling measured from the pair, but C2 was more strongly coupled with two other neighboring cells, indicated by the dye spread, and likely having a g_j > 1.5 nS. Stronger coupling was observed between osteocytes illustrated by rapid LY diffusion into its neighboring cell (**Fig. 28**), in accordance with its measured junctional conductance of 7.8 nS.

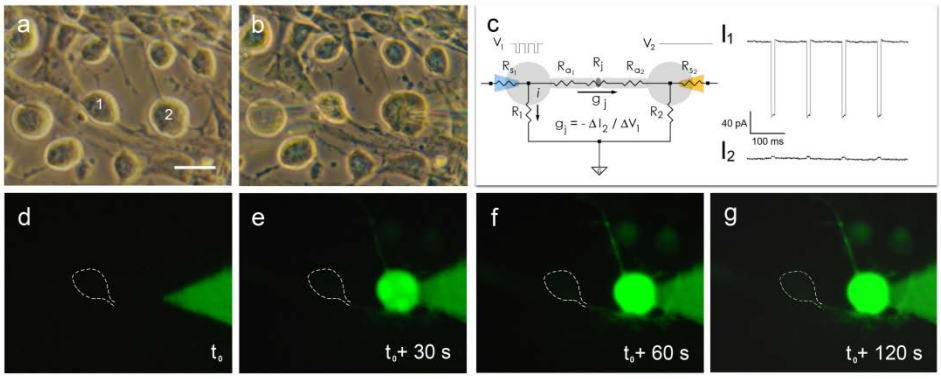

Figure 27 Measurement of junctional conductance in MLO-Y4 pairs, weak coupling

(a) MLO-Y4 cell pair prior to dual whole-cell patch-clamp and Lucifer Yellow dye transfer (b) Microelectrode placement during dual whole-cell patch-clamp and dye injection (c) Equivalent circuit superimposed on idealized cell pair to illustrate system resistances and position of LY dye filled microelectrode. Voltage protocols V_1 (hyperpolarizing voltage steps of 10 mV for 30 ms at 10 Hz) and V_2 (voltage held constant at -60 mV) were introduced to the pair and currents I_1 and I_2 were measured in response to voltage changes applied to C1. The measured junctional conductance (g_j=-$\Delta I_j/\Delta V_j$) of this pair was 1.5 nS. (d-g) To visualize intercellular communication through gap junctions, LY dye was injected into C2 and diffused into neighboring cells via gap junction channels. Epifluorescence image sequence captures the LY dye transfer for 3 min. Scale bar = 10 µm.

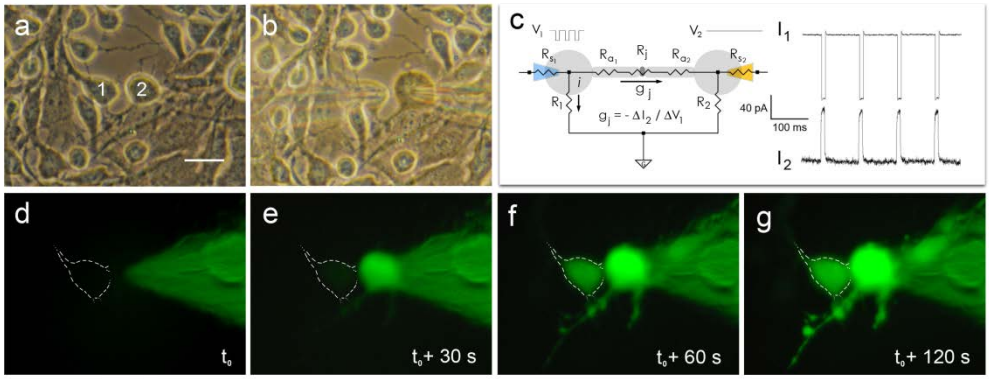

Figure 28 Measurement of junctional conductance in MLO-Y4 pairs, strong coupling

(a) MLO-Y4 cell pair prior to dual whole-cell patch-clamp and Lucifer Yellow dye transfer (b) Microelectrode placement during dual whole-cell patch-clamp and dye injection (c) Equivalent circuit superimposed on idealized cell pair to illustrate system resistances and position of LY dye filled microelectrode. Voltage protocols V_1 (hyperpolarizing voltage steps of 10 mV for 30 ms at 10 Hz) and V_2 (voltage held constant at -60 mV) were introduced to the pair while currents I_1 and I_2 were measured in response to voltage changes applied to C1. The measured junctional conductance (g_j=-$\Delta I_j/\Delta V_j$) of this pair was 7.8 nS. (d-g) To visualize intercellular communication through gap junctions, LY dye was injected into C2 and diffused into neighboring cells through gap junction channels. Epifluorescence image sequence captures the LY dye transfer for 3 min. Scale bar = 10 µm.

4.3.2. Junctional conductance and connectivity

The magnitude of junctional conductance between cells quantifies the degree of coupling between pairs and its ability to exchange chemical messengers with its neighboring cells. MLO-Y4 cell pairs that had at least 1 cell process between them were selected and measured for coupling. Measured junctional conductance between pairs ranged from 0 to 7.8 nS with a mean of 1.49±0.19 nS, n=111 for all pairs (**Fig.29a**). Not all chosen pairs were coupled even when cytoplasmic connections were apparent

between cells; coupling was found in 58% of pairs tested (**Fig. 29b**). It was important to take into account potential electrical impedances that slender and elongated cell processes would introduce (R_{a1} and R_{a2} in **Fig. 24b**) when junctional conductance was measured in cell pairs. Therefore, to determine whether or not access resistance affected the measurement of junctional conductance, MLO-Y4 pairs were separated into two categories of input resistance (< 100 MΩ or > 100 MΩ). The mean of high R_{in} recordings was not statistically different (t-test, p=0.19, n=111) from that of lower R_{in} pairs (1.18 ± 0.25 nS, $n = 46$ vs. 1.66 ± 0.26 nS, $n = 65$) (**Fig. 29c**), and therefore all g_j values were pooled for analysis. The lack of statistical difference between junctional conductance values in low or high input resistance cells indicates that the access resistance provided by the cell process is not a major restriction of current or dye spread between MLO-Y4 cells. Cell pairs with appositional cell process lengths < 5 µm and juxtaposed cell bodies had junctional conductance values up to 10 nS, n=5, and exhibited higher values because of cytoplasmic bridging or cell division. These pairs were excluded in the input resistance analysis and connectivity analysis, but were included in the percentage-coupled analysis, since those pairs would contribute to the direct intercellular signaling potential of a cellular network.

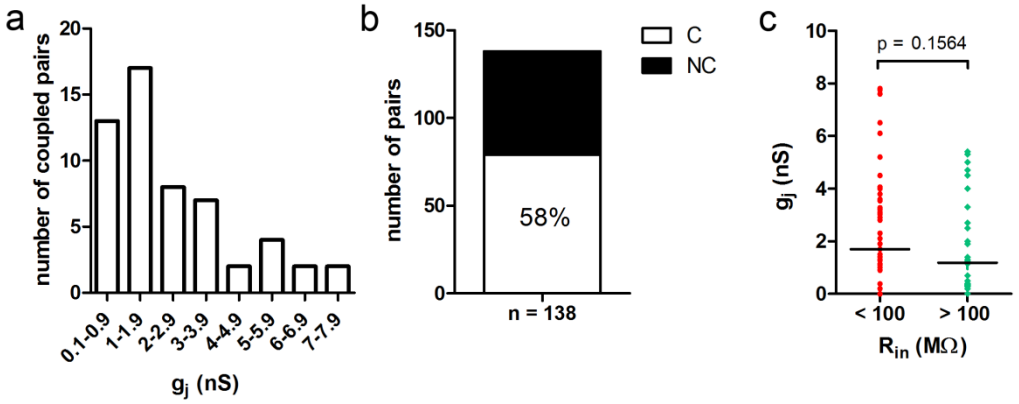

Figure 29 Comparison of junctional conductance and input resistance

(a) Electrical coupling was tested in pairs that had at least 1 appositional cell process between the pair. Junctional conductance in MLO-Y4 cell pairs ranged from 0 – 7.8 nS with a mean of 1.49±0.19 nS, n=111. (b) All MLO-Y4 pairs tested for coupling had apparent appositional cell processes, and 58% of these pairs exhibited electrical coupling mediated by gap junctions. Coupled pairs, including

juxtaposed pairs and pairs with appositional cell processes < 5 µm are included in the % coupled analysis (n=5) since those pairs would contribute to the potential for direct intercellular communication of the cell network. (c) MLO-Y4 pairs investigated for junctional conductance (g_j) were separated into two categories of input resistance (< 100 MΩ or > 100 MΩ) to identify any consequence of access resistance on the observed junctional conductance. The mean g_j between the two groups were not significantly different (t-test, $p = 0.19$, $n = 111$), and therefore g_j for all pairs tested were pooled for analysis.

The degree of coupling between cell pairs was found to be dependent upon the number of appositional cell process junctions (CPJ) between cells. A standardized and objective methodology was developed to classify connectivity between cell pairs and illustrated with 3 examples of connectedness in Figure 29a. The term connectivity of MLO-Y4 cells pairs is used to describe the number of pathways of electrical access between cells. The convergence of cell processes segments of topological order *0*, with no apparent bifurcations from the cell body to the point at which they converge, was classified as one CPJ indicated by a red line. Topological orders of cell process segments in pairs with > 1 appositional cell processes were similarly determined, and cell pairs were categorized by their assigned CPJ number, see **Fig. 30c-e** for examples of each CPJ group. Mean junctional conductance values of each CPJ group were not significantly different from one another (ANOVA, $p = 0.08$, $n = 58$), but a linear trend for increasing junctional conductance with increasing junctional connections was identified (linear regression post-test, slope $= 0.53$ $R^2 = 0.83$, *$p = 0.01$), see **Figure 30f.** This linear trend suggested cytoplasmic connectivity in coupled cells as a morphologic influence on g_j in MLO-Y4 cells. The contribution that one cell process had on junctional conductance within a pair with more than one cell process was difficult to assess. However, it was evident that no significant differences were found between groups with 1 appositional cell process (CPJ-1) or 2 (CPJ-2), and similarly between CPJ-2 and CPJ-3. Only between the groups of pairs with one appositional cell process (CPJ-1) and pairs with more than 4 appositional cell processes (CPJ-4^+), was the mean g_j of the CPJ-4^4 group significantly higher by 1.8 times than that of the CPJ-1 group (t-test, *p=0.02, n=37). The mean of the CPJ-4^+ group was still substantially higher than that of all remaining

pairs with less than 4 cell processes (t-test,** $p = 0.01, n = 58$), (**Fig. 30g**) This observation suggested that pairs with 4 or more intercellular junctions would achieve coupling near 3.6 nS or higher in MLO-Y4 networks to increase its potential for direct intercellular communication in the network. Distances between neighboring MLO-Y4 cell body centroids were 33.86±1.75 µm, n=58.

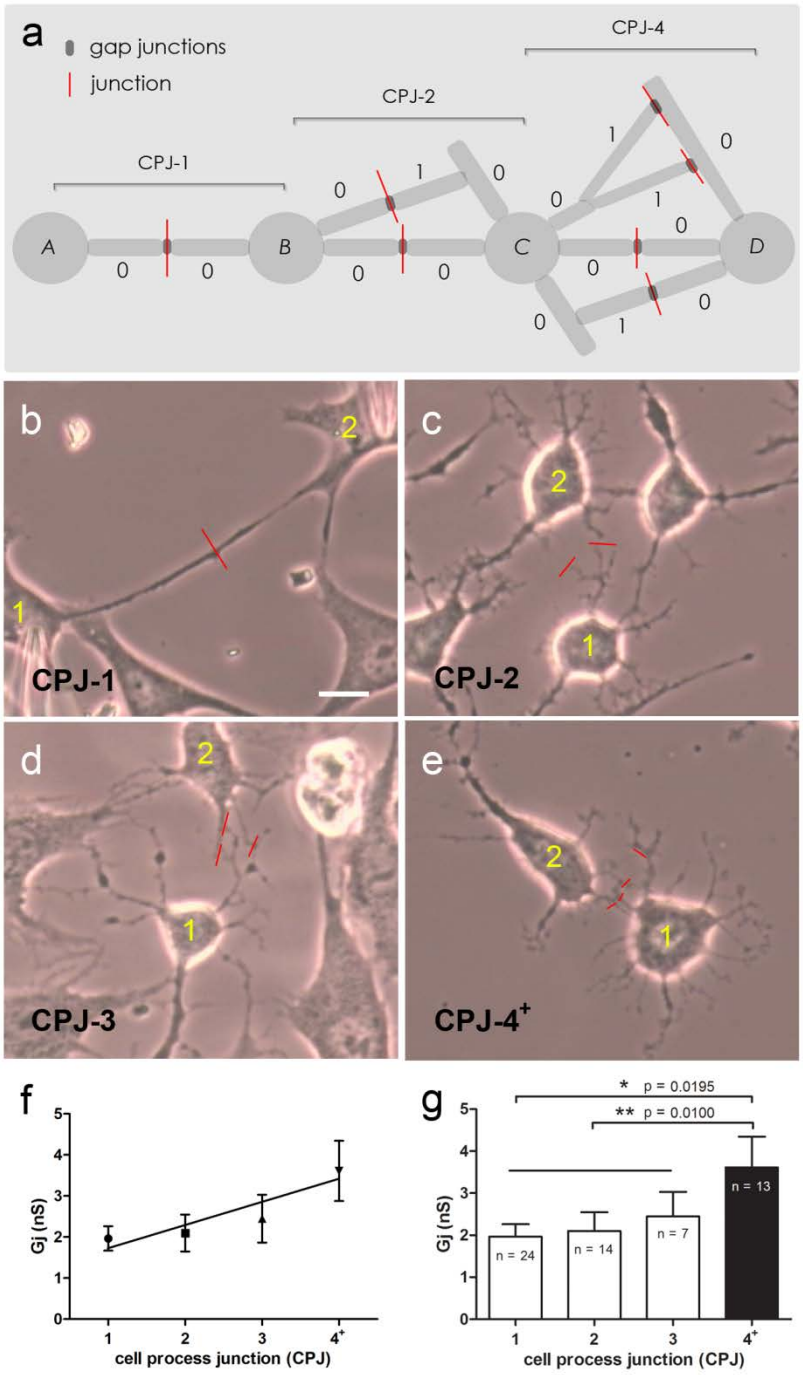

Figure 30 Junctional Conductance in MLO-Y4 pairs

(a) MLO-Y4 pairs were grouped according to the number of cell process junctions (CPJ) in a cell pair. The illustration describes the methodology of how the CPJ number for a pair was determined where each cell process segment was assigned a topological order starting at *0* for segments that originate from the cell

body and do not bifurcate. Three examples are shown using this methodology to determine the CPJ number of the pair. (b-e) Light micrographs of example pairs for each CPJ-*n* group. Junctions are indicated by the red line. (f) Significant differences between group means of g_j were not apparent (ANOVA, p=0.32, n=57), but a linear trend was found to be statistically significant (linear regression post-test, slope $= 0.53$, $R^2 = 0.83$ $p = 0.01$). (g) Significant differences in g_j were not found between CPJ-1 through CPJ-3, but pairs in CPJ-4^+ had a significantly higher mean of g_j than that of CPJ-1, and still much higher than that of CPJ-1 through CPJ-3 groups combined. Coupled pairs with at least 4 appositional cell processes had a g_j of at least ~ 3.6 nS.

4.3.3. Force mediated intercellular communication in MLO-Y4 pairs

Cell process stimulation produced by the SFSP probe is instantaneous and force rapidly dissipates from peak force (< 3 pN) to 0 pN within 100 ms. Rapid and transient changes in coupling were observed after focal cell process stimulation, and were apparent when stimulation was restricted to two particular regions: appositional cell process stimulation or distal un-apposed cell process stimulation. R_1 and R_2 are resistances introduced by the membrane of C1 and C2 respectively. R_{a1} and R_{a2} are access resistances introduced by the slender and elongated cell process membranes. R_j is the junctional resistance introduced by the appositional cell process membranes at cell-cell junctions and of the gap junctions.

Appositional cell process stimulation (**Fig. 31a**) was directed at a point along the appositional cell process between C1 and C2 (highlighted in **Fig. 31b**), and induced a rapid and transient decrease in coupling of 19% within 200 ms (**Fig 31c**). The decrease in coupling observed was either (1) a true decrease in junctional conductance by gap junction closure (R_j increase) or (2) a resultant of current shunting by an increase in non-junctional channel openings in cells. The rapid decrease in coupling indicated a transient shunting of current flow between the coupled cells when stimulated at their appositional cell processes to decrease direct intercellular communication and perhaps increase indirect intercellular communication through non-junctional pathways.

Alternatively, distal un-apposed cell process stimulation (**Fig. 31d**) directed at a cell process from only

one cell induced an increase in coupling of 11% within 200 ms (**Fig. 31f**). The stimulation either induced (1) a real increase in g_j by opening of gap junctions at the junction (highlighted region in **Fig. 31e**) or (2) a resultant increase in coupling from non-junctional membrane closures of the cell body (R_2 increase) induced by cell process stimulation (R_{a2} decrease) to preferentially direct current toward the junction. The increase in coupling suggested a force-induced change in junctional resistance, since it was less likely that this increase in g_j resulted from force mediated membrane channel closures (an increase in R_2). Focal force perturbation did not permanently alter the baseline junctional conductance between pairs, but illustrated an underlying dynamic of intercellular communication between osteocytes mediated by forces.

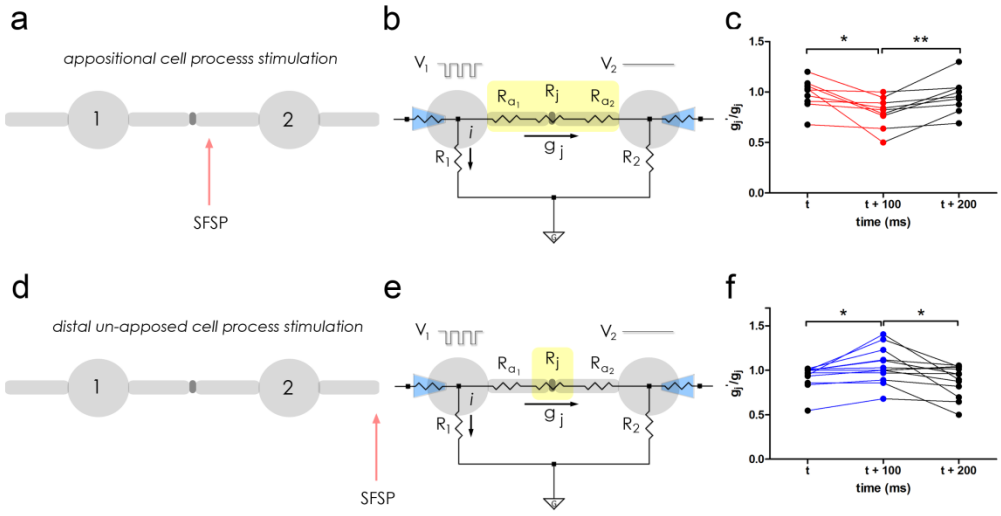

Figure 31 SFSP-induced transient changes in coupling

Changes in coupling between pairs were observed when stimulated at points within two particular regions. Stimulation directed at a point (a) along the appositional cell process (b) while electrical coupling was measured using a hyperpolarizing voltage protocol V_1, likely caused shunting of current near the junction represented in (c) the decrease in junctional conductance of 19% (paired t-test, n=9, p=0.015) followed by rapid recovery in coupling of 17% (paired t-test, p=0.005, n=9) observed. Stimulation directed at a (d) distal un-apposed cell process of the pair (e) while electrical coupling was measured, likely altered the junctional resistance R_j, to (f) induce an increase in junctional conductance by 13% (paired t-test, n=13, p=0.013) followed by recovery of 17% (paired t-test, p=0.013,

n=13). The changes in junctional conductance after stimulation were not significantly different from the baseline junctional conductance in both cases, but illustrated an underlying dynamic of intercellular communication between osteocytes mediated by focal forces.

Direct pathways of intercellular communication were not the only form of communication with which MLO-Y4 cell pairs communicated. To explore the role of the paracrine ATP-mediated signaling, we stimulated the cells in the presence of suramin. In the suramin study, we chose pairs that formed multiple connections with each other but minimal connections, if any, with other neighboring cells. A distal un-apposed cell process from C1 received the SFSP stimulation and induced a C1 response. C2 received the SFSP-induced response of C1 and subsequently responded. C1 and C2 responses were paired and measured in the absence or presence of suramin. The responses of two particular pairs in both conditions are shown in **Figure 32a,b,d,e**, and affirmed force-induced ATP-release mediated by P2Rs in MLO-Y4 cells (black traces) and illustrated a reduction of intercellular communication in the presence of suramin (red traces). Measurements of C1 and C2 responses in conditions with and without suramin incubation (**Fig. 32c**) were normalized (**Fig. 32f**) and a significant decrease in C2 responses of ~27% was observed in the presence of suramin (t-test,p=0.02, n=4). The decrease in response of the effector cell was less for electrically coupled pairs ~ 6-16%, and provided evidence that MLO-Y4 cell pairs communicated using both direct and indirect signaling pathways simultaneously.

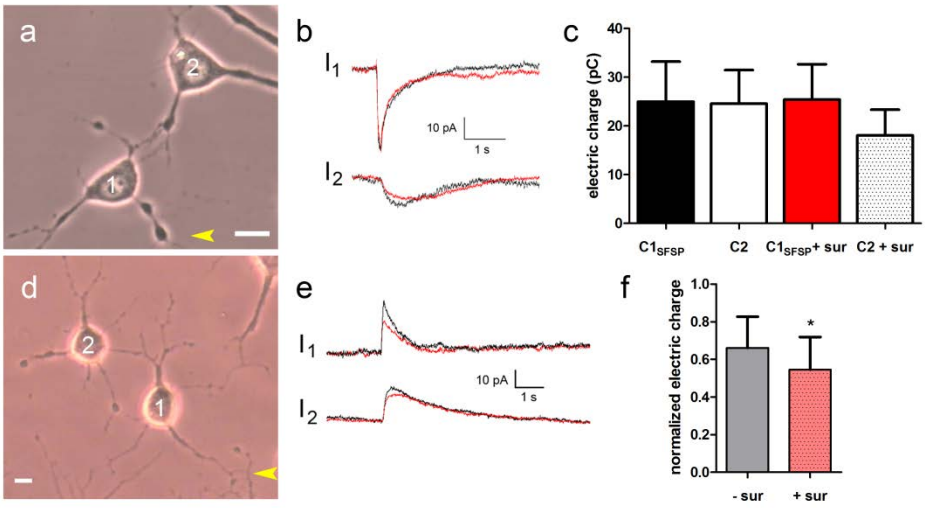

Figure 32 Effect of suramin on SFSP-induced intercellular signaling

(a) A light micrograph of an MLO-Y4 pair with a junctional conductance of 0.2 nS. Distal un-apposed cell process stimulation of C1 (indicated by the yellow arrow) (b) induced a response in C1 and C2 without suramin (black traces) and with suramin (red traces) incubation. The broad-spectrum P2R antagonist, suramin (50 μM), reduced the electric charge response in the effector cell (normalized to its respective C1 response) by 16% and also confirmed ATP-mediated P2R signaling in MLO-Y4 cells. (c) Electric charge responses of C1 and C2 after C1 cell process stimulation in conditions without and with suramin, *sur*. (d) A light micrograph of an MLO-Y4 pair that exhibited no electrical coupling. Distal un-apposed cell process stimulation of C1 (indicated by the yellow arrow) (e) induced a response in C1 and C2 without suramin (black traces) and with suramin (red traces) incubation. Suramin suppressed the normalized electric charge response in the effector cell by 20%. (f) A significant 27% suppression in P2R mediated intercellular communication induced by suramin incubation was observed (paired two-tailed t-test, $p = 0.02$, $n = 4$). Scale bars were 5 μm and yellow arrow heads indicated location of focal SFSP stimulation.

4.4. Discussion

Force-induced cell membrane conductance changes by activation of signaling mechanisms were initiated by the SFSP probe (Wu et al., 2011) and monitored using electrophysiology of high temporal resolution to observe autocrine and paracrine signaling through the action of numerous nucleotides and mobilization of ions and paracrine signaling molecules. Other culture systems have shown that larger networks of osteocytes respond to forces imposed by fluid shear stress (FSS) and substrate stretch as well as to higher magnitude plasmalemmal indentation by releasing nucleotides and divalent cations such as Ca^{2+} as well as PGE_2 and NO into the extracellular space. Principal plasma membrane associated mechanisms such as integrins (Litzenberger et al., 2010; Litzenberger et al., 2009; Miyauchi et al., 2006; Plotkin et al., 2005) and ligand-gated receptors, particularly purinergic receptors (Genetos et al., 2007; Li et al., 2005) and hormone receptors (Gu et al., 2001b) are implicated to rapidly initiate cellular responses of osteocytes.

These candidate molecular mediators were investigated to characterize rapid and transient intercellular signaling dynamics between MLO-Y4 cell pairs. SFSP stimulation and activation of these mechanisms directly mobilized small allosteric second messengers and potentially larger signaling molecules through cell junctions and non-junctional membrane pores. Intercellular communication has been known to be effective when mediated by second messengers, since they freely diffuse because of their small size and have low binding affinity to produce fast responses over some distance.

Two types of signaling, direct junctional- and indirect non-junctional communication, were observed to mediate intercellular communication between MLO-Y4 pairs in culture. Coupling between pairs was evident in 58% of cell pairs investigated and coupled pairs exhibited a mean junctional conductance of 2.4 ± 0.3 nS that rapidly and transiently changed at the onset of cell process stimulation. An expected shunting of current was observed when the current path in the cell process was perturbed, and suggested opening of non-junctional channels to mediate indirect pathways for chemical signaling. However, an increase in coupling was observed when non-junctional cell processes were stimulated. Non-junctional cell processes are also representative of appositional cell processes that were not communicating directly via gap junctions that were also present in our culture. The unexpected transient increase in coupling between MLO-Y4 could have opened gap junctions to increase the potential for metabolic exchange

between the pair. An increase in junctional conductance has previously been reported to be the action of cyclic adenosine monophosphate (cAMP) that increased coupling between cells up to 46% (van Rijen et al., 2000). It is plausible that osteocytes can mediate how they communicate with their neighboring cells over short and larger distances when initiated by particular forces.

MLO-Y4 pairs also communicated after cell process stimulation through indirect signaling mechanisms. P2R signaling dynamics were investigated using the broad-spectrum P2 receptor antagonist, suramin. Effector responses of MLO-Y4 cells were reduced after suramin incubation consistent with suramin binding to P2Y and P2X receptors blocking the action of ATP on these receptors and subsequent signaling cascades (Gunosewoyo et al., 2007). The effect of suramin was less potent on electrically coupled pairs, and provided evidence that tandem signaling, direct and indirect, in MLO-Y4 cells was advantageous under inhibited conditions. It also demonstrated that the direct exchange of metabolites through gap junctions and indirect autocrine/paracrine signaling were not mutually exclusive events. Different polarities of responses may be attributed those ions, Na^+, K^+, and Cl^-, that carry the current flowing across the cell membrane during activation.

G-protein coupled P2Y receptors are also activated by ATP to initiate IP_3 production via phospholipase C (PLC) which initiated IP_3 binding to IP_3 receptors on the endoplasmic reticulum (ER) inducing Ca^{2+} release that can also trigger the calcium-induced calcium-release signaling cascade. Activation of the G-protein coupled receptor such as the P2YR would assist in the potentiation of calcium signals throughout the bone network, and is captured using calcium imaging dyes visualizing transients that last for many seconds to minutes. The activation and signaling of fast-acting inotropic P2X receptors (P2XRs) is more likely what is seen in these recordings of rapid and transient changes in conductance lasting only a few seconds. P2XRs are involved in the activation of particular signaling cascades, for example, $P2X_7R$ pores, activated by ATP can induce an elevation of intracellular calcium levels that diffuse through gap junctions, and release cytosolic Ca^{2+} as a second messenger can act on a population of neighboring cells (Scemes and Giaume, 2006). Also, continuous stimulation of the $P2X_7R$, in astrocytes cause further release of larger molecules up to 900 Da, including ATP, through the recruitment of the pannexin1 (Panx1) channel forming complex (Iglesias et al., 2009), and the release of ATP further activates purinergic receptors on neighboring cells (Scemes and Spray, 2012; Suadicani et al., 2003) .

Larger autocrine and paracrine signaling molecules in bone, for example, and OPG, RANKL, and VEGF would be released from the cell along with PGE_2 (Kitase et al., 2010; Li et al., 2005), NO (Zaman et al., 1999), K^+ (Gu et al., 2001a) and other non-selective divalent ion channels (Guo et al., 2006), with the persistent ATP (Genetos et al., 2007) activation of the $P2X_7R$-pannexin1 (Panx1) hemichannel forming complex. This particular P2 receptor signaling pathway may partially explain the alteration in metabolic influence that mechanical loading had on bone formation in the absence of $P2X_7Rs$ (Li et al., 2005) and may work in coordination with other P2Rs present in bone (Ke et al., 2003; Orriss et al., 2010).

MLO-Y4 cells could improve coupling with their neighboring cells by increasing cell process convergence and/or connections within its network. An increase in connections between coupled MLO-Y4 cells in culture improved junctional conductance between pairs. The degree of interconnectivity of osteocyte cell processes in cortical bone are illustrated by stains (Kusuzaki et al., 1995) and tracers (Ciani et al., 2009) filling the lacunar-canalicular system (LCS), and by 3D computational renderings of the osteocyte cell network (Himeno-Ando et al., 2012). Osteocytes *in vivo* contain at least 41 to 50 emanating cell processes, in human bone (Beno et al., 2006) and mouse parietal bone (Sugawara et al., 2011) respectively, and those cell processes provided pathways for direct communication with more than one neighboring cell at any time. Osteocytes may regulate the amount of Cx43 at its membrane by regulating β-catenin production through the Wnt-1 signaling pathway as evidenced in cardiac myocytes (Ai et al., 2000). The connectivity of cell processes only modestly predicted intercellular communication, since electrical coupling was confirmed in 58% of those cytoplasmically connected pairs. An inherent redundancy created by the multitude of appositional cell processes between osteocytes *in vivo* would not remove gap junctional communication completely. Also, since the use of alternative signaling pathways was apparent, osteocytes could maintain some degree of intercellular communication with neighboring cells independent of their degree of coupling.

In summary, the force-mediated indirect and direct intercellular signaling mechanisms are illustrated in **Figure 33**. SFSP stimulation initiated an adhesion-mediated opening of ion channels (**Fig. 33-1**). The opening of ion channels induced release of ATP (**Fig. 33-2**) that in turn activates P2Rs (**Fig. 33-3**). Activation of the P2XR induces an influx of calcium that may diffuse to the neighboring cell through gap junctions or through a recruited pore forming Panx1 channel that would further mobilize calcium or other

signaling molecules into the extracellular space. ATP-mediated activation of phospholipase C (PLC) via the P2YR induces IP_3 production to regulate the release of Ca^{2+} from internal stores by IP_3 receptor (IP_3R) activation (**Fig. 33-4**). Mitochondria also play a role in modulating intracellular calcium levels through the Na^+/Ca^{2+} exchanger (Reyes and Parpura, 2008) (**Fig. 33-4**) and would also contribute to available cytosolic calcium for the potentiation of calcium signaling in osteocytes.

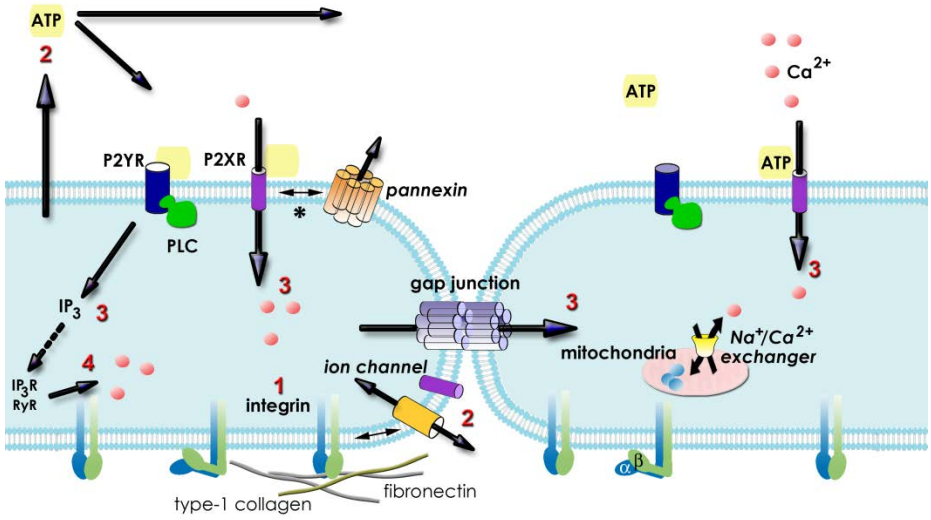

Figure 33 Parallel Intercellular Signaling in MLO-Y4 cells

MLO-Y4 cells plated on a thin layer of type-1 collagen to encourage cell-substrate attachment utilize rapid direct and indirect signaling in response focal stimulation. SFSP stimulation activates an adhesion-mediated ion channel opening (Fig. 33-1) to release ATP into the extracellular space (Fig. 33-2). ATP is known to activate G-protein coupled P2Y and ionotropic P2X receptors to induce the mobilization of chemical messengers, such as Ca^{2+}, into the cell that further spread throughout the cell network via gap junctions (Fig. 33-2). ATP and possibly other chemical messengers can be released from the cell through a non-selective Panx1 hemichannel pore that is recruited after sustained ATP activation of the $P2X_7R$. Simultaneous activation of plasma membrane bound phospholipase C (PLC), via P2YR activation, induces IP_3 production to mediate the release of Ca^{2+} from internal stores by IP_3 receptor (IP_3R) activation on the endoplasmic reticulum (ER)

(Fig. 33-4). The subsequent increase in cytosolic calcium induces calcium release through membrane channels into the extracellular space to maintain a high calcium concentration gradient across the membrane. Mitochondrial Na^{+}/Ca^{2+} exchangers would also contribute to elevated cytosolic calcium concentrations by ionic buffering in the regions distant from other internal calcium stores to potentiate direct and indirect intercellular signaling within the cellular network.

Osteocyte signaling, in the context of its native microenvironment, is induced by tensile forces at membrane attachment sites along cell processes created by fluid-flow in the LCS porosity. These signals are mediated by 'loose' cell process attachment to its canalicular wall via traversing tethering fibers and 'firm' cell process attachment to the canalicular protrusions that span the pericellular space (Han et al., 2004; Wang et al., 2007). Mechanisms of amplification within the osteocytic network facilitate the activation and potentiation of intercellular signals between osteocytes. A recent study using a postmenopausal osteoporotic murine model identified a significant increase in lacunar-canalicular porosity in the ovariectomized animals compared to controls (Sharma et al., 2012), and this increased spacing of the pericellular matrix likely compromised the adhesion-mediated activation of osteocytes in the LCS where a major phenotype for these estrogen-deficient animals is the loss of bone mass.

The osteocyte network could utilize parallel signaling pathways to overcome inherent instabilities in the network that may arise during homeostasis and remodeling. Intermittent and persistent changes in a complex loading environment may be sensed by osteocytes to preferentially send signals to influence various micro-architectural changes at the tissue level. The potency of this influence is dictated by available minerals and metabolic substances within the microenvironment as well as the integrity of the osteocytes and the LCS microenvironment in which they reside. The understanding of how osteocytes initiate chemical signals in response to mechanical cues to trigger osteogenic influence on neighboring bone cells *in vitro* and *in vivo* would have major implications for bone tissue engineering and rehabilitative treatments that address conditions of injury/pathology of bone to restore its osteogenic nature.

Chapter 5: Summary statements and future directions

5.1. Summary statements

The aim of this dissertation was to stimulate osteocytes in a physiologically relevant manner to identify mechanosensitive regions involved at the early onset of osteocyte signaling. Osteocytes are implicated to be the mechanosensitive cell in bone connected to other osteocytes to form networks ideal for transmission of signals throughout the bone matrix. When an osteocyte is loaded in its three dimensional matrix, the cell body and the cell processes are not exposed to the same forces. Mimicking *in vivo* forces *in vitro* has been a major challenge in studying mechanotransduction in osteocytes, and a new technique has been developed to overcome this challenge: the Stokesian Fluid Stimulus Probe (SFSP). Two major findings from these functional experiments using the SFSP were: (1) osteocyte dendritic cell processes are the mechanosensitive regions of the cell and (2) stimulation of a focal attachment complex along the cell process at 1-10 pN was enough to initiate early changes in cellular conductance

. The primary objective was to develop a probe that hydrodynamically stimulated focal regions of the osteocyte cell process separately from the cell body and the characterization of the new SFSP is described in Chapter 2. A microejection system previously used for pharmacological studies was used to eject a spherical hydrodynamic stimulus designed to produce pN level forces that were applied to osteocyte-like MLO-Y4 cells *in vitro*. Tracer studies were performed to determine the shape of bolus and two key relationships were apparent: $Re_t = \frac{2\rho U_t R_t}{\mu}$ and $Re_s \frac{2\rho U_s R_s}{\mu}$. In order to calibrate the forces produced by the SFSP, a laboratory model of hydrodynamic similarity was developed to study the ejected bolus in detail. The growth of the bolus was found to operate in a new tip Re regime where the spreading bolus was nearly spherical and closely approximated by Sampson flow. Position and pressure profiles were determined at a Re_t ~ 0.03, and predicted the SFSP to produce focal hydrodynamic forces in the range of 1-30 pN in a region 2-5 μm from the probe tip. The cellular strain amplification model most recently predicted forces from 1-10 pN to occur at discrete locations of the cell process *in vivo* (Wang et al., 2007). A force probe capable of delivering physiologically relevant forces *in vitro* is now used to focally stimulate osteocytes in culture to explore mechanosensitive regions of the cell.

In Chapter 3, mechanosesitive regions of the MLO-Y4 cell were explored using focal stimulation from the newly developed SFSP. A high sensitivity whole-cell voltage-clamp technique was used to record cellular responses of single cells during focal activation along the cell process and at the cell body. Prior to SFSP stimulation, cells were patched and held at -60 mV. It was found that focal activation at discrete attachment sites along the dendritic processes produced changes in cellular conductance indicative of ionic or molecular fluxes through the membrane. Stimulation of the cell process at non-attached sites or at the cell body did not elicit changes in cellular conductance. These findings were especially interesting since stretch activated ion channels were largely implicated to mediate intercellular communication induced by mechanical deformation caused by whole tissue loading. Our results have clearly highlighted the importance of cell process adhesions in MLO-Y4 cells for signal transduction initiation, and its multiple dendritic extensions has inherently increased the signaling potential of a single osteocyte.

A unique aspect of SFSP stimulation on the osteocyte cell process was the deflection of the cell process in cases where the cell process was loosely or not attached to the substrate. The deflection of the cell process provided a method to estimate forces exerted on the cell process as well as the lateral decay of pressures of the bolus relative to its line of action. Elastic beam theory was applied to the cell process where the concentric force acting at the midpoint of a beam is $F = \frac{48EI\delta_m}{L^3}$. The Young's modulus of a single actin filament was $E = 2.6x10^3$ pN/nm^2, and had been accurately measured by *in vitro* nanomanipulation (Kojima et al., 1994), where the effective cross-sectional area of an individual actin filament is 25 nm^2. The area moment of inertia of the 19 filament central actin bundle, from in the ultrastructural model of Han et al. (2004), is calculated to be I=8.6x10^4 nm^4. In cases where there was observed cell process deflection, measurements of the maximum deflection δ_m of the cell process, and the distance *L* between integrin attachment sites, were measured from light images of the cell process during SFSP application. These forces were calculated to be in the range of 1–2.3 pN, well within the range of forces predicted by Wang et al. (2007) for the hypothesized integrin attachments at canalicular projections.

The utility of the force probe was evidenced in the experiments designed to characterize the intercellular communication pathways in osteocyte networks described in Chapter 4. Investigation of cellular responses to physiological forces was taken from a single-cell experiment to a dual-cell experiment

to capture how osteocytes communicate in a network in response to focal and physiological stimulation. Mechanisms involved in the cell-cell communication enabled direct and indirect signaling. MLO-Y4 cells expressed Cx43 gap junction proteins in their cytoplasmic processes that provided a low resistance pathway for metabolic exchange between cells. They also demonstrated ATP-mediated P2R signaling, a pathway for indirect signaling through non-junctional transmembrane channels, in response to focal cell process stimulation. The use of direct and indirect pathways of intercellular communication was observed in MLO-Y4 pairs and these signaling pathways were not mutually exclusive. MLO-Y4 cells could utilize these signaling pathways in parallel, and signal initiation was highly dependent on their adhesion to the substrate. Direct intercellular signaling through gap junctions was also observed to be directional in response to cell process stimulation to suggest that the osteocytes could mediate the direction of signals to its neighboring cells focally and transiently within a network. MLO-Y4 cells are well equipped to modulate the metabolic state of their microenvironment as well as the activity of other neighboring bone cells in the presence of mechanical load.

In summary, three major contributions from this work are (1) the development of an entirely new force probe capable of delivering hydrodynamic pN level forces in a quantifiable and repeatable manner to focal regions of a cell, (2) the accomplishment of cell process stimulation separate from cell body stimulation at physiologically relevant forces to explore functional polarity of the osteocyte, and (3) the investigation of osteocyte network responses by physiological cell process stimulation. Together these results support the hypothesis that the osteocyte cell process is the mechanosensitive region of the cell where adhesion mediated signaling is initiated.

5.2. Future directions

Osteocytes are known to communicate with other osteocytes, osteoblasts and osteoclasts to maintain a local homeostasis; however, mechanisms of coordinated signaling at the cellular level to influence net resorption and deposition in bone tissue remain unclear. The investigation of signal transduction within a single osteocyte discovered that integrin mediated signal transduction was triggered at osteocyte cell process and not the cell body. Investigation of how these initial signals are propagated and transmitted from the stimulated osteocyte to a neighboring osteocyte, osteoblasts or osteoclasts would further improve

the knowledge of intercellular communication among bone cells.

The SFSP described in Chapter 2 is currently used in a force-mode to produce focal hydrodynamic stimulation on regions of the cell. It would be of interest to use the SFSP in a chemical mode where pharmacological agents were used to focally stimulate or block discrete regions of a cell. Focal application of an agonist, such as BzATP, a known potent $P2X_7R$ agonist, or specific pharmacological blockers, such as mefloquine or carbonoxolone, known gap junction blockers, can aid in elucidating complexes responsible for mediating pore forming channels involved in intercellular communication.

The whole-cell voltage clamp technique described in Chapter 3 currently investigated real-time single-cell responses to hydrodynamic stimulation and has proven to be a highly sensitive technique to capture early signaling responses from an osteocyte. Modifications were made to perform experiments on more than one cell where dual whole-cell patch-clamp was used to investigate intercellular signaling between an osteocyte pair, as discussed in Chapter 4. Further investigation of intercellular signaling in isolated primary osteocytes, which did exhibit electrical coupling in culture (n=5), using pharmacological agonists/antagonists, integrin peptides, and substrate patterning could help identify and refine the list of mechanosensitive signaling mechanism(s) suggested in the osteocyte cell process. These techniques could also be utilized in co-cultures of bone cells, and would be useful in characterizing intercellular communication between osteoblast-osteocyte pairs, for example.

With respect to the utility of the probe, its development enabled the investigation and identification of fast-transient adhesion-mediated intercellular communications pathways utilized by MLO-Y4 cells. The probe was also instrumental in identifying the mechanosensitive regions of the osteocyte and provided supporting experimental evidence that osteocyte cell signals are initiated at the cell processes as hypothesized by theoretical models of sub-cellular amplification in osteocytes. Understanding how osteocytes convert mechanical stimulation to biochemical signals at the cellular level could assist in:

(1) advances in substrate development to promote adhesion in tissue engineering,

(2) discovery of therapeutic targets using pharmacology, and

(3) optimizing parameters of mechanical stimulation to promote osteogenic responses in osteocytes.

Advances in imaging techniques and bone sample preparation provided the ultrastructural evidence

necessary to refine the sophisticated theoretical models of bone fluid flow to date. Force predications of these theoretical models guided the development of a novel stimulation technique that stimulated osteocytes in a physiological manner. The SFSP enabled the investigation of physiological responses of osteocytes in real-time which resembled the manner in which osteocytes communicate in their dynamic microenvironment. These findings further emphasized the active role osteocytes play in bone and their potential to influence their microenvironment under dynamic loading. These advances and findings also highlighted the utility of a nurturing interdisciplinary environment, where engineering and physiology have continued to converge, discover, and innovate.

References

Aarden, E., Wassenaar, A., Alblas, M. and Nijweide, P., 1996. Immunocytochemical demonstration of extracellular matrix proteins in isolated osteocytes. Histochemistry and Cell Biology 106(5), 495-501.

Abbracchio, M. P. and Burnstock, G., 1994. Purinoceptors: Are there families of p2x and p2y purinoceptors? Pharmacology & Therapeutics 64(3), 445-475.

Adachi, T., Aonuma, Y., Ito, S. i., Tanaka, M., Hojo, M., Takano-Yamamoto, T. and Kamioka, H., 2009a. Osteocyte calcium signaling response to bone matrix deformation. Journal of Biomechanics 42(15), 2507-2512.

Adachi, T., Aonuma, Y., Tanaka, M., Hojo, M., Takano-Yamamoto, T. and Kamioka, H., 2009b. Calcium response in single osteocytes to locally applied mechanical stimulus: Differences in cell process and cell body. Journal of Biomechanics 42(12), 1989-1995.

Aguirre, J. I., Plotkin, L. I., Stewart, S. A., Weinstein, R. S., Parfitt, A. M., Manolagas, S. C. and Bellido, T., 2006. Osteocyte apoptosis is induced by weightlessness in mice and precedes osteoclast recruitment and bone loss. Journal of Bone and Mineral Research 21(4), 605-615.

Ai, Z., Fischer, A., Spray, D. C., Brown, A. M. C. and Fishman, G. I., 2000. Wnt-1 regulation of connexin43 in cardiac myocytes. The Journal of Clinical Investigation 105(2), 161-171.

Ajubi, N. E., Klein-Nulend, J., Nijweide, P. J., Vrijheid-Lammers, T., Alblas, M. J. and Burger, E. H., 1996. Pulsating fluid flow increases prostaglandin production by cultured chicken osteocytes--a cytoskeleton-dependent process. Biochemical and Biophysical Research Communications 225(1), 62-68.

Akst, J., 2009. Full speed ahead: Physical forces acting in and around cells are fast - and making waves in the world of molecular biology. The Scientist 23(12), 26-32.

Al-Dujaili, S. A., Lau, E., Al-Dujaili, H., Tsang, K., Guenther, A. and You, L., 2011. Apoptotic osteocytes regulate osteoclast precursor recruitment and differentiation in vitro. Journal of Cellular Biochemistry 112(9), 2412-2423.

Alam, I., Warden, S. J., Robling, A. G. and Turner, C. H., 2005. Mechanotransduction in bone does not require a functional cyclooxygenase-2 (cox-2) gene. Journal of Bone and Mineral Research 20(3), 438-446.

Alenghat, F. J. and Ingber, D. E., 2002. Mechanotransduction: All signals point to cytoskeleton, matrix, and integrins. Sci.STKE 2002, E6-E6.

Alford, A. I., Jacobs, C. R. and Donahue, H. J., 2003. Oscillating fluid flow regulates gap junction communication in osteocytic mlo-y4 cells by an erk1/2 map kinase-dependent mechanism. Bone 33(1), 64-70.

Armstrong, S., Pereverzev, A., Dixon, S. J. and Sims, S. M., 2009. Activation of p2x7 receptors causes isoform-specific translocation of protein kinase c in osteoclasts. Journal of Cell Science 122(1), 136-144.

Bader, B. L., Rayburn, H., Crowley, D. and Hynes, R. O., 1998. Extensive vasculogenesis, angiogenesis, and organogenesis precede lethality in mice lacking all αv integrins. Cell 95(4), 507-519.

Bakker, A. D., Klein-Nulend, J. and Burger, E. H., 2003. Mechanotransduction in bone cells proceeds via activation of cox-2, but not cox-1. Biochemical and Biophysical Research Communications 305(3), 677-683.

Bao, L., Locovei, S. and Dahl, G., 2004a. Pannexin membrane channels are mechanosensitive conduits for atp. FEBS Letters 572(1-3), 65-68.

Bao, L., Sachs, F. and Dahl, G., 2004b. Connexins are mechanosensitive. AJP - Cell Physiology 287(5), C1389-C1395.

Barbe, M. T., Monyer, H. and Bruzzone, R., 2006. Cell-cell communication beyond connexins: The pannexin channels. Physiology 21(2), 103-114.

Baron, R. and Rawadi, G., 2007. Wnt signaling and the regulation of bone mass. Current Osteoporosis Reports 5(2), 73-80.

Bartl, R. and Frisch, B., 2009. Biology of bone. In: (Eds.), Osteoporosis. Springer Berlin Heidelberg, pp. 7-28.

Bausch, A. R., Zeimann, F., Boulbitch, A. A., Jacobson, K. and Sackman, E., 1998. Local measurements of viscoelastic parameters of adherent cell surfaces by magnetic bead microrheometry. Biophysical Journal 75(4), 2038-2049.

Baylink, D. and Wergedal, J., 1971. Bone formation by osteocytes. American Journal of Physiology -- Legacy Content 221(3), 669-678.
Baylink, T. M., Mohan, S., Fitzsimmons, R. J. and Baylink, D. J., 1996. Evaluation of signal transduction mechanisms for the mitogenic effects of prostaglandin e2 in normal human bone cells in vitro. Journal of Bone and Mineral Research 11(10), 1413-1418.
Beglova, N., Blacklow, S. C., Takagi, J. and Springer, T. A., 2002. Cysteine-rich module structure reveals a fulcrum for integrin rearrangement upon activation. Nature Structural Biology 9(4), 282-287.
Benedetti, E. L. and Emmelot, P., 1965. Electron microscopic observations on negatively stained plasma membranes isolated from rat liver. The Journal of Cell Biology 26(1), 299-305.
Benedetti, E. L. and Emmelot, P., 1968. Hexagonal array of subunits in tight junctions separated from isolated rat liver plasma membranes. The Journal of Cell Biology 38(1), 15-24.
Beningo, K. A., Dembo, M., Kaverina, I., Small, J. V. and Wang, Y.-l., 2001. Nascent focal adhesions are responsible for the generation of strong propulsive forces in migrating fibroblasts. The Journal of Cell Biology 153(4), 881-888.
Bennett, J. H., Carter, D. H., Alavi, A. L., Beresford, J. N. and Walsh, S., 2001. Patterns of integrin expression in a human mandibular explant model of osteoblast differentiation. Archives of Oral Biology 46(3), 229-238.
Bennett, M. V. L., 1966. Physiology of electrotonic junctions. Annals of the New York Academy of Sciences 137, 509-539.
Bennett, M. V. L. and Trinkaus, J. P., 1970. Electrical coupling between embryonic cells by way of extracellular space and specialized junctions. The Journal of Cell Biology 44(3), 592-610.
Beno, T., Yoon, Y.-J., Cowin, S. C. and Fritton, S. P., 2006. Estimation of bone permeability using accurate microstructural measurements. Journal of Biomechanics 39(13), 2378-2387.
Berthiaume, F. and Frangos, J. A., 1992. Flow-induced prostacyclin production is mediated by a pertussis toxin-sensitive g protein. FEBS Letters 308(3), 277-279.
Bett, G. C. L. and Sachs, F., 2000. Whole-cell mechanosensitive currents in rat ventricular myocytes activated by direct stimulation. Journal of Membrane Biology 173(3), 255-263.
Beyer, E. C., Paul, D. L. and Goodenough, D. A., 1987. Connexin43: A protein from rat heart homologous to a gap junction protein from liver. The Journal of Cell Biology 105(6), 2621-2629.
Beyer, E. C., Paul, D. L. and Goodenough, D. A., 1990. Connexin family of gap junction proteins. Journal of Membrane Biology 116(3), 187-194.
Bhattacharjee, R., Kaneda, M., Nakahama, K.-i. and Morita, I., 2009. The steady-state expression of connexin43 is maintained by the pi3k/akt in osteoblasts. Biochemical and Biophysical Research Communications 382(2), 440-444.
Binnig, G., Quate, C. F. and Gerber, C., 1986. Atomic force microscope. Physical Review Letters 56(9), 930-933.
Bissell, M. J., Radisky, D. C., Rizki, A., Weaver, V. M. and Petersen, O. W., 2002. The organizing principle: Microenvironmental influences in the normal and malignant breast. Differentiation; Research In Biological Diversity 70(9-10), 537-546.
Biswas, P. and Zanello, L. P., 2009. 1α,25(oh)2 vitamin d3 induction of atp secretion in osteoblasts. Journal of Bone and Mineral Research 24(8), 1450-1460.
Boassa, D., Qiu, F., Dahl, G. and Sosinsky, G., 2008. Trafficking dynamics of glycosylated pannexin 1 proteins. Cell Communication & Adhesion 15(1), 119-132.
Bonewald, L. F., 1999. Establishment and characterization of an osteocyte-like cell line, mlo-y4. Journal of Bone and Mineral Metabolism 17(1), 61-65.
Bonucci, E., 2009. The osteocyte: The underestimated conductor of the bone orchestra. Rendiconti Lincei 20(3), 237-254.
Bretschneider, F., Klapperstuck, M., Lohn, M. and Markwardt, F., 1995. Nonselective cationic currents elicited by extracellular atp in human b-lymphocytes. Pflügers Archiv European Journal of Physiology 429(5), 691-698.
Brophy, C. M., Mills, I., Rosales, O., Isales, C. and Sumpio, B. E., 1993. Phospholipase c: A putative mechanotransducer for endothelial cell response to acute hemodynamic changes. Biochemical and Biophysical Research Communications 190(2), 576-581.
Bruzzone, R., White, T. W. and Goodenough, D. A., 1996. The cellular internet: On-line with connexins. BioEssays 18(9), 709-718.
Burnstock, G. and Kennedy, C., 1985. Is there a basis for distinguishing two types of p2-purinoceptor?

General Pharmacology: The Vascular System 16(5), 433-440.
Burr, D. B., Milgrom, C., Fyhrie, D., Forwood, M., Nyska, M., Finestone, A., Hoshaw, S., Saiag, E. and Simkin, A., 1996. In vivo measurement of human tibial strains during vigorous activity. Bone 18(5), 405-410.
Burra, S., Nicolella, D. P., Francis, W. L., Freitas, C. J., Mueschke, N. J., Poole, K. and Jiang, J. X., 2010. Dendritic processes of osteocytes are mechanotransducers that induce the opening of hemichannels. Proceedings of the National Academy of Sciences 107(31), 13648-13653.
Burridge, K. and Chrzanowska-Wodnicka, M., 1996. Focal adhesions, contractility, and signaling. Annual Review of Cell and Developmental Biology 12(1), 463-519.
Butcher, M. T., White, B. J., Hudzik, N. B., Gosnell, W. C., Parrish, J. H. A. and Blob, R. W., 2011. In vivo strains in the femur of the virginia opossum (didelphis virginiana) during terrestrial locomotion: Testing hypotheses of evolutionary shifts in mammalian bone loading and design. The Journal of Experimental Biology 214(15), 2631-2640.
Cardoso, L., Herman, B. C., Verborgt, O., Laudier, D., Majeska, R. J. and Schaffler, M. B., 2009. Osteocyte apoptosis controls activation of intracortical resorption in response to bone fatigue. Journal of Bone and Mineral Research 24(4), 597-605.
Caspar, D. L., Goodenough, D. A., Makowski, L. and Phillips, W. C., 1977. Gap junction structures. I. Correlated electron microscopy and x-ray diffraction. The Journal of Cell Biology 74(2), 605-628.
Charras, G. T., Williams, B. A., Sims, S. M. and Horton, M. A., 2004. Estimating the sensitivity of mechanosensitive ion channels to membrane strain and tension. Biophysical Journal 87(4), 2870-2884.
Cheng, B., Kato, Y., Zhao, S., Luo, J., Sprague, E., Bonewald, L. F. and Jiang, J. X., 2001a. Pge2 is essential for gap junction-mediated intercellular communication between osteocyte-like mlo-y4 cells in response to mechanical strain. Endocrinology 142(8), 3464-3473.
Cheng, B., Zhao, S., Luo, J., Sprague, E., Bonewald, L. F. and Jiang, J. X., 2001b. Expression of functional gap junctions and regulation by fluid flow in osteocyte-like mlo-y4 cells. Journal of Bone and Mineral Research 16(2), 249-259.
Cherian, P. P., Siller-Jackson, A. J., Gu, S., Wang, X., Bonewald, L. F., Sprague, E. and Jiang, J. X., 2005. Mechanical strain opens connexin 43 hemichannels in osteocytes: A novel mechanism for the release of prostaglandin. Molecular Biology of the Cell 16(7), 3100-3106.
Cherian, P. P., Xia, X. and Jiang, J. X., 2008. Role of gap junction, hemichannels, and connexin 43 in mineralizing in response to intermittent and continuous application of parathyroid hormone. Cell Communication & Adhesion 15(1), 43-54.
Cheung, W.-Y., Liu, C., Tonelli-Zasarsky, R. M. L., Simmons, C. A. and You, L., 2011. Osteocyte apoptosis is mechanically regulated and induces angiogenesis in vitro. Journal of Orthopaedic Research 29(4), 523-530.
Chow, J. W. M., Fox, S. W., Lean, J. M. and Chambers, T. J., 1998. Role of nitric oxide and prostaglandins in mechanically induced bone formation. Journal of Bone and Mineral Research 13(6), 1039-1044.
Chyun, Y. S. and Raisz, L. G., 1984. Stimulation of bone formation by prostaglandin e2. Prostaglandins 27(1), 97-103.
Ciani, C., Doty, S. B. and Fritton, S. P., 2009. An effective histological staining process to visualize bone interstitial fluid space using confocal microscopy. Bone 44(5), 1015-1017.
Civitelli, R., Beyer, E. C., Warlow, P. M., Robertson, A. J., Geist, S. T. and Steinberg, T. H., 1993. Connexin43 mediates direct intercellular communication in human osteoblastic cell networks. The Journal of Clinical Investigation 91(5), 1888-1896.
Cluzel, C., Saltel, F., Lusis, J., Paulhe, F., Imhof, B. A. and Wehrle-Haller, B., 2005. The mechanisms and dynamics of avb3 integrin clustering in living cells. Journal of Cell Biology 171 (2), 383-392.
Dagan, Z., Weinbaum, S. and Pfeffer, R., 1982. An infinite-series solution for the creeping motion through an orifice of finite length. Journal of Fluid Mechanics Digital Archive 115(1), 505-523.
Dahl, G. and Locovei, S., 2006. Pannexin: To gap or not to gap, is that a question? IUBMB Life 58(7), 409-419.
Davidson, R. M., Tatakis, D. W. and Auerbach, A. L., 1990. Multiple forms of mechanosensitive ion channels in osteoblast-like cells. Pflügers Archiv European Journal of Physiology 416(6), 646-651.
De Arcangelis, A. and Georges-Labouesse, E., 2000. Integrin and ecm functions: Roles in vertebrate development. Trends in Genetics 16(9), 389-395.
del Corsso, C., Srinivas, M., Urban-Maldonado, M., Moreno, A. P., Fort, A. G., Fishman, G. I. and Spray, D.

C., 2006. Transfection of mammalian cells with connexins and measurement of voltage sensitivity of their gap juncitons. Nature Protocols 1(4), 1799-1809.
Demes, B., Qin, Y.-X., Stern, J. T., Larson, S. G. and Rubin, C. T., 2001. Patterns of strain in the macaque tibia during functional activity. American Journal of Physical Anthropology 116(4), 257-265.
Demes, B., Stern, J. T., Hausman, M. R., Larson, S. G., McLeod, K. J. and Rubin, C. T., 1998. Patterns of strain in the macaque ulna during functional activity. American Journal of Physical Anthropology 106(1), 87-100.
Dietrich, J. W., Goodson, J. M. and Raisz, L. G., 1975. Stimulation of bone resorption by various prostaglandins in organ culture. Prostaglandins 10(2), 231-240.
Donahue, H. J., 2000. Gap junctions and biophysical regulation of bone cell differentiation. Bone 26(5), 417-422.
Donahue, H. J., McLeod, K. J., Rubin, C. T., Andersen, J., Grine, E. A., Hertzberg, E. L. and Brink, P. R., 1995. Cell-to-cell communication in osteoblastic networks: Cell line–dependent hormonal regulation of gap junction function. Journal of Bone and Mineral Research 10(6), 881-889.
Doty, S. B., 1981. Morphological evidence of gap junctions between bone cells. Calcified Tissue International 33, 509-512.
Duffy, H., Fort, A. and Spray, D. C., 2006. Cardiac connexins: Genes to nexus. Advances in Cardiology 42, 1-17.
Duncan, R. and Misler, S., 1989. Voltage-activated and stretch-activated ba2+ conducting channels in an osteoblast-like cell line (umr 106). FEBS Letters 251(1-2), 17-21.
Duncan, R. L. and Hruska, K. A., 1994. Chronic, intermittent loading alters mechanosensitive channel characteristics in osteoblast-like cells. AJP - Renal Physiology 267(6), F909-F916.
Duncan, R. L. and Misler, S., 1989. Voltage-activated and stretch-activated ba2+ conducting channels in an osteoblast-like cell line (umr 106). FEBS Letters 125(1,2), 17-21.
Duszyk, M., Schwab, B., Zahalak, G. I., Qian, H. and Elson, E. L., 1989. Cell poking: Quantitative analysis of indentation of thick viscoelastic layers. Biophysical Journal 55, 683-690.
Emerman, J. and Pitelka, D., 1977. Maintenance and induction of morphological differentiation in dissociated mammary epithelium on floating collagen membranes. In Vitro Cellular & Developmental Biology - Plant 13(5), 316-328.
Evans, E., Ritchie, K. and Merkel, R., 1995. Sensitive force technique to probe molecular adhesion and structural linkages at biological interfaces. Biophysical Journal 68(6), 2580-2587.
Finbow, M. E. and Pitts, J. D., 1981. Permeability of junctions between animal cells : Intercellular exchange of various metabolites and a vitamin-derived cofactor. Experimental Cell Research 131(1), 1-13.
Folkman, J. and Moscona, A., 1978. Role of cell shape in growth control. Nature 273(5661), 345-349.
Forwood, M. R., 1996. Inducible cyclo-oxygenase (cox-2) mediates the induction of bone formation by mechanical loading in vivo. Journal of Bone and Mineral Research 11(11), 1688-1693.
Fox, J., Miller, M., Recker, R., Turner, C. and Smith, S., 2007. Effects of treatment of ovariectomized adult rhesus monkeys with parathyroid hormone 1-84 for 16 months on trabecular and cortical bone structure and biomechanical properties of the proximal femur. Calcified Tissue International 81(1), 53-63.
Fritton, S. P., McLeod, K. J. and Rubin, C. T., 2000. Quantifying the strain history of bone: Spatial uniformity and self-similarity of low-magnitude strains. Journal of Biomechanics 33(3), 317-325.
Fritton, S. P. and Weinbaum, S., 2009. Fluid and solute transport in bone: Flow-induced mechanotransduction. Annual Review of Fluid Mechanics 41(1), 347-374.
Galilei, G., 1638. First new science, treating of the resistance which solid bodies offer to fracture. In: Crew, H. and Salvio, A. D. (Eds.), Discorsi e dimostrazioni mathematiche intorno a due nuove scienze. MacMillan, New York, pp. 1-8.
Gardinier, J., Majumdar, S., Duncan, R. and Wang, L., 2009. Cyclic hydraulic pressure and fluid flow differentially modulate cytoskeleton re-organization in mc3t3 osteoblasts. Cellular and Molecular Bioengineering 2(1), 133-143.
Gartland, A., Buckley, K. A., Bowler, W. B. and Gallagher, J. A., 2003. Blockade of the pore-forming $p2x_7$ receptor inhibits formation of multinucleated human osteoclasts *in vitro*. Calcified Tissue International 73(4), 361-369.
Geneau, G., Lamiche, C., Niger, C., Strale, P.-O., Clarhaut, J., Defamie, N., Debiais, F., Mesnil, M. and Cronier, L., 2010. Effect of endothelin-1 on osteoblastic differentiation is modified by the level of connexin43: Comparative study on calvarial osteoblastic cells isolated from $cx43^{+/-}$ and $cx43^{+/+}$ mice.

Cell and Tissue Research 340(1), 103-115.
Genetos, D. C., Geist, D. J., Liu, D., Donahue, H. J. and Duncan, R. L., 2005. Fluid shear-induced atp secretion mediates prostaglandin release in mc3t3-e1 osteoblasts. Journal of Bone and Mineral Research 20(1), 41-49.
Genetos, D. C., Kephart, C. J., Zhang, Y., Yellowley, C. E. and Donahue, H. J., 2007. Oscillating fluid flow activation of gap junction hemichannels induces atp release from mlo-y4 osteocytes. Journal of Cellular Physiology 212(1), 207-214.
Gershey, E. L. and Alisa, R. M., 1980. Characterization of a cv-1 cell cycle. Journal of Cell Science 42, 357-365.
Gilula, N. B., Branton, D. and Satir, P., 1970. The septate junction: A structural basis for intercellular coupling. Proceedings of the National Academy of Sciences 67(1), 213-220.
Globus, R. K., 2007. Extracellular matrix and integrin interactions in the skeletal responses to mechanical loading and unloading. Clinical Reviews in Bone and Mineral Metabolism 5, 210-221.
Gohel, A. R., Hand, A. R. and Gronowicz, G. A., 1995. Immunogold localization of beta 1-integrin in bone: Effect of glucocorticoids and insulin-like growth factor i on integrins and osteocyte formation. Journal of Histochemistry & Cytochemistry 43(11), 1085-96.
Goodenough, D. A., Goliger, J. A. and Paul, D. L., 1996. Connexins, connexons, and intercellular communication. Annual Review of Biochemistry 65(1), 475-502.
Goodenough, D. A. and Revel, J. P., 1970. A fine structural analysis of intercellular junctions in the mouse liver. The Journal of Cell Biology 45(2), 272-290.
Goodenough, D. A. and Stoeckenius, W., 1972. The isolation of mouse hepatocyte gap junctions. The Journal of Cell Biology 54(3), 646-656.
Grimston, S. K., Brodt, M. D., Silva, M. J. and Civitelli, R., 2008. Attenuated response to in vivo mechanical loading in mice with conditional osteoblast ablation of the connexin43 gene (gja1). Journal of Bone and Mineral Research 23(6), 879-886.
Gu, G., Nars, M., Hentunen, T., Metsikkö, K. and Väänänen, H., 2006. Isolated primary osteocytes express functional gap junctions in vitro. Cell and Tissue Research 323(2), 263-271.
Gu, Y., Preston, M. R., El Haj, A. J., Howl, J. D. and Publicover, S. J., 2001a. Three types of k+ currents in murine osteocyte-like cells (mlo-y4). Bone 28 (1), 29-3.
Gu, Y., Preston, M. R., Magnay, J., El Haj, A. J. and Publicover, S. J., 2001b. Hormonally-regulated expression of voltage-operated ca2+ channels in osteocytic (mlo-y4) cells. Biochemical and Biophysical Research Communications 282(2), 536-542.
Guharay, F. and Sachs, F., 1984. Stretch-activated single ion channel currents in tissue-cultured embryonic chick skeletal muscle. The Journal of Physiology 352(1), 685-701.
Gunosewoyo, H., Coster, M. J. and Kassiou, M., 2007. Molecular probes for p2x7 receptor studies. Current Medicinal Chemistry 14(14), 1505-1523.
Guo, X. E., Takai, E., Jiang, X. J., Xu, Q., Whitesides, G. M., Yardley, J. T., Hung, C. T., Chow, E. M., Hantschel, T. and Costa, K. D., 2006. Intracellular calcium waves in bone cell networks under single cell nanoindentation. Molecular and Cellular Biomechanics 3(3), 95-107.
Guyton, A. and Hall, J. E., 2006. Parathyroid hormone, calcitonin, calcium and phosphate metabolism, vitamin d, bone and teeth. In: Gruliow, R. and Schmitt, W. (Eds.), Textbook of medical physiology. Elsevier, Philadelphia, Pennysylvania, pp.
Han, Y., Cowin, S. C., Schaffler, M. B. and Weinbaum, S., 2004. Mechanotransduction and strain amplification in osteocyte cell processes. Proceedings of the National Academy of Sciences of the United States of America 101(47), 16689-16694.
Hanani, M., 1997. Microscopic analysis of pressure ejection of drugs from micropipettes. J.Basic Clin.Physiol Pharmacol. 8(1-2), 57-71.
Happel, J. and Brenner, H., 1973. Low reynolds number hydrodynamics In: (Eds.), Low reynolds number hydrodynamics Prentice Hall, New York, pp.
Haskill, S., Johnson, C., Eierman, D., Becker, S. and Warren, K., 1988. Adherence induces selective mrna expression of monocyte mediators and proto-oncogenes. The Journal of Immunology 140(5), 1690-1694.
High, W. B., 1987. Effects of orally administered prostaglandin e-2 on cortical bone turnover in adult dogs: A histomorphometric study. Bone 8(6), 363-373.
Himeno-Ando, A., Izumi, Y., Yamaguchi, A. and Iimura, T., 2012. Structural differences in the osteocyte network between the calvaria and long bone revealed by three-dimensional fluorescence

morphometry, possibly reflecting distinct mechano-adaptations and sensitivities. Biochemical and Biophysical Research Communications 417(2), 765-770.
Hoyle, C. H., Knight, G. E. and Burnstock, G., 1990. Suramin antagonizes responses to p_2-purinoceptor agonists and purinergic nerve stimulation in the guinea-pig urinary bladder and taenia coli. British Journal of Pharmacology 99, 617-621.
Huang, H., Chikazu, D., Voznesensky, O. S., Herschman, H. R., Kream, B. E., Drissi, H. and Pilbeam, C. C., 2010. Parathyroid hormone induction of cyclooxygenase-2 in murine osteoblasts: Role of the calcium-calcineurin-nfat pathway. Journal of Bone and Mineral Research 25(4), 819-829.
Hughes, D., Salter, D., Dedhar, S. and Simpson, R., 1993. Integrin expression in human bone. Journal of Bone and Mineral Research 8(5), 527-533.
Hung, C. T., Pollack, S. R., Reilly, T. M. and Brighton, C. T., 1995. Real-time calcium response of cultured bone cells to fluid flow. Clinical Orthopaedics and Related Research 313, 256-269.
Huo, B., Lu, X., Hung, C., Costa, K., Xu, Q., Whitesides, G. and Guo, X., 2008. Fluid flow induced calcium response in bone cell network. Cellular and Molecular Bioengineering 1(1), 58-66.
Huo, B., Lu, X. L., Costa, K. D., Xu, Q. and Guo, X. E., 2010. An atp-dependent mechanism mediates intercellular calcium signaling in bone cell network under single cell nanoindentation. Cell Calcium 47(3), 234-241.
Hynes, R. O., 2002. Integrins: Bidirectional, allosteric signaling machines. Cell 110 673-687.
Iglesias, R., Dahl, G., Qiu, F., Spray, D. C. and Scemes, E., 2009. Pannexin 1: The molecular substrate of astrocyte "hemichannels". The Journal of Neuroscience 29(21), 7092-7097.
Ingber, D., 1991. Integrins as mechanochemical transducers. Current Opinion in Cell Biology 3(5), 841-848.
Ingber, D. E., 1997. Tensegrity: The architectural basis of cellular mechanotransduction. Annual Review of Physiology 59(1), 575-599.
Ingber, D. E. and Folkman, J., 1987. Regulation of endothelial growth factor action: Solid state control by extracellular matrix. Mechanisms of Signal Transduction by Hormones, 273-282.
Ishihara, Y., Kamioka, H., Honjo, T., Ueda, H., Takano-Yamamoto, T. and Yamashiro, T., 2008. Hormonal, ph, and calcium regulation of connexin 43–mediated dye transfer in osteocytes in chick calvaria. Journal of Bone and Mineral Research 23(3), 350-360.
Ishihara, Y., Sugawara, Y., Kamioka, H., Kawanabe, N., Kurosaka, H., Naruse, K. and Yamashiro, T., 2012. In situ imaging of the autonomous intracellular ca^{2+} oscillations of osteoblasts and osteocytes in bone. Bone 50(4), 842-852.
Ito, K. and Dulon, D., 2002. Nonselective cation conductance activated by muscarinic and purinergic receptors in rat spiral ganglion neurons. American Journal of Physiology - Cell Physiology 282(5), C1121-C1135.
Janle, E. and Sojka, J., 2001. Use of ultrafiltration probes in sheep to collect interstitial fluid for measurement of calcium and magnesium. Contemporary Topics in Laboratory Animal Science 39(6), 47-50.
Járos, G., Guyton, A. and Coleman, T., 1980. The role of bone in short-term calcium homeostasis: An analog-digital computer simulation. Annals of Biomedical Engineering 8(2), 103-141.
Jee, W. S. S., Akamine, T., Ke, H. Z., Li, X. J., Tang, L. Y. and Zeng, Q. Q., 1992. Prostaglandin e2 prevents disuse-induced cortical bone loss. Bone 13(2), 153-159.
Jee, W. S. S., Ueno, K., Kimmel, D. B., Woodbury, D. M., Price, P. and Woodbury, L. A., 1987. The role of bone cells in increasing metaphyseal hard tissue in rapidly growing rats treated with prostaglandin e2. Bone 8(3), 171-178.
Jorgensen, F. and Kroese, A. B., 1995. Ca selectivity of the transduction channels in the hair cells of the frog sacculus. Acta Physiol.Scand. 155, 363-376.
Jørgensen, N. R., Henriksen, Z., Sørensen, O. H., Eriksen, E. F., Civitelli, R. and Steinberg, T. H., 2002. Intercellular calcium signaling occurs between human osteoblasts and osteoclasts and requires activation of osteoclast p2x7 receptors. Journal of Biological Chemistry 277(9), 7574-7580.
Kalinowski, R. R., Berlot, C. H., Jones, T. L. Z. and Ross, L. F., 2004. Maintenance of meiotic prophase arrest in vertebrate oocytes by a gs protein-mediated pathway. Developmental Biology 267, 1-13.
Kamioka, H., Ishihara, Y., Ris, H., Murshid, S. A., Sugawara, Y., Takano-Yamamoto, T. and Lim, S.-S., 2007. Primary cultures of chick osteocytes retain functional gap junctions between osteocytes and between osteocytes and osteoblasts. Microscopy and Microanalysis 13(2), 108-117.
Kato, Y., Windle, J. J., Koop, B. A., Mundy, G. R. and Bonewald, L. F., 1997. Establishment of an

osteocyte-like cell line, mlo-y4. Journal of Bone and Mineral Research 12(12), 2014-2023.
Kawata, A. and Mikuni-Takagaki, Y., 1998. Mechanotransduction in stretched osteocytes--temporal expression of immediate early and other genes. Biochemical and Biophysical Research Communications 246(2), 404-408.
Ke, H. Z., Qi, H., Weidema, A. F., Zhang, Q., Panupinthu, N., Crawford, D. T., Grasser, W. A., Paralkar, V. M., Li, M., Audoly, L. P., Gabel, C. A., Jee, W. S. S., Dixon, S. J., Sims, S. M. and Thompson, D. D., 2003. Deletion of the p2x7 nucleotide receptor reveals its regulatory roles in bone formation and resorption. Molecular Endocrinology 17(7), 1356-1367.
Keely, P. J., Westwick, J. K., Whitehead, I. P., Der, C. J. and Parise, L. V., 1997. Cdc42 and rac1 induce integrin-mediated cell motility and invasiveness through pi(3)k. Nature 390(6660), 632-636.
Keller, J., Klamer, A., Bak, B. and Suder, P., 1993. Effect of local prostaglandin e2 on fracture callus in rabbits. Acta Orthop.Scand. 64(1), 59-63.
Kennedy, O. D., Herman, B. C., Laudier, D. M., Majeska, R. J., Sun, H. B. and Schaffler, M. B., 2012. Activation of resorption in fatigue-loaded bone involves both apoptosis and active pro-osteoclastogenic signaling by distinct osteocyte populations. Bone 50(5), 1115-1122.
Kimmel, D. B., Fong, T., Akhter, M. P., Coats, J. and Wronski, T., 2011. Effects of pth(1-34) and estrogen status on osteocyte lacunar properties in rats. Bone 48(Supplement 2), S97-S98.
Kitase, Y., Barragan, L., Qing, H., Kondoh, S., Jiang, J. X., Johnson, M. L. and Bonewald, L. F., 2010. Mechanical induction of pge2 in osteocytes blocks glucocorticoid-induced apoptosis through both the β-catenin and pka pathways. Journal of Bone and Mineral Research 25(12), 2657-2668.
Kizer, N., Guo, X. L. and Hruska, K., 1997. Reconstitution of stretch-activated cation channels by expression of the α-subunit of the epithelial sodium channel cloned from osteoblasts. Proc.Natl Acad.Sci.USA 94, 1013-1018.
Klein-Nulend, J., Burger, E. H., Semeins, C. M., Raisz, L. G. and Pilbeam, C. C., 1997. Pulsating fluid flow stimulates prostaglandin release and inducible prostaglandin g/h synthase mrna expression in primary mouse bone cells. Journal of Bone and Mineral Research 12(1), 45-51.
Klein-Nulend, J., van der Plas, A., Semeins, C. M., Ajubi, N. E., Frangos, J. A., Nijweide, P. J. and Burger, E. H., 1995. Sensitivity of osteocytes to biomechanical stress in vitro. The FASEB Journal 9(5), 441-445.
Knothe Tate, M. L., Knothe, U. and Niederer, P., 1998a. Experimental elucidation of mechanical load-induced fluid flow and its potential role in bone metabolism and functional adaptation. The American Journal of the Medical Sciences 316(3), 189-195.
Knothe Tate, M. L., Niederer, P. and Knothe, U., 1998b. In vivo tracer transport through the lacunocanalicular system of rat bone in an environment devoid of mechanical loading. Bone 22(2), 107-117.
Kojima, H., Ishijima, A. and Yanagida, T., 1994. Direct measurement of stiffness of single actin filaments with and without tropomyosin by in vitro nanomanipulation. Proceedings of the National Academy of Sciences of the United States of America 91(26), 12962-12966.
Korcok, J., Raimundo, L. N., Ke, H. Z., Sims, S. M. and Dixon, S. J., 2004. Extracellular nucleotides act through p2x7 receptors to activate nf-κb in osteoclasts. Journal of Bone and Mineral Research 19(4), 642-651.
Kuroda, Y., Hisatsune, C., Nakamura, T., Matsuo, K. and Mikoshiba, K., 2008. Osteoblasts induce ca2+ oscillation-independent nfatc1 activation during osteoclastogenesis. Proceedings of the National Academy of Sciences 105(25), 8643-8648.
Kusuzaki, K., Kageyama, N., Shinjo, H., Murata, H., Takeshita, H., Ashihara, T. and Hirasawa, Y., 1995. A staining method for bone canaliculi. Acta Orthopaedica 66(2), 166-168.
Lane, N. E., Yao, W., Balooch, M., Nalla, R. K., Balooch, G., Habelitz, S., Kinney, J. H. and Bonewald, L. F., 2006. Glucocorticoid-treated mice have localized changes in trabecular bone material properties and osteocyte lacunar size that are not observed in placebo-treated or estrogen-deficient mice. Journal of Bone and Mineral Research 21(3), 466-476.
Lanyon, L. E., Hampson, W. G. J., Goodship, A. E. and Shah, J. S., 1975. Bone deformation recorded in vivo from strain gauges attached to the human tibial shaft. Acta Orthopaedica 46(2), 256-268.
Lau, E., Al Dujaili, S., Guenther, A., Liu, D., Wang, L. and You, L., 2010. Effect of low-magnitude, high-frequency vibration on osteocytes in the regulation of osteoclasts. Bone 46(6), 1508-1515.
Lecanda, F., Warlow, P. M., Sheikh, S., Furlan, F., Steinberg, T. H. and Civitelli, R., 2000. Connexin43 deficiency causes delayed ossification, craniofacial abnormalities, and osteoblast dysfunction. The

Journal of Cell Biology 151(4), 931-944.
Lee, K. C. L., Maxwell, A. and Lanyon, L. E., 2002. Validation of a technique for studying functional adaptation of the mouse ulna in response to mechanical loading. Bone 31(3), 407-412.
Lester, M. E., Urso, M. L., Evans, R. K., Pierce, J. R., Spiering, B. A., Maresh, C. M., Hatfield, D. L., Kraemer, W. J. and Nindl, B. C., 2009. Influence of exercise mode and osteogenic index on bone biomarker responses during short-term physical training. Bone 45(4), 768-776.
Leybaert, L., Braet, K., Vandamme, W., Cabooter, L., Martin, P. E. M. and Evans, W. H., 2003. Connexin channels, connexin mimetic peptides and atp release. Cell Communication & Adhesion 10(4-6), 251-257.
Li, G.-H., Lee, E. M., Blair, D., Holding, C., Poronnik, P., Cook, D. I., Barden, J. A. and Bennett, M. R., 2000. The distribution of p2x receptor clusters on individual neurons in sympathetic ganglia and their redistribution on agonist activation. Journal of Biological Chemistry 275(37), 29107-29112.
Li, J., Liu, D., Ke, H. Z., Duncan, R. L. and Turner, C. H., 2005. The p2x7 nucleotide receptor mediates skeletal mechanotransduction. The Journal of Biological Chemistry 280(52), 42592-42595.
Li, M. L., Aggeler, J., Farson, D. A., Hatier, C., Hassell, J. and Bissell, M. J., 1987. Influence of a reconstituted basement membrane and its components on casein gene expression and secretion in mouse mammary epithelial cells. Proc.Natl Acad.Sci.USA.
Li, X. J., Jee, W. S. S., Li, Y. L. and Patterson-Buckendahl, P., 1990. Transient effects of subcutaneously administered prostaglandin e2 on cancellous and cortical bone in young adult dogs. Bone 11(5), 353-364.
Lieberman, D. E., Polk, J. D. and Demes, B., 2004. Predicting long bone loading from cross-sectional geometry. American Journal of Physical Anthropology 123(2), 156-171.
Litvinov, R. I., Vilaire, G., Shuman, H., Bennett, J. S. and Weisel, J. W., 2003. Quantitative analysis of platelet avb3 binding to osteopontin using laser tweezers. Journal of Biological Chemistry 278(51), 51285-51290.
Litzenberger, J., Kim, J. B., Tummala, P. and Jacobs, C., 2010. Beta1 integrins mediate mechanosensitive signaling pathways in osteocytes. Calcified Tissue International 86(4), 325-332.
Litzenberger, J., Tang, W., Castillo, A. and Jacobs, C., 2009. Deletion of β1 integrins from cortical osteocytes reduces load-induced bone formation. Cellular and Molecular Bioengineering 2(3), 416-424.
Liu, D., Genetos, D. C., Shao, Y., Geist, D. J., Li, J., Ke, H. Z., Turner, C. H. and Duncan, R. L., 2008. Activation of extracellular-signal regulated kinase (erk1/2) by fluid shear is ca2+- and atp-dependent in mc3t3-e1 osteoblasts. Bone 42(4), 644-652.
Locovei, S., Scemes, E., Qiu, F., Spray, D. C. and Dahl, G., 2007. Pannexin1 is part of the pore forming unit of the p2x7 receptor death complex. FEBS Letters 581(3), 483-488.
Loewenstein, W. R., 1966. Permeability of membrane junctions*. Annals of the New York Academy of Sciences 137(2), 441-472.
Lohmann, C. H., Schwartz, Z., Liu, Y., Li, Z., Simon, B. J., Sylvia, V. L., Dean, D. D., Bonewald, L. F., Donahue, H. J. and Boyan, B. D., 2003. Pulsed electromagnetic fields affect phenotype and connexin 43 protein expression in mlo-y4 osteocyte-like cells and ros 17/2.8 osteoblast-like cells. Journal of Orthopaedic Research 21(2), 326-334.
Mack, P. J., Kaazempur-Mofrad, M. R., Karcher, H., Lee, R. T. and Kamm, R. D., 2004. Force-induced focal adhesion translocation: Effects of force amplitude and frequency. Am.J.Physiol.Cell Physiol. 287, C954-C962.
Malone, A. M. D., Anderson, C. T., Tummala, P., Kwon, R. Y., Johnston, T. R., Stearns, T. and Jacobs, C. R., 2007. Primary cilia mediate mechanosensing in bone cells by a calcium-independent mechanism. Proceedings of the National Academy of Sciences 104(33), 13325-13330.
Marotti, G., 1996. The structure of bone tissues and the cellular control of their deposition. Italian journal of anatomy and embryology = Archivio italiano di anatomia ed embriologia 101(4), 25-79.
Mazet, F., Wittenberg, B. and Spray, D., 1985. Fate of intercellular junctions in isolated adult rat cardiac cells. Circulation Research 56(2), 195-204.
McHugh, K. P., Hodivala-Dilke, K., Zheng, M.-H., Namba, N., Lam, J., Novack, D. V., Feng, X., Ross, F. P., Hynes, R. O. and Teitelbaum, S. L., 2000. Mice lacking β3 integrins are osteosclerotic because of dysfunctional osteoclasts. The Journal of Clinical Investigation 105(4), 433-440.
McNamara, L. M., Majeska, R. J., Weinbaum, S., Friedrich, V. and Schaffler, M. B., 2009. Attachment of osteocyte cell processes to the bone matrix. Anatomical Records 292(3), 355-363.

Menko, A. S. and Boettiger, D., 1987. Occupation of the extracellular matrix receptor, integrin, is a control point for myogenic differentiation. Cell 51(1), 51-57.
Meyer, D. J., Yancey, S. B. and Revel, J. P., 1981. Intercellular communication in normal and regenerating rat liver: A quantitative analysis. The Journal of Cell Biology 91(2), 505-523.
Milgrom, C., Finestone, A., Simkin, A., Ekenman, I., Mendelson, S., Millgram, M., Nyska, M., Larsson, E. and Burr, D., 2000. In vivo strain measurements to evaluate the strengthening potential of exercises on the tibial bone. J Bone Joint Surg Br 82-B(4), 591-594.
Miyauchi, A., Gotoh, M., Kamioka, H., Notoya, K., Sekiya, H., Takagi, Y., Yoshimoto, Y., Ishikawa, H., Chihara, K., Takano-Yamamoto, T., Fujita, T. and Mikuni-Takagaki, Y., 2006. Avb3 integrin ligands enhance volume-sensitive calcium influx in mechanically stretched osteocytes. Journal of Bone and Mineral Metabolism 24(6), 498-504.
Miyauchi, A., Notoya, K., Mikuni-Takagaki, Y., Takagi, Y., Goto, M., Miki, Y., Takano-Yamamoto, T., Jinnai, K., Takahashi, K., Kumegawa, M., Chihara, K. and Fujita, T., 2000. Parathyroid hormone-activated volume-sensitive calcium influx pathways in mechanically loaded osteocytes. Journal of Biological Chemistry 275(5), 3335-3342.
Modderman, W., Weidema, A., Vrijheid-Lammers, T., Wassenaar, A. and Nijweide, P., 1994. Permeabilization of cells of hemopoietic origin by extracellular atp: Elimination of osteoclasts, macrophages, and their precursors from isolated bone cell populations and fetal bone rudiments. Calcified Tissue International 55(2), 141-150.
Mori, S., Jee, W. S. S., Li, X. J., Chan, S. and Kimmel, D. B., 1990. Effects of prostaglandin e2 on production of new cancellous bone in the axial skeleton of ovariectomized rats. Bone 11(2), 103-113.
Morris, C. E., 1990. Mechanosensitive ion channels. Journal of Membrane Biology 113(2), 93-107.
Moustafa, A., Sugiyama, T., Prasad, J., Zaman, G., Gross, T., Lanyon, L. and Price, J., 2011. Mechanical loading-related changes in osteocyte sclerostin expression in mice are more closely associated with the subsequent osteogenic response than the peak strains engendered. Osteoporosis International, 1-10.
Nobes, C. D. and Hall, A., 1995. Rho, rac, and cdc42 gtpases regulate the assembly of multimolecular focal complexes associated with actin stress fibers, lamellipodia, and filopodia. Cell 81(1), 53-62.
Norrdin, R. and Shih, M., 1988. Systemic effects of prostaglandin e_2 on vertebral trabecular remodeling in beagles used in a healing study. Calcified Tissue International 42(6), 363-368.
Ohlendorff, S. D., Tofteng, C. L., Jensen, J.-E. B., Petersen, S., Civitelli, R., Fenger, M., Abrahamsen, B., Hermann, A. P., Eiken, P. and Jørgensen, N. R., 2007. Single nucleotide polymorphisms in the p2x7 gene are associated to fracture risk and to effect of estrogen treatment. Pharmacogenetics and Genomics 17(7), 555-567.
Orriss, I. R., Burnstock, G. and Arnett, T. R., 2010. Purinergic signalling and bone remodelling. Current Opinion in Pharmacology 10, 1-9.
Orriss, I. R., Knight, G. E., Ranasinghe, S., Burnstock, G. and Arnett, T. R., 2006. Osteoblast responses to nucleotides increase during differentiation. Bone 39(2), 300-309.
Orriss, I. R., Knight, G. E., Utting, J. C., Taylor, S. E. B., Burnstock, G. and Arnett, T. R., 2009. Hypoxia stimulates vesicular atp release from rat osteoblasts. Journal of Cellular Physiology 220(1), 155-162.
Owan, I., Burr, D. B., Turner, C. H., Qiu, J., Tu, Y., Onyia, J. E. and Duncan, R. L., 1997. Mechanotransduction in bone: Osteoblasts are more responsive to fluid forces than mechanical strain. AJP - Cell Physiology 273(3), C810-C815.
Palumbo, C., Palazzini, S. and Marotti, G., 1990. Morphological study of intercellular junctions during osteocyte differentiation. Bone 11(6), 401-406.
Panupinthu, N., Rogers, J. T., Zhao, L., Solano-Flores, L. P., Possmayer, F., Sims, S. M. and Dixon, S. J., 2008. P2x7 receptors on osteoblasts couple to production of lysophosphatidic acid: A signaling axis promoting osteogenesis. The Journal of Cell Biology 181(5), 859-871.
Panupinthu, N., Zhao, L., Possmayer, F., Ke, H. Z., Sims, S. M. and Dixon, S. J., 2007. P2x7 nucleotide receptors mediate blebbing in osteoblasts through a pathway involving lysophosphatidic acid. Journal of Biological Chemistry 282(5), 3403-3412.
Parfitt, A. M., 1977. The cellular basis of bone turnover and bone loss: A rebuttal of the osteocytic resorption-bone flow theory. Clinical Orthopaedics and Related Research 127, 236-247.
Pavalko, F. M., Gerard, R. L., Ponik, S. M., Gallagher, P. J., Jin, Y. and Norvell, S. M., 2003a. Fluid shear stress inhibits tnf-+ý-induced apoptosis in osteoblasts: A role for fluid shear stress-induced

activation of pi3-kinase and inhibition of caspase-3. Journal of Cellular Physiology 194(2), 194-205.
Pavalko, F. M., Norvell, S. M., Burr, D. B., Turner, C. H., Duncan, R. L. and Bidwell, J. P., 2003b. A model for mechanotransduction in bone cells: The load-bearing mechanosomes. Journal of Cellular Biochemistry 88(1), 104-112.
Phillips, J. A., Almeida, E. A. C., Hill, E. L., Aguirre, J. I., Rivera, M. F., Nachbandi, I., Wronski, T. J., van der Meulen, M. C. H. and Globus, R. K., 2008. Role for β1 integrins in cortical osteocytes during acute musculoskeletal disuse. Matrix Biology 27(7), 609-618.
Pidaparti, R. M. V. and Turner, C. H., 1997. Cancellous bone architecture: Advantages of nonorthogonal trabecular alignment under multidirectional joint loading. Journal of Biomechanics 30(9), 979-983.
Piekarski, K. and Munro, M., 1977. Transport mechanism operating between blood supply and osteocytes in long bones. Nature 269(5623), 80-82.
Pitts, J. D. and Simms, J. W., 1977. Permeability of junctions between animal cells : Intercellular transfer of nucleotides but not of macromolecules. Experimental Cell Research 104(1), 153-163.
Plotkin, L. I., Manolagas, S. C. and Bellido, T., 2007. Glucocorticoids induce osteocyte apoptosis by blocking focal adhesion kinase-mediated survival. Journal of Biological Chemistry 282(33), 24120-24130.
Plotkin, L. I., Mathov, I., Aguirre, J. I., Parfitt, A. M., Manolagas, S. C. and Bellido, T., 2005. Mechanical stimulation prevents osteocyte apoptosis: Requirement of integrins, src kinases, and erks. American Journal of Physiology - Cell Physiology 289(3), C633-C643.
Ponik, S. M. and Pavalko, F. M., 2004. Formation of focal adhesions on fibronectin promotes fluid shear stress induction of cox-2 and pge2 release in mc3t3-e1 osteoblasts. Journal of Applied Physiology 97(1), 135-142.
Ponik, S. M., Triplett, J. W. and Pavalko, F. M., 2007. Osteoblasts and osteocytes respond differently to oscillatory and unidirectional fluid flow profiles. Journal of Cellular Biochemistry 100(3), 794-807.
Price, C., Zhou, X., Li, W. and Wang, L., 2010. Real-time measurement of solute transport within the lacunar-canalicular system of mechanically loaded bone: Direct evidence for load-induced fluid flow. Journal of Bone and Mineral Research, n/a-n/a.
Raisz, L. G., Pilbeam, C. C. and Fall, P. M., 1993. Prostaglandins: Mechanisms of action and regulation of production in bone. Osteoporosis International 3(0), 136-140.
Rawlinson, S. C. F., Pitsillides, A. A. and Lanyon, L. E., 1996. Involvement of different ion channels in osteoblasts' and osteocytes' early responses to mechanical strain. Bone 19(6), 609-614.
Reich, K. M. and Frangos, J. A., 1991. Effect of flow on prostaglandin e2 and inositol trisphosphate levels in osteoblasts. American Journal of Physiology - Cell Physiology 261(3), C428-C432.
Reich, K. M. and Frangos, J. A., 1993. Protein kinase c mediates flow-induced prostaglandin e_2 production in osteoblasts. Calcified Tissue International 52(1), 62-66.
Reich, K. M., Gay, C. V. and Frangos, J. A., 1990. Fluid shear stress as a mediator of osteoblast cyclic adenosine monophosphate production. Journal of Cellular Physiology 143(1), 100-104.
Reich, K. M., McAllister, T. N., Gudi, S. and Frangos, J. A., 1997. Activation of g proteins mediates flow-induced prostaglandin e2 production in osteoblasts. Endocrinology 138(3), 1014-1018.
Reilly, G. C., Haut, T. R., Yellowley, C. E., Donahue, H. J. and Jacobs, C. R., 2003. Fluid flow induced pge2 release by bone cells is reduced by glycocalyx degradation whereas calcium signals are not. Biorheology 40(6), 591-603.
Revel, J. P. and Karnovsky, M. J., 1967. Hexagonal array of subunits in intercellular junctions of the mouse heart and liver. The Journal of Cell Biology 33(3), C7-12.
Reyes, R. C. and Parpura, V., 2008. Mitochondria modulate ca2+-dependent glutamate release from rat cortical astrocytes. The Journal of Neuroscience 28(39), 9682-9691.
Ringel, R. E., Brenner, J. I., Haney, P. J., Burns, J. E., Moulton, A. L. and Berman, M. A., 1982. Prostaglandin-induced periostitis: A complication of long-term pge_1 infusion in an infant with congenital heart disease. Radiology 142, 657-658.
Rizzoli, R., Reginster, J.-Y., Boonen, S., Bréart, G., Diez-Perez, A., Felsenberg, D., Kaufman, J.-M., Kanis, J. and Cooper, C., 2011. Adverse reactions and drug–drug interactions in the management of women with postmenopausal osteoporosis. Calcified Tissue International 89(2), 91-104.
Robertson, J. D., 1963. The occurrence of a subunit pattern in the unit membranes of club endings in mauthner cell synapses in goldfish brains. The Journal of Cell Biology 19(1), 201-221.
Robling, A. G., Niziolek, P. J., Baldridge, L. A., Condon, K. W., Allen, M. R., Alam, I., Mantila, S. M., Gluhak-Heinrich, J., Bellido, T. M., Harris, S. E. and Turner, C. H., 2008. Mechanical stimulation of

bone in vivo reduces osteocyte expression of sost/sclerostin. Journal of Biological Chemistry 283(9), 5866-5875.
Roca-Cusachs, P., Gauthier, N. C., del Rio, A. and Sheetz, M. P., 2009. Clustering of α5β1 integrins determines adhesion strength whereas αvβ3 and talin enable mechanotransduction. Proceedings of the National Academy of Sciences 106(38), 16245-16250.
Rodan, G., Bourret, L., Harvey, A. and Mensi, T., 1975. Cyclic amp and cyclic gmp: Mediators of the mechanical effects on bone remodeling. Science 189(4201), 467-469.
Roesler, H., 1987. The history of some fundamental concepts in bone biomechanics. Journal of Biomechanics 20(11-12), 1025-1034.
Ross, F. P., Chappel, J., Alvarez, J. I., Sander, D., Butler, W. T., Farach-Carson, M. C., Mintz, K. A., Robey, P. G., Teitelbaum, S. L. and Cheresh, D. A., 1993. Interactions between the bone matrix proteins osteopontin and bone sialoprotein and the osteoclast integrin alpha v beta 3 potentiate bone resorption. Journal of Biological Chemistry 268(13), 9901-7.
Rozental, R., C, G. and Spray, D. C., 2000. Gap junctions in the nervous system. Brain Research Reviews 32(1), 11-15.
Rubin, C., Turner, A. S., Mallinckrodt, C., Jerome, C., McLeod, K. and Bain, S., 2002. Mechanical strain, induced noninvasively in the high-frequency domain, is anabolic to cancellous bone, but not cortical bone. Bone 30(3), 445-452.
Rubin, C. T. and Lanyon, L. E., 1982. Limb mechanics as a function of speed and gait: A study of functional strains in the radius and tibia of horse and dog. Journal of Experimental Biology 101(1), 187-211.
Rubin, C. T. and Lanyon, L. E., 1984. Regulation of bone formation by applied dynamic loads. Journal of Bone and Joint Surgery 66(3), 397-402.
Rubin, J., Rubin, C. and Jacobs, C. R., 2006. Molecular pathways mediating mechanical signaling in bone. Gene 367, 1-16.
Ryder, K. D. and Duncan, R. L., 2001. Parathyroid hormone enhances fluid shear-induced [ca2+]i signaling in osteoblastic cells through activation of mechanosensitive and voltage-sensitive ca2+ channels. Journal of Bone and Mineral Research 16(2), 240-248.
Saito, T., Albelda, S. M. and Brighton, C. T., 1994. Identification of integrin receptors on cultured human bone cells. Journal of Orthopaedic Research 12(3), 384-394.
Sakai, H., Kobayashi, Y., Sakai, E., Shibata, M. and Kato, Y., 2000. Cell adhesion is a prerequisite for osteoclast survival. Biochemical and Biophysical Research Communications 270(2), 550-556.
Sakai, K., Mohtai, M. and Iwamoto, Y., 1998. Fluid shear stress increases transforming growth factor beta 1 expression in human osteoblast-like cells: Modulation by cation channel blockades. Calcified Tissue International 63(6), 515-520.
Salzstein, R. A. and Pollack, S. R., 1987. Electromechanical potentials in cortical bone—ii. Experimental analysis. Journal of Biomechanics 20(3), 271-280.
Salzstein, R. A., Pollack, S. R., Mak, A. F. T. and Petrov, N., 1987. Electromechanical potentials in cortical bone—i. A continuum approach. Journal of Biomechanics 20(3), 261-270.
Saunders, M. M., You, J., Zhou, Z., Li, Z., Yellowley, C. E., Kunze, E. L., Jacobs, C. R. and Donahue, H. J., 2003. Fluid flow-induced prostaglandin e2 response of osteoblastic ros 17/2.8 cells is gap junction-mediated and independent of cytosolic calcium. Bone 32(4), 350-356.
Sauren, Y. M. H. F., Mieremet, R. H. P., Groot, C. G. and Scherft, J. P., 1992. An electron microscopic study on the presence of proteoglycans in the mineralized matrix of rat and human compact lamellar bone. The Anatomical Record 232(1), 36-44.
Sawakami, K., Robling, A. G., Ai, M., Pitner, N. D., Liu, D., Warden, S. J., Li, J., Maye, P., Rowe, D. W., Duncan, R. L., Warman, M. L. and Turner, C. H., 2006. The wnt co-receptor lrp5 is essential for skeletal mechanotransduction but not for the anabolic bone response to parathyroid hormone treatment. Journal of Biological Chemistry 281(33), 23698-23711.
Scemes, E. and Giaume, C., 2006. Astrocyte calcium waves: What they are and what they do. Glia 54(7), 716-725.
Scemes, E. and Spray, D., 2012. Extracellular k^+ and astrocyte signaling via connexin and pannexin channels. Neurochemical Research, 1-7.
Scemes, E., Spray, D. and Meda, P., 2009. Connexins, pannexins, innexins: Novel roles of hemi-channels. Pflgers Archiv European Journal of Physiology 457(6), 1207-1226.
Scemes, E., Suadicani, S. O., Dahl, G. and Spray, D. C., 2007. Connexin and pannexin mediated cell-cell communication. Neuron Glia Biology 3, 199-208.

Schirrmacher, K., Wiemann, M., Bingmann, D. and Busselberg, D., 1998. Effects of lead, mercury, and methyl mercury on gap junctions and [ca2+]i in bone cells. Calcified Tissue International 63 134-139.

Shao, Y., Alicknavitch, M. and Farach-Carson, M. C., 2005. Expression of voltage sensitive calcium channel (vscc) l-type cav1.2 (a1c) and t-type cav3.2 (a1h) subunits during mouse bone development. Developmental Dynamics 234(1), 54-62.

Sharma, D., Ciani, C., Marin, P. A. R., Levy, J. D., Doty, S. B. and Fritton, S. P., 2012. Alterations in the osteocyte lacunar-canalicular microenvironment due to estrogen deficiency. Bone (0). DOI: 10.1016/j.bone.2012.05.014

Sheridan, J. D., 1968. Electrophysiological evidence for low-resistance intercellular junctions in the early chick embryo. The Journal of Cell Biology 37(3), 650-659.

Silver, I. A., Murrills, R. J. and Etherington, D. J., 1988. Microelectrode studies on the acid microenvironment beneath adherent macrophages and osteoclasts. Experimental Cell Research 175(2), 266-276.

Sissons, H., Kelman, G. and Marotti, G., 1984. Mechanisms of bone resorption in calcium-deficient rats. Calcified Tissue International 36(1), 711-721.

Sloan, A. V., Martin, J. R., Li, S. and Li, J., 2010. Parathyroid hormone and bisphosphonate have opposite effects on stress fracture repair. Bone 47(2), 235-240.

Small, J. V., Rottner, K., Kaverina, I. and Anderson, K. I., 1998. Assembling an actin cytoskeleton for cell attachment and movement. Biochimica et Biophysica Acta (BBA) - Molecular Cell Research 1404(3), 271-281.

Smalt, R., Mitchell, F. T., Howard, R. L. and Chambers, T. J., 1997. Induction of no and prostaglandin e2 in osteoblasts by wall-shear stress but not mechanical strain. AJP - Endocrinology and Metabolism 273(4), E751-E758.

Smith, D. V. and Uteshev, V. V., 2008. Heterogeneity of nicotinic acetylcholine receptor expression in the caudal nucleus of the solitary tract. Neuropharmacology 54(2), 445-453.

Spray, D. C., Bai, S., Burk, R. D. and Saez, J. C., 1994. Regulation and function of liver gap junctions and their genes. Progress in Liver Diseases 12, 1-18.

Spray, D. C., Harris, A. L. and Bennett, M. V. L., 1979. Voltage dependence on junctional conductance in early amphibian embryos. Science 204(4391), 432-434.

Spray, D. C., White, R. L., Mazet, F. and Bennett, M. V., 1985. Regulation of gap junctional conductance. American Journal of Physiology - Heart and Circulatory Physiology 248(6), H753-H764.

Spray, D. C., Ye, Z.-C. and Ransom, B. R., 2006. Functional connexin “hemichannels”: A critical appraisal. Glia 54(7), 758-773.

Starkebaum, W., Pollack, S. R. and Korostoff, E., 1979. Midroelectrode studies of stress-generated potentials in four-point bending of bone. Journal of Biomedical Materials Research 13(5), 729-751.

Steinberg, T. H., Civitelli, R., Geist, S. T., Robertson, A. J., Hick, E., Veenstra, R. D., Wang, H. Z., Warlow, P. M., Westphale, E. M. and Laing, J. G., 1994. Connexin43 and connexin45 form gap junctions with different molecular permeabilities in osteoblastic cells. The EMBO Journal 13(4), 744-750.

Stoker, M., 1970. New growth and viruses. British Medical Journal 5 (5722), 541-545.

Stupack, D. G., Puente, X. S., Boutsaboualoy, S., Storgard, C. M. and Cheresh, D. A., 2001. Apoptosis of adherent cells by recruitment of caspase-8 to unligated integrins. The Journal of Cell Biology 155(3), 459-470.

Suadicani, S. O., Cherkas, P. S., Zuckerman, J., Smith, D. N., Spray, D. C. and Hanani, M., 2010. Bidirectional calcium signaling between satellite glial cells and neurons in cultured mouse trigeminal ganglia. Neuron Glia Biology 6(Special Issue 01), 43-51.

Suadicani, S. O., De Pina-Benabou, M. H., Urban-Maldonado, M., Spray, D. C. and Scemes, E., 2003. Acute downregulation of cx43 alters p2y receptor expression levels in mouse spinal cord astrocytes. Glia 42(2), 160-171.

Sugawara, Y., Ando, R., Kamioka, H., Ishihara, Y., Honjo, T., Kawanabe, N., Kurosaka, H., Takano-Yamamoto, T. and Yamashiro, T., 2011. The three-dimensional morphometry and cell-cell communication of the osteocyte network in chick and mouse embryonic calvaria. Calcified Tissue International, 1-9.

Sugawara, Y., Ando, R., Kamioka, H., Ishihara, Y., Murshid, S. A., Hashimoto, K., Kataoka, N., Tsujioka, K., Kajiya, F., Yamashiro, T. and Takano-Yamamoto, T., 2008. The alteration of a mechanical property of bone cells during the process of changing from osteoblasts to osteocytes. Bone 43(1), 19-24.

Takagi, J., Petre, B. M., Walz, T. and Springer, T. A., 2002. Global conformational rearrangements in integrin extracellular domains in outside-in and inside-out signaling. Cell 110(5), 599-611.
Tami, A. E., Nasser, P., Verborgt, O., Schaffler, M. B. and Tate, M. L. K., 2002. The role of interstitial fluid flow in the remodeling response to fatigue loading. Journal of Bone and Mineral Research 17(11), 2030-2037.
Tami, A. E., Schaffler, M. B. and Tate, M. L. K., 2003. Probing the tissue to subcellular level structure underlying bone's molecular sieving function. Biorheology 40(6), 577-590.
Tan, J. L., Tien, J., Pirone, D. M., Gray, D. S., Bhadriraju, K. and Chen, C. S., 2003. Cells lying on a bed of microneedles: An approach to isolate mechanical force. Proceedings of the National Academy of Sciences 100(4), 1484-1489.
Tanaka-Kamioka, K., Kamioka, H., Ris, H. and Lim, S. S., 1998. Osteocyte shape is dependent on actin filaments and osteocyte processes are unique actin-rich projections. Journal of Bone and Mineral Research 13(10), 1555-1568.
Tanaka, T. and Sakano, A., 1985. Differences in permeability of microperoxidase and horseradish peroxidase into the alveolar bone of developing rats. Journal of Dental Research 64(6), 870-876.
Tazawa, K., Hoshi, K., Kawamoto, S., Tanaka, M., Ejiri, S. and Ozawa, H., 2004. Osteocytic osteolysis observed in rats to which parathyroid hormone was continuously administered. Journal of Bone and Mineral Metabolism 22(6), 524-529.
Termine, J. and Posner, A., 1967. Amorphous/crystalline interrelationships in bone mineral. Calcified Tissue Research 1(1), 8-23.
Teti, A. and Zallone, A., 2009. Do osteocytes contribute to bone mineral homeostasis? Osteocytic osteolysis revisited. Bone 44(1), 11-16.
Thi, M. M., Kojima, T., Cowin, S. C., Weinbaum, S. and Spray, D. C., 2003. Fluid shear stress remodels expression and function of junctional proteins in cultured bone cells. American Journal of Physiology - Cell Physiology 284(2), C389-C403.
Thi, M. M., Suadicani, S. O. and Spray, D. C., 2010a. Fluid flow-induced soluble vascular endothelial growth factor (vegf) isoforms regulate actin adaptation in osteoblasts. Journal of Biological Chemistry.
Thi, M. M., Urban-Maldonado, M., Spray, D. C. and Suadicani, S. O., 2010b. Characterization of htert-immortalized osteoblast cell lines generated from wild-type and connexin43-null mouse calvaria. American Journal of Physiology - Cell Physiology 299(5), C994-C1006.
Thompson, W. R., Rubin, C. T. and Rubin, J., Mechanical regulation of signaling pathways in bone. Gene (0).
Tilney, L. G., Egelman, E. H., DeRosier, D. J. and Saunder, J. C., 1983. Actin filaments, stereocilia, and hair cells of the bird cochlea. Ii. Packing of actin filaments in the stereocilia and in the cuticular plate and what happens to the organization when the stereocilia are bent. The Journal of Cell Biology 96(3), 822-834.
Traub, O., Druge, P. M. and Willecke, K., 1983. Degradation and resynthesis of gap junction protein in plasma membranes of regenerating liver after partial hepatectomy or cholestasis. Proceedings of the National Academy of Sciences 80(3), 755-759.
Turner, C. and Robling, A., 2005. Mechanisms by which exercise improves bone strength. Journal of Bone and Mineral Metabolism 23, 16-22.
Turner, C. H., Forwood, M. R., Rho, J. Y. and Yoshikawa, T., 1994. Mechanical loading thresholds for lamellar and woven bone formation. Journal of Bone and Mineral Research 9(1), 87-97.
Ueno, K., Haba, T., Woodbury, D., Price, P., Anderson, R. and Jee, W. S. S., 1985. The effects of prostaglandin e2 in rapidly growing rats: Depressed longitudinal and radial growth and increased metaphyseal hard tissue mass. Bone 6(2), 79-86.
van Rijen, H. V. M., van Veen, T. A. B., Hermans, M. M. P. and Jongsma, H. J., 2000. Human connexin40 gap junction channels are modulated by camp. Cardiovascular Research 45(4), 941-951.
Vatsa, A., Semeins, C. M., Smit, T. H. and Klein-Nulend, J., 2008. Paxillin localisation in osteocytes--is it determined by the direction of loading? Biochemical and Biophysical Research Communications 377(4), 1019-1024.
Vatsa, A., Smit, T. H. and Klein-Nulend, J., 2007. Extracellular no signalling from a mechanically stimulated osteocyte. Journal of Biomechanics 40, S89-S95.
von Meyer, G., 1867. Die architektur der spongiosa. Archives fur Anatomie, Physiologie und wissenschaftliche Medizin 34, 615-628.

Wang, H., Ma, W.-g., Tejada, L., Zhang, H., Morrow, J. D., Das, S. K. and Dey, S. K., 2004. Rescue of female infertility from the loss of cyclooxygenase-2 by compensatory up-regulation of cyclooxygenase-1 is a function of genetic makeup. Journal of Biological Chemistry 279(11), 10649-10658.

Wang, L., Ciani, C., Doty, S. B. and Fritton, S. P., 2004. Delineating bone's interstitial fluid pathway in vivo. Bone 34(3), 499-509.

Wang, Y., McNamara, L. M., Schaffler, M. B. and Weinbaum, S., 2007. A model for the role of integrins in flow induced mechanotransduction in osteocytes. Proc.Natl.Acad.Sci.U.S.A. 104(40), 15941-15946.

Weinbaum, S., Cowin, S. C. and Zeng, Y., 1994. A model for the excitation of osteocytes by mechanical loading-induced bone fluid shear stresses. Journal of Biomechanics 27(3), 339-360.

Wennerberg, K., Lohikangas, L., Gullberg, D., Pfaff, M., Johansson, S. and Fässler, R., 1996. Beta 1 integrin-dependent and -independent polymerization of fibronectin. The Journal of Cell Biology 132(1), 227-238.

Werb, Z., Tremble, P. M., Behrendtsen, O., Crowley, E. and Damsky, C. H., 1989. Signal transduction through the fibronectin receptor induces collagenase and stromelysin gene expression. The Journal of Cell Biology 109(2), 877-889.

Whitfield, J. F., 2003. Primary cilium--is it an osteocyte's strain-sensing flowmeter? J.Cell Biochem. 89(2), 233-237.

Wolff, J., 1892. Das gesetz der transformation der knochen. In: (Eds.), Das gesetz der transformation der knochen. Hirschwald, Berlin, pp.

Wozniak, M. A., Modzelewska, K., Kwong, L. and Keely, P. J., 2004. Focal adhesion regulation of cell behavior. Biochimica et Biophysica Acta (BBA) - Molecular Cell Research 1692(2–3), 103-119.

Wu, D., Ganatos, P., Spray, D. C. and Weinbaum, S., 2011. On the electrophysiological response of bone cells using a stokesian fluid stimulus probe for delivery of quantifiable localized piconewton level forces. Journal of Biomechanics 44(9), 1702-8.

Yellowley, C. E., Hancox, J. C., Skerry, T. M. and Levi, A. J., 1998. Whole-cell membrane currents from human osteoblast-like cells. Calcified Tissue International 62(2), 122-132.

Yellowley, C. E., Li, Z., Zhou, Z., Jacobs, C. R. and Donahue, H. J., 2000. Functional gap junctions between osteocytic and osteoblastic cells. Journal of Bone and Mineral Research 15(2), 209-217.

You, J., Yellowley, C. E., Donahue, H. J., Zhang, Y., Chen, Q. and Jacobs, C. R., 2000. Substrate deformation levels associated with routine physical activity are less stimulatory to bone cells relative to loading-induced oscillatory fluid flow. Journal of Biomechanical Engineering 122(4), 387-393.

You, L., Temiyasathit, S., Lee, P., Kim, C. H., Tummala, P., Yao, W., Kingery, W., Malone, A. M., Kwon, R. Y. and Jacobs, C. R., 2008. Osteocytes as mechanosensors in the inhibition of bone resorption due to mechanical loading. Bone 42(1), 172-179.

You, L. D., Cowin, S. C., Schaffler, M. B. and Weinbaum, S., 2001. A model for strain amplification in the actin cytoskeleton of osteocytes due to fluid drag on pericellular matrix. Journal of Biomechanics 34(11), 1375-1386.

You, L. D., Weinbaum, S., Cowin, S. C. and Schaffler, M. B., 2004. Ultrastructure of the osteocyte process and its pericellular matrix. The Anatomical Record Part A: Discoveries in Molecular, Cellular, and Evolutionary Biology 278A(2), 505-513.

Young, S. R. L. and Pavalko, F. M., 2011. Cellular mechanisms of mechanotransduction in bone. In: Kamkin, A. and Kiseleva, I. (Eds.), Mechanosensitivity and mechanotransduction. Springer Netherlands, pp. 277-296.

Zaman, G., Pitsillides, A. A., Rawlinson, S. C. F., Suswillo, R. F. L., Mosley, J. R., Cheng, M. Z., Platts, L. A. M., Hukkanen, M., Polak, J. M. and Lanyon, L. E., 1999. Mechanical strain stimulates nitric oxide production by rapid activation of endothelial nitric oxide synthase in osteocytes. Journal of Bone and Mineral Research 14(7), 1123-1131.

Zeng, Y., Lv, X.-h., Zeng, S.-q., Tian, S.-l., Li, M. and Shi, J., 2008. Sustained depolarization-induced propagation of [ca2+]i oscillations in cultured drg neurons: The involvement of extracellular atp and p2y receptor activation. Brain Research 1239, 12-23.